Metformin-induced Effects on Human Skeletal Muscle Metabolism and Function

Dissertation

der Mathematisch-Naturwissenschaftlichen Fakultät
der Eberhard Karls Universität Tübingen
zur Erlangung des Grades eines
Doktors der Naturwissenschaften
(Dr. rer. nat.)

vorgelegt von
Jennifer Maurer
aus München

Tübingen
2024

Gedruckt mit Genehmigung der Mathematisch-Naturwissenschaftlichen Fakultät der Eberhard Karls Universität Tübingen.

Tag der mündlichen Qualifikation: 19.07.2024

Dekan:	Prof. Dr. Thilo Stehle
1. Berichterstatter:	Prof. Dr. Peter Ruth
2. Berichterstatterin:	Prof. Dr. Cora Weigert

Contents

Abbreviations

2-DG	2-deoxyglucose
4E-BP1	eukaryotic translation initiation factor 4E binding protein 1
ABRA	actin binding Rho activating protein
ACC	acetyl-CoA carboxylase
AEC	adenylate energy charge
AGE	advanced glycation end product
Akt	Akt serine/threonine kinase
AMPK	AMP activated protein kinase
AS160	Akt substrate of 160 kDa
AUC	area under the curve
BCA	bicinchonic acid
CaMK	calmodulin-dependent protein kinase
CE	capillary electrophoresis
CK	creatine kinase
CRTC2	CREB regulated transcription coactivator 2
CS	citrate synthase
CYP2D6	cytochrome P450 2D6
CXCL1	CXC motif chemokine ligand 1
D0	day 0 of differentiation
D3	day 3 of differentiation
D5	day 5 of differentiation
D6	day 6 of differentiation
D8	day 8 of differentiation
DPP4	dipeptidyl peptidase 4
DRX	disordered-relaxed
ECAR	extracellular acidification rate
ECC	excitation contraction coupling
ECM	extracellular matrix
EPS	electro-pulse stimulation
ERK	extracellular signal-regulated kinases
FACS	fluorescence-activated cell sorting
FAO	fatty acid oxidation
FBP1	fructose bisphosphatase 1
FDA	Food and Drug Administration

FDG	fluorodeoxyglucose
fps	frames per second
GAPDH	glyceraldehyde-3-phosphate dehydrogenase
GDF15	growth differentiation factor 15
GIT	gastrointestinal tract
GLP1	glucagon-like peptide 1
GLUT1	glucose transporter 1
GLUT2	glucose transporter 2
GLUT4	glucose transporter 4
GPR81	G-protein coupled receptor 81
HbA1c	glycated haemoglobin A1c
HIIT	high intensity interval training
HK	hexokinase
HR	heart rate
IFG	impaired fasting glucose
IGF1	insulin-like growth factor 1
IGT	impaired glucose tolerance
IL6	interleukin 6
IL8	interleukin 8
Lac-Phe	lactoyl-phenylalanine
LC-MS	liquid chromatography-mass spectrometry
LDH	lactate dehydrogenase
LKB1	liver kinase B1
MACS	magnetic cell separation
MATE	multidrug and toxin extruder
MCT	monocarboxylate transporter
ME2	malic enzyme 2
mG3PDH	mitochondrial glycerol-3-phosphate dehydrogenase
MHfast	fast type myosin heavy chain
MHslow	slow type myosin heavy chain
MPC	mitochondrial pyruvate carrier
MRTF-A	myocardin related transcription factor A
mTOR	mechanistic target of rapamycin
mTORC1	mechanistic target of rapamycin complex 1
MyBP	myosin binding protein
MYH1	myosin heavy chain 1
MYH2	myosin heavy chain 2
MYH7	myosin heavy chain 7

MyoD	myogenic differentiation
NDUFB8	NADH:ubiquinone oxidoreductase subunit B8
OCR	oxygen consumption rate
OCT	organic cation transporter
oGTT	oral glucose tolerance test
P0	passage 0
P1	passage 1
p70S6K1	ribosomal protein S6 kinase beta 1
PBPK	physiologically based pharmacokinetic
PDH	pyruvate dehydrogenase
PDK	pyruvate dehydrogenase kinase
PEN2	presenilin enhancer 2
PET	positron emission tomography
PFK	phosphofructokinase
PGC1α	peroxisome proliferator-activated receptor gamma co-activator 1 alpha
PI3K	phosphoinositide 3 kinase
PK	pyruvate kinase
PLL	poly-L-lysine
PMAT	plasma membrane monoamine transporter
qRT-PCR	quantitative real time polymerase chain reaction
Rab4	Ras-related protein Rab-4
RER	respiratory exchange ratio
RIN	RNA integrity number
RLC	regulatory light chain
RLU	relative light unit
RPE	rate of perceived exertion
RPS6	ribosomal protein S6
RSPO3	R-spondin 3
RT	room temperature
RyR	ryanodine receptor
SA medium	seahorse assay medium
sd	standard deviation
SERCA	sarcoplasmic/endoplasmic reticulum calcium ATPase
SERT	serotonin reuptake transporter
SGLT1	sodium glucose cotransporter 1
SGLT2	sodium glucose cotransporter 2
SRF	serum response factor
SRX	super-relaxed

Stars	striated muscle activator of Rho signaling
SUIT	substrate-uncoupler-inhibitor-titration
T1D	type 1 diabetes
T2D	type 2 diabetes
TBC1D1	TBC1 domain family member 1
THTR2	thiamine transporter 2
TSC	tuberous sclerosis complex
VDAC	voltage-dependent anion channel
VO_{2peak}	peak oxygen uptake
w/	with
w/o	without
WHO	World Health Organization
Wnt	wingless-related integration site

Abstract

Metformin, the primary oral antidiabetic agent for type 2 diabetes (T2D), has been FDA-approved for three decades. Today more than 150 million people worldwide benefit from metformin via effectively reduced blood glucose levels with low risk of hypoglycemia. However, the precise mechanism of action has not yet been conclusively clarified. Skeletal muscle is an important player in insulin-mediated glucose uptake, but the number of studies on the effects of metformin on this tissue is limited. This thesis aims to improve the understanding of the effects of metformin on skeletal muscle by investigating two specific questions:

1. What are the molecular mechanisms by which metformin leads to increased lactate production? This phenomenon is associated with the known adverse effects of hyperlactatemia and metabolic acidosis. At the same time, it has been hypothesized that moderate increases in plasma lactate levels may contribute to the pleiotropic beneficial effects of metformin.

2. Which molecular mechanisms provide an explanation for the attenuated muscular adaptations to regular performed physical exercise during metformin therapy as reported in some clinical studies? This question arises in the context that regular exercise is an integral part of T2D therapy and skeletal muscle plays a central role in physical activity.

Both questions were addressed by a 48-hour treatment of primary human myotubes with a range of different metformin concentrations (16–776 µM) to cover both pharmacological and supra-pharmacological doses of the drug. Global effects were investigated by RNA sequencing analysis. For the determination of lactate production and glucose consumption cell culture supernatant was analyzed. Individual mechanisms were investigated on the basis of immunoblots, immunohistochemistry, respirometry and luminescence assays. Mimicking exercise *in vitro*, electro-pulse stimulation was applied and cellular energy status was investigated by quantification of adenosine nucleotides via capillary electrophoresis (CE).

Increasing concentrations of metformin led to its intracellular accumulation. As from 78 µM, the metformin treatment resulted in a dose-dependent increase in extracellular lactate, predominantly due to increased lactate production covered by increased glucose uptake and glycolysis. Lactate production was forced through a shift in the equilibrium of the LDH reaction in myotubes. First, metformin inhibited mitochondrial respiration in complex I causing a shift in cellular redox state represented by the accumulation of NADH. Second, metformin mediated an accumulation of pyruvate through the inhibition of PDH complex. Which of the two mechanisms is at work in the skeletal muscle of metformin-treated patients with T2D needs to be investigated.

Assessing the second question, reduced mTOR-C1/S6K1 signaling was found in metformin-treated myotubes, indicating a blunted hypertrophic response mediated by metformin. In addition, even at low concentrations, metformin impaired the electro-pulse-stimulated contraction of myotubes. No evidence of structural changes could be found, so that this does not appear to be the cause of the limited functionality of the myotubes. The hypothesis that a metformin-induced energy deficit is the underlying cause could not be conclusively confirmed. Nucleotide quantification using CE did not reveal any differences, but in contrast, an increased activation of the energy sensor AMPK was found.

In conclusion, the results suggest a novel mechanism by which metformin can increase lactate production through altered activity of the PDH complex. The impaired contractility of metformin-treated myotubes provides *in vitro* evidence that metformin may interfere with biochemical processes during exercise *in vivo*. Given the high prevalence of metformin-exercise combination therapies in patients with T2D, further *in vivo* studies are required.

Zusammenfassung

Metformin ist das wichtigste orale Antidiabetikum zur Behandlung von Diabetes Typ 2 (T2D) und bereits seit drei Jahrzehnten von der FDA zugelassen. Heute profitieren weltweit mehr als 150 Millionen Menschen von einer effektiven Senkung des Blutzuckerspiegels, während gleichzeitig das Risiko einer Hypoglykämie gering ist. Der genaue Wirkmechanismus von Metformin ist jedoch noch nicht abschließend geklärt. Der Skelettmuskel ist ein wichtiger Akteur bei der Insulin-vermittelten Glukoseaufnahme, dennoch ist die Anzahl an Studien über die Auswirkungen von Metformin auf dieses Gewebe begrenzt. Daher zielt diese Arbeit darauf ab, das Verständnis der Effekte von Metformin auf die Skelettmuskulatur zu verbessern, indem zwei spezifische Fragestellungen untersucht werden:

1. Über welche molekularen Mechanismen induziert Metformin eine erhöhte Laktatproduktion? Dieses Phänomen ist mit den bekannten unerwünschten Nebenwirkungen Hyperlaktatämie und metabolischer Azidose assoziiert. Gleichzeitig existiert die Hypothese, dass moderate Erhöhungen des Plasmalaktatspiegels zu den pleiotropen positiven Wirkungen von Metformin beitragen könnten.

2. Welche molekularen Mechanismen liefern eine Erklärung für die reduzierte Wirksamkeit von regelmäßig durchgeführtem Sport während einer Metformin Therapie, wie dies in einigen klinischen Studien berichtet wurde? Diese Frage stellt sich vor dem Hintergrund, dass regelmäßiger Sport fester Bestandteil der Therapie von T2D ist und die Skelettmuskulatur eine zentrale Rolle bei körperlicher Aktivität einnimmt.

Beide Fragen wurden durch eine 48-stündige Behandlung primärer humaner Myotuben mit einer Reihe unterschiedlicher Metforminkonzentrationen (16–776 µM) untersucht, um pharmakologische und supra-pharmakologische Dosen des Wirkstoffes abzudecken. Die globalen Effekte von Metformin auf die Myotuben wurden im Rahmen einer RNA-Sequencing Analyse untersucht. Für die Bestimmung der Laktatproduktion und des Glukoseverbrauchs wurde der Zellkulturüberstand analysiert. Einzelne Mechanismen wurden anhand von Immunoblots, Immunhistochemie, Respirometrie und Lumineszenz Assays untersucht. Zur Simulation von Sport *in vitro* wurde die Elektropuls-Stimulation angewendet und der zelluläre Energiestatus der Myotuben wurde durch die Quantifizierung der Adenosin-Nukleotide mittels Kapillarelektrophorese (CE) ermittelt.

Steigende Konzentrationen von Metformin führten zu dessen intrazellulärer Anreicherung. Ab 78 µM führte die Metformin-Behandlung zu einem dosisabhängigen Anstieg des extrazellulären Laktats, der in erster Linie auf eine erhöhte Laktatproduktion zurückzuführen war, die durch eine erhöhte Glukoseaufnahme und Glykolyse gedeckt wurde. Die verstärkte Laktatproduktion wurde durch eine Verschiebung des Gleichgewichts der LDH-Reaktion bewirkt. Erstens hemmte Metformin die mitochondriale Atmung des Komplex I, was eine Verschiebung des zellulären Redox-Status zur Folge hatte und somit zur Erhöhung der NADH/NAD^+ Ratio führte. Zweitens induzierte Metformin die Akkumulation von Pyruvat durch die Hemmung des PDH-Komplexes. Welcher der beiden Mechanismen im Skeletmuskel von mit Metformin behandelten Patienten mit T2D eine Rolle spielt, muss weitergehend untersucht werden.

In Bezug auf die zweite Fragestellung wurde in mit Metformin behandelten Myotuben ein verringertes mTOR-C1/S6K1-Signaling nachgewiesen, was eine durch Metformin vermittelte abgeschwächte hypertrophe Antwort erklären kann. Darüber hinaus zeigte die Elektropuls-Stimulation der Myotuben eine beeinträchtigte Kontraktion bereits durch die Behandlung mit niedrigen Metformindosen. Es konnten keine Hinweise auf strukturelle Veränderungen gezeigt werden, so dass hierin

nicht die Ursache für die eingeschränkte Funktionalität der Myotuben zu liegen scheint. Die Hypothese, dass ein Metformin-induziertes Energiedefizit die Ursache ist, konnte nicht abschließend bestätigt werden. Die Nukleotidquantifizierung mittels CE ergab keine Unterschiede, wohingegen eine erhöhte Aktivierung des Energiesensors AMPK gemessen wurde.

Die Ergebnisse deuten auf einen neuen Mechanismus hin, durch den Metformin die Laktatproduktion durch eine veränderte Aktivität des PDH-Komplexes erhöhen kann. Die beeinträchtigte Kontraktilität der mit Metformin behandelten Myotuben liefert einen Beweis dafür, dass Metformin biochemische Prozesse während des Trainings beeinträchtigen kann. Angesichts der hohen Prävalenz von Kombinationstherapien aus Metformin und regelmäßigem Sport bei Patienten mit T2D erscheinen weitere *in vivo* Studien notwendig, um diesem Sachverhalt nachzugehen.

CHAPTER 1

Introduction

1.1 Type 2 diabetes

Diabetes mellitus defines a heterogeneous metabolic disease which is characterized by chronically elevated plasma glucose levels. The disease is caused by impaired or even absent insulin secretion and impaired insulin sensitivity, usually a combination of both. A general distinction for the two major types is made as to whether there is an absolute insulin deficiency caused by β-cell damage (type 1 diabetes (T1D), 5–10%) or a relative insulin deficiency (type 2 diabetes (T2D), 90–95%) due to insulin resistance [193]. Following criteria for diagnosis are used [193]:

- Impaired fasting glucose (IFG): venous fasting plasma glucose $\geq$ 126 mg/dL
- Random venous plasma glucose $\geq$ 200 mg/dL
- Impaired glucose tolerance (IGT): 120 min plasma glucose $\geq$ 200 mg/dL during oral glucose tolerance test (oGTT)
- Glycated haemoglobin A1c (HbA1c) $\geq$ 6.5%

Predetermined risk factors for T2D include age, genetic traits, and family history, while acquired factors cover obesity, physical inactivity, and related metabolic disorders, often associated with an unhealthy lifestyle (smoking, alcohol, high-caloric food intake) [131]. Global diabetes prevalence reached 529 million individuals, representing 6.1% of the world population, with a projected increase to 1.31 billion by 2050, predominantly T2D [175]. In 2022, the US incurred total costs of 412.9 billion dollars, covering direct medical treatment and indirect costs, emphasizing the societal burden of the disease [184]. Diabetes-related complications include macrovascular (coronary artery disease, peripheral arterial disease, stroke) and microvascular complications (diabetic nephropathy, neuropathy, retinopathy) [61], which contribute to 12.2% of global deaths (ages 20–79) [56].

The treatment of T2D therefore involves not only regulation of blood glucose levels but also reduction of risk factors and complications. Guideline-based treatment consists of basic therapy, which can be used preventative, and additional pharmacotherapy [7, 131, 141]. Basic therapy comprises multiple actions aiming for a healthier lifestyle incorporating dietary interventions and increased physical activity as key factors. Metformin is the first-choice oral antidiabetic drug for pharmacological treatment, irrespective of cardiovascular and renal risk. For intensified therapy, dipeptidyl peptidase 4 (DPP4) inhibitors, glucagon-like peptide 1 (GLP1) receptor agonists, sodium glucose cotransporter 2 (SGLT2) inhibitors or sulfonylureas can be used. Considering patient risk factors SGLT2 and/or DPP4 inhibitors can even be combined with metformin. With progression of the disease, insulin treatment might become necessary.

1.2 Clinical application and pharmacology of metformin in T2D

Metformin was introduced as early as 1958 in the UK and other European countries for the treatment of diabetes, but it was not until FDA approval in 1994 that it became popular. Since 2011 metformin is included in WHO's essential medicines list emphasizing its medical, social, and economic significance [14]. Several guidelines for the treatment of T2D recommend metformin as the first-line oral antidiabetic drug [7, 131, 141]. It is further often used for combination therapy

with SGLT2 or DPP4 inhibitors or is continued when patients become insulin dependent showing an additive effect on glycemic control [13]. In clinical practice, a maximum daily dose of 2x 1 000 mg is typically administered [131]. After initially slowly increasing the dose to reduce gastrointestinal side effects, metformin is generally well tolerated.

Metformin (1,1-dimethylbiguanide, Fig. 1) is chemically classified as biguanide and is allocated to class 3 of the Biopharmaceutics Drug Disposition Classification System, which is characterized by high solubility coupled with poor membrane permeability [247]. Its bioavailability, following oral administration, ranges from 40% to 60%, and it is primarily absorbed in the small intestine [76]. Pharmacological doses yield plasma concentrations mainly ranging from 1 to 40 µM with pronounced inter-individual variability [101, 128, 231]. Peak levels are achieved about 2 h post-administration [231]. Notably, hepatic metformin concentrations are 2 to 3-fold higher, as the absorbed drug is transported via the portal vein to the liver where it accumulates [128]. With a half-life of approximately 5 h in patients with normal renal function metformin is eliminated by the kidneys without being metabolized [76]. In accordance, in a human ^{11}C-metformin positron emission tomography (PET) dosimetry study highest concentrations were measured in liver, kidneys and bladder while less tracer was detected in intestine and skeletal muscle [75].

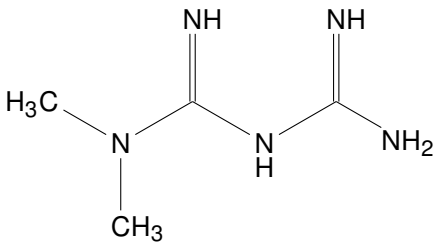

Figure 1: Chemical structure of the biguanide metformin.

Metformin is a highly hydrophilic substance and with a pKa value of 12.4 [172] more than 99.9% of the drug are in the mono-protonated form under physiological conditions. Consequently, passive diffusion through membranes is unlikely and active transport by specific transporters is required for substantial cellular uptake of metformin. Several transporters have been described to transport metformin across the route of administration, distribution and elimination: organic cation transporters (OCTs), multidrug and toxin extruders (MATEs), plasma membrane monoamine transporter (PMAT), thiamine transporter 2 (THTR2), and serotonin reuptake transporter (SERT) (Table 1).

Table 1: Major tissue distribution of identified metformin transporters. The direction of transport summarizes results as observed in either *in vitro* or *in vivo* studies.

Gene	Transporter	Major tissue	Direction
SLC6A4	SERT	Intestine	uptake
SLC19A3	THTR2	Intestine, Liver	uptake
SLC22A1	OCT1	Liver, Kidney	bidirectional
SLC22A2	OCT2	Kidney	bidirectional
SLC22A3	OCT3	Liver, Skeletal Muscle, Fat, Brain, Intestine	bidirectional
SLC22A4	OCTN1	Intestine	uptake
SLC29A4	PMAT	Intestine	uptake
SLC47A1	MATE1	Kidney, Liver	release
SLC47A2	MATE2	Kidney	release

Table modified from [139].

Multiple transporters have been suggested to play a role in intestinal uptake of metformin including OCT1, PMAT, and SERT, each contributing to 15–25% to the apical uptake of metformin in Caco-2 cells [82]. In the liver, OCT1 plays a significant role in the hepatic uptake of metformin [242], contributing to its distribution and pharmacological effects as demonstrated by depletion and reduced function genetic variants of OCT1, which abolish metformin effects on the regulation of blood glucose levels in humans [220]. Additionally, OCT3 is associated with the hepatic uptake of metformin in cell culture and may modulate its pharmacological action as demonstrated by genetic variants [37]. For the hepatic elimination of metformin MATE1 has been shown to be of great relevance by dynamic PET imaging in mice [98]. *In vivo* studies found that OCT2 plays a dominant role in the renal uptake and accumulation of metformin [110, 233]. Furthermore, OCT1 is expressed at the apical side of proximal and distal tubules in human kidneys, suggesting its potential role in metformin renal clearance [233]. However, the renal clearance of metformin is significantly influenced by the activity of MATE transporters, particularly MATE1 [19, 229, 230]. Limited information is available regarding the potential transport mechanisms in skeletal muscle. OCT3 is expressed ubiquitously and is the most frequent expressed member of the OCT family in skeletal muscle and adipose tissue [36] showing similar substrate specificity to OCT1 and OCT2. In rat skeletal muscle metformin uptake occurs via OCTs in a time-dependent manner [177]. Studies on OCT3 knockout mice show a reduced intramuscular accumulation of metformin compared to wildtype mice going along with a blunted hypoglycemic effect [36]. Further evidence for OCT3-mediated uptake of metformin derive from experiments in primary human muscle cells showing a reduced effect of metformin on the phosphorylation of AMP activated protein kinase (AMPK) induced by both the general OCT inhibitor cimetidine and OCT3 shRNA [37].

1.3 The mechanisms of action of metformin to mediate its hypoglycemic effect

Metformin is a synthetic derivate of the natural compound galegine (*Galega officinalis*) and was evidence-based introduced as an antidiabetic drug [14]. Which mechanisms are mostly responsible for the glucoregulatory effects of metformin and how they interact is still not fully understood. The liver is considered the main target, while there is increasing evidence that the gastrointestinal tract (GIT) also plays an important role. The skeletal muscle has been studied to a lesser extent, although it is an important regulator of whole-body glucose homeostasis showing a high and flexible capacity to remove glucose from circulation.

Many mechanistic *in vitro* studies are criticized because metformin concentrations above 1 mM were used [52, 189, 195, 180], which are in the supra-pharmacological range. The review by LaMoia et al. [128] reports that therapeutic metformin concentrations in human plasma are in the range of 1 to 40 µM (approximately 0.1–4 mg/L). Not less important for the *in vivo* comparison are the tissue distribution of the drug and the intracellular concentrations that can be achieved in the individual tissues. PET dosimetry studies applying ^{11}C-metformin report increased tracer concentrations in liver and intestine of mice [98] and in liver and kidneys for humans, while skeletal muscle shows slow tracer accumulation [75]. With regard to hepatic metformin effects it is also important to note that metformin concentrations in portal vein are 2 to 3-fold higher compared to the systemic levels [84, 246].

The upcoming section will provide a concise overview of the pleiotropic effects of metformin currently discussed to play a role in the liver and GIT based on *in vivo* and *in vitro* studies, followed by summarizing the identified mechanisms in skeletal muscle (Fig. 2).

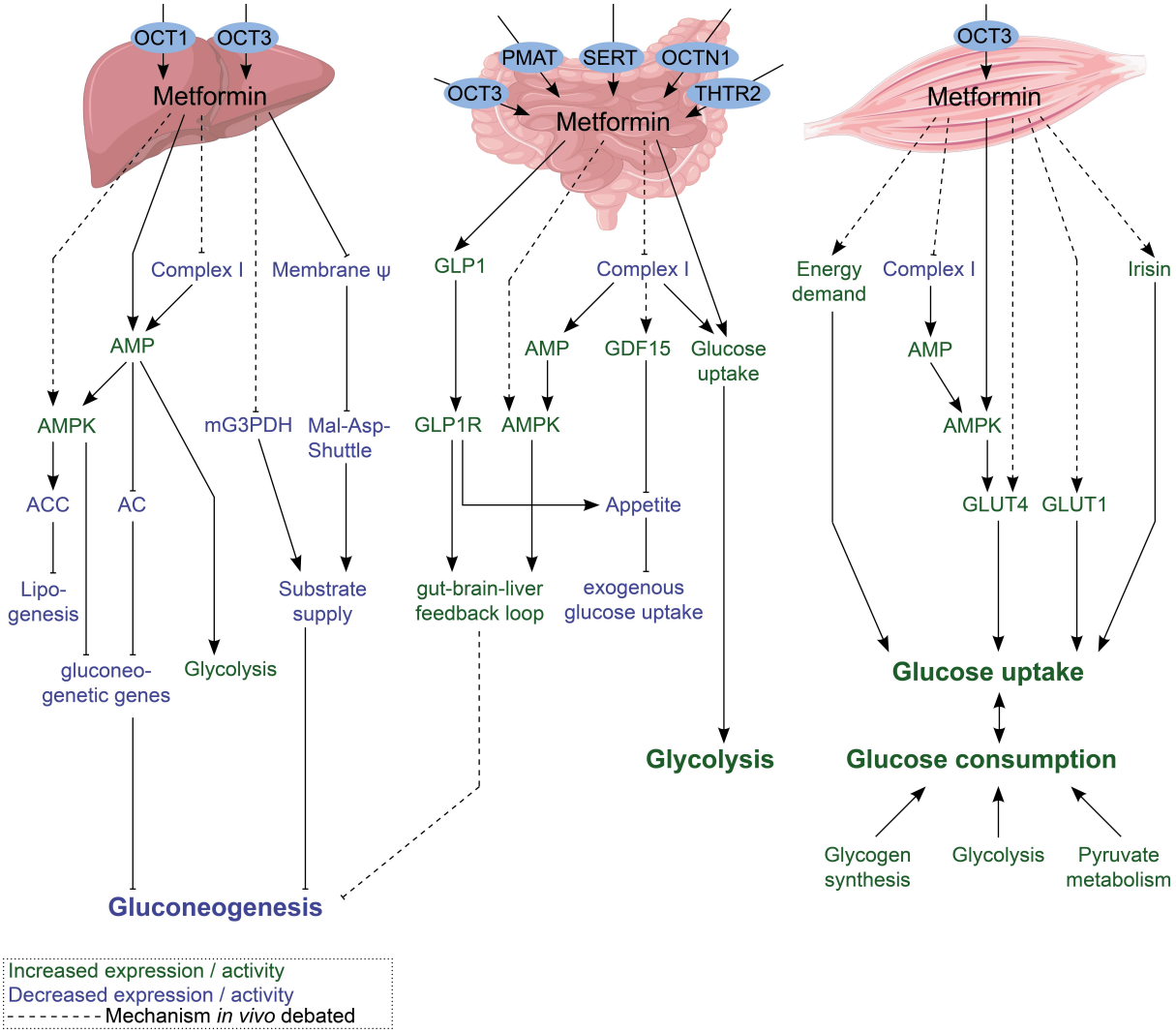

Figure 2: Overview of identified mechanisms of action of metformin to mediate its hypoglycemic effect.
The overview of major identified mechanisms of action of metformin to mediate the hypoglycemic effect illustrates a complex interplay between signaling pathways not only in liver, GIT and skeletal muscle but also in inter-organ crosstalk. By different AMPK-dependent and independent mechanisms hepatic gluconeogenesis is established as a major mechanism of action, while increased muscular glucose uptake and consumption contribute as well. Solid lines indicate mechanisms observed in human clinical studies and mechanisms induced by pharmacological relevant concentrations *in vitro* as well as in animal models. Dashed lines represent mechanisms of debatable relevance *in vivo* as they were observed at supra-pharmacological concentrations.

1.3.1 Targets in the liver

Clinical evidence for the liver as a major target of metformin is provided by studies reporting a reduction of up to 20% in hepatic glucose production in patients with poorly controlled T2D [42, 94]. The hypoglycemic effect can conclusively be attributed to reduced hepatic gluconeogenesis caused either by energy-dependent mechanisms through elevated AMP concentrations or redox-dependent mechanisms affecting the NADH:NAD^+ ratio [59]. Gluconeogenesis is physiologically reduced in states of low energy availability as six ATP equivalents per molecule of glucose are required. Early work showed that metformin inhibits mitochondrial complex I respiration in hepatocytes and isolated mitochondria [52, 180] impairing ATP production and consequently, compensatory activation of AMPK can occur. However, the relevance of complex I inhibition *in vivo* is highly debated as

effective concentrations were in the millimolar range. High concentrations of metformin can activate the AMPK-upstream kinase liver kinase B1 (LKB1), which is required to mediate the repressive effect of metformin on hepatic glucose production by inhibiting CREB regulated transcription coactivator 2 (CRTC2)-dependent gluconeogenic gene expression in mice [83, 219]. Therapeutic concentrations of metformin have been recently demonstrated to target the lysosomal AMPK pathway through PEN2 in mice, leading to the inhibition of v-ATPase and the activation of AMPK, while cellular AMP levels remain unaffected [146]. Further, activation of AMPK by metformin in hepatocytes results in suppression of lipogenic gene expression and inhibition of lipogenesis through the phosphorylation of acetyl-CoA carboxylase (ACC) [260]. Of note, prolonging the treatment time in hepatocytes results in AMPK activation at clinically relevant metformin concentrations of 10 µM [260], suggesting that during long-term treatment, the chronic AMPK activation modulates lipid metabolism and thereby improves hepatic insulin sensitivity by indirectly inhibiting hepatic gluconeogenesis [59]. The AMPK-mediated transcriptional changes induced by metformin are challenged by the finding that overexpression of peroxisome proliferator-activated receptor gamma co-activator 1 alpha (PGC1α), a major co-activator of gluconeogenic gene expression, in hepatocytes does not affect the inhibitory effect of metformin on hepatic glucose production [60]. The authors conclude that metformin-induced suppression of hepatic glucose production is linked to the regulation of the gluconeogenic flux rather than directly inhibiting gluconeogenic gene expression [60]. In addition, they demonstrate that the inhibitory effect of metformin on glucose production in primary murine hepatocytes is conserved when LKB1-AMPK signaling is impaired [60]. Moreover, in several other studies AMPK-independent mechanisms are repeatedly described [60, 88, 178], leaving room for discussion of the relevance of AMPK as a metformin target. Irrespective of energy-dependent activation of AMPK, metformin-induced increases in AMP levels in mice lead to allosteric inhibition of fructose bisphosphatase 1 (FBP1), a key regulatory enzyme of hepatic gluconeogenesis [93]. The accompanying accumulation of fructose-2,6-bisphosphate increases the glycolytic flux through increased pyruvate kinase (PK) activity, which in turn has an inhibitory effect on gluconeogenesis [9, 93]. Further, increased AMP levels lead to blunted glucagon-stimulated glucose production under high concentrations of metformin through inhibition of adenylate cyclase in mice [161].

Further mechanisms of metformin can be categorized on the basis of the altered cellular redox state, which has been identified as a regulatory factor in gluconeogenesis, with the regeneration of NADH in the cytosol influencing the process [225]. In rats, both acute and chronic administration of low doses of metformin result in direct inhibition of mitochondrial glycerol-3-phosphate dehydrogenase (mG3PDH) [148, 149], which is part of the glycerol-phosphate shuttle. As a consequence it is suggested that gluconeogenesis is impaired by diminished supply of glycerol and increased NADH levels, which in turn affects the allocation of lactate as a gluconeogenic precursor. The relevance of this mechanism is debated as malate-aspartate shuttle is the primary transport mechanism of NADH in liver [59]. In that direction, Alshawi et al. [6] suggest, that mitochondrial accumulation of metformin leads to the depolarisation of the mitochondrial membrane inhibiting the malate-aspartate shuttle and results in insufficient supply of gluconeogenesis with oxidized and reduced substrates.

In summary, metformin mediates parts of its hypoglycemic effect through a reduction of hepatic gluconeogenesis. Metformin-induced alterations in cellular energy and redox state are the basis for a number of potential mechanisms, whose interrelationship and clinical relevance is not yet fully understood.

1.3.2 Targets in the gastrointestinal tract

After oral administration of metformin, approximately 50% remain unabsorbed in the small intestine resulting in concentrations 30–300 times higher than plasma levels [15, 246] and accumulation in enterocytes, which is attributed to a more efficient uptake compared to the release [194]. Thus, the GIT is a promising target for mediating hypoglycemic effects of metformin. Buse et al. [32]

demonstrated the relevance of intestinal mechanisms by using a pH-dependent delayed-release formulation of metformin. This technological modification results in drug release within the ileum, where absorption is diminished and thus lower plasma concentrations are achieved. Nevertheless, participants with T2D do improve in fasting plasma glucose levels in a comparable manner regardless of whether delayed-release or common immediate-release formulation was administrated over 12 weeks. A human PET study conducted on individuals with type 2 diabetes found that metformin primarily stimulates uptake of intravenously applicated ^{18}F-FDG in the colon, with secondary effects observed in the small intestine [71]. This observation is associated with improved glycemic control and it is hypothesized that the intestine may act as a reservoir for circulating glucose [113]. However, which glucose transporters (GLUT1, GLUT2, and SGLT1) could be involved in increasing glucose uptake from circulation remains controversial [59, 181].

The inhibition of complex I of the respiratory chain, which is critically discussed in the liver due to the high metformin concentrations required, may indeed play a role in intestinal cells. A recent study links the impairment in mitochondrial respiration with increases of glucose uptake, glycolysis and secretion of growth differentiation factor 15 (GDF15) in murine intestinal cells treated with 1 mM metformin [252]. GDF15 is known to cause a reduced appetite *in vivo*, which on the one hand reduces exogenous glucose uptake and on the other hand may explain the patients' moderate weight loss under metformin treatment [45].

The incretin GLP1, produced by enteroendocrine L-cells, is another important regulator of whole-body glucose homeostasis. Upon postprandial release, it stimulates insulin secretion, inhibits glucagon secretion, slows gastric emptying and promotes satiety [170, 217]. Metformin increases GLP1 plasma levels [155], which can be attributed to increased GLP1 secretion in humans [12] or reduced degradation via DPP4, at least in mice [77]. Mechanistically, Kim et al. [109] link the interaction between Wnt and insulin signaling pathways with an increase in GLP1 production, which was induced by low concentrations of metformin (0.25 mM; 12.5 mg/kg body weight) in human L-cells *in vitro* as well as in mice. Further discussed mechanisms affecting GLP1 secretion include indirect effects caused by the release of bile acids or changes in the gut microbiome. Besides mediating positive effects, metformin-induced changes in the gut microbiome are also associated with the gastrointestinal side effects of the drug [59, 181].

The concept of a gut-brain-liver feedback loop describes an additional glucoregulatory mechanism, which is activated by nutrient intake and finally inhibits hepatic glucose production [49]. By metformin-mediated activation of duodenal mucosal AMPK and GLP1 receptor the neuronal axis of the feedback loop gets activated. This illustrates once again the pleiotropic effects of metformin, but also the contribution of several organs to the blood glucose lowering effect. Against that background it is important to gain a precise understanding of the effects in all relevant organs and their interplay to further improve the individual clinical efficiency and safety for the patient and to open up new treatment options.

1.3.3 Targets in skeletal muscle

Previous studies mainly investigated the effect of metformin on glucose metabolism and insulin signaling in skeletal muscle cell culture or rodent models. These studies provide some evidence that skeletal muscle can contribute to the hypoglycemic effect of metformin by inducing an increased glucose uptake [35, 43, 121, 163, 210, 211]. Nevertheless, the transferability of the findings to humans and therapeutic relevance of metformin's action in skeletal muscle must be questioned, since the experimentally used concentrations of metformin are again very high.

There have been several investigations into the involvement of expression and translocation of the major muscular glucose transporters glucose transporter 1 (GLUT1) and glucose transporter 4 (GLUT4) in the underlying mechanisms, but the results have been contradictory. A large point of discussion is again whether energy-dependent activation of AMPK is involved. It was recently

shown that metformin induces AMPK-dependent the expression of Ras-related protein Rab-4 (Rab4) in C2C12 cells [135, 163], which is an important regulator of GLUT4 membrane trafficking. Further studies found that the imidazoline I_{2B} receptor, ERK signaling, and conventional PKCs could be involved in metformin effects on GLUT4 [35, 210, 232]. In contrast to all the studies showing effects on GLUT4, Hundal et al. [92] report heightened GLUT1 in plasma membrane of L6 cells, while GLUT4 subcellular distribution is unaffected by 800 µM metformin. Moreover, in one of the few human studies, 26 weeks of metformin treatment of patients with newly diagnosed T2D shows no changes in insulin-dependent glucose uptake and GLUT4 expression [105].

Metformin also causes an increase in muscle glucose consumption. However, it is not yet possible to differentiate whether this is a consequence of the increased glucose uptake or forced by an heightened cellular energy demand. 10 weeks of metformin administration in patients with T2D results in reduced concentrations of phosphocreatine and ATP in skeletal muscle, which are further reflected by increased AMPK activity [169]. Similar to the mechanisms described in the liver and GIT, mitochondrial respiration can be disturbed in skeletal muscle due to the inhibition of complex I [28, 244], leading to an insufficient supply of energy. Beside some studies showing an increased production of H_2O_2 independent of O_2 flux [104, 157], the ongoing debate about the *in vivo* relevance of complex I inhibition is of particular importance in relation to skeletal muscle due to the low intramuscular concentrations of metformin that can be expected and because the effect is described at supra-pharmacological concentrations ($\geq$ 10 mM in rat muscle [28], 300 mg/kg body weight in mice [244]). As another mechanism, the reduced activity of the glycolytic enzymes hexokinase (HK) and phosphofructokinase (PFK) could be regenerated by metformin in diabetic mice, which increased glycolysis and lactate production [43]. Moreover, changes in pyruvate metabolism in skeletal muscle from older people [119] and an increase in insulin-stimulated glycogen synthesis in human muscle cells [3] have been described.

Irisin is an exercise-inducable myokine, which is associated with glucose regulatory mechanisms in different organs and organ-crosstalk, including a direct action onto skeletal muscle by increasing glucose uptake and lipid metabolism while reducing glycogenolysis [187]. Metformin treatment results in irisin release from both mouse muscle and C2C12 cells with evidence for both an AMPK-independent and AMPK-dependent PGC1α regulated mechanisms [137, 253].

In summary, metformin might lead to increased glucose turnover by increasing glucose uptake and glucose consuming metabolic pathways in skeletal muscle. However, the *in vivo* data regarding the relevance of skeletal muscle for the hypoglycemic effect of metformin are insufficient and therefore the contribution of skeletal muscle remains speculative.

1.4 Role of metformin in hyperlactatemia and metabolic acidosis

Metformin is generally a well tolerated drug. But in some cases, patients suffer from so-called "metformin-associated lactic acidosis" as a life-threatening side effect, which is estimated to occur at a prevalence of 47 per 100 000 patients per year [234]. The risk of acidosis is increased when comorbidities such as liver failure, kidney disease or dehydration are present [127]. The clinical criteria for diagnosing the complication comprise blood lactate levels $\geq$ 5 mmol/L and pH < 7.35 [103].

From a pathophysiological perspective, it is important to differentiate between mechanisms that lead to the accumulation of lactate and those that cause acidification [204, 205]. Hyperlactatemia is caused by an imbalance between lactate production and clearance. Under basal conditions, muscle, adipose tissue and the brain are the main producers of lactate, while the liver, kidneys and heart are responsible for its clearance [235]. As an energy source, lactate is oxidized to pyruvate, which can either be used as a substrate for gluconeogenesis or converted to acetyl-CoA via the pyruvate dehydrogenase (PDH) complex as fuel for the TCA cycle to provide electrons for the respiratory chain [27]. Thus, any disturbance in these metabolic pathways could theoretically contribute to

the accumulation of lactate in blood. In addition, an impairment in the transporters relevant for the mitochondrial transport of lactate and pyruvate (VDACs, MCTs, MPCs [69]) can also negatively affect lactate clearance. A major source for cellular H^+ causing metabolic acidosis is ATP breakdown to ADP. Under normal conditions these protons are of relevance to preserve the proton gradient of the respiratory chain in order to maintain ATP production. In contrast, non-mitochondrial ATP production through glycolysis leads to a net production of H^+, a pathway that becomes more important when the ATP demand can no longer be covered by the respiratory chain. The final step of glycolysis, the reduction of pyruvate to lactate, acts as a buffer by consuming one H^+ per converted molecule. Thus, the risk of acidification exists in situations in which a high energy demand must be covered, the glycolysis rate is high and the buffering capacity of the lactate dehydrogenase (LDH) reaction is exhausted due to the accumulation of lactate. To prevent the latter, cytosolic lactate is released through monocarboxylate transporters (MCTs) into the circulation as symport with H^+, explaining the good correlation between blood lactate levels and pH. In conclusion, lactate production per se does not cause acidosis, but hyperlactatemia and metabolic acidosis often occur together. It is important to note that the association between metformin and increased lactate production is not fully understood, and further research is needed to clarify the relationship between metformin, hyperlactatemia, and metabolic acidosis.

Metformin-associated clinically relevant hyperlactatemia with plasma lactate levels between 7.6 and 28.1 mmol/L in most cases also show markedly elevated plasma metformin concentrations in a range of 30 to 660 µM [126]. While one case could be attributed to metformin overdose, many are related to reduced renal excretion highlighting the role of comorbidities as risk factor for developing hyperlactatemia and metabolic acidosis under metformin treatment. On the other hand, there is also evidence that metformin therapy can lead to slightly elevated plasma lactate levels that do not require clinical intervention [44, 190]. A community-based study demonstrated that plasma lactate levels are elevated by a mean of 0.28 mmol/L in patients with T2D under metformin therapy [44]. Huang et al. [90] conclude in their review that plasma lactate levels are at most slightly elevated in chronically metformin-treated otherwise healthy patients with T2D.

Regardless of the extent to which the increase in plasma lactate levels is pronounced by metformin *in vivo*, it raises the question of the underlying mechanisms. First, an association between a metformin-induced increase in the cellular lactate:pyruvate ratio or lactate production and the inhibition of mitochondrial respiratory chain complex I was demonstrated in different species, tissues and cell lines [28, 52, 180, 195]. Using human platelets, Piel et al. [189] provide not only evidence for increased lactate production through complex I inhibition but demonstrate also accompanying extracellular acidification. An increased lactate:pyruvate ratio in both liver and plasma is explained by inhibition of the redox shuttle enzyme mG3PDH in acutely or chronically metformin-treated rats [148]. The inhibitory effect of metformin on AMP deaminase is considered as another lactate producing pathway in L6 cells [179].

In conclusion, a few mechanisms have been already suggested to explain metformin-induced lactate accumulation. However, the role of skeletal muscle with its high capacity for lactate production is still unclear. In addition, most experimental studies do not consider differences between pharmacological and supra-pharmacological metformin doses, so that there are still substantial gaps in knowledge at the molecular level.

1.5 Lactate as mediator of beneficial metformin effects

The health-beneficial effects of metformin therapy extend beyond blood glucose control and include protective effects on the cardiovascular and renal system [78, 200], particularly important regarding diabetes-related complications. In the human body, lactate has three important functions:

- Lactate is a major source for oxidative energy production.

- Lactate is the major gluconeogenic precursor.
- Lactate is a signaling molecule mediating auto-, para-, and endocrine effects.

Based on this so-called lactate shuttle concept [26], Giaccari et al. [67] recently suggested that lactate might be a mediator of some of the pleiotropic effects of metformin. A renoprotective effect of metformin could be due to the fact that the increased production of lactate provides an additional energy source for the energy-intensive maintenance of renal function. Lactate is advantageous in comparison to glucose utilization in this respect as no potentially harmful waste products, like advanced glycation end products (AGEs), are produced [67]. In a similar manner, it is possible that metformin also has a positive effect on the heart and central nervous system providing increasingly lactate as an energy source [67]. With regard to lactate's signaling function, metformin has been shown to up-regulate the lactate receptor G-protein coupled receptor 81 (GPR81) in hepatocytes and to rescue obesity-induced suppression of the receptor [248].

This rather new hypothesis requires experimental investigations and is particularly interesting considering that metformin therapy causes a slight increase in human lactate plasma levels [44, 90].

1.6 Exercise in prevention and treatment of type 2 diabetes

Regular physical activity and exercise unquestionably promote health-beneficial effects and reduce all-cause mortality [125, 186, 259]. Several studies provide convincing evidence that regular exercising prevents or delays the onset of T2D [70, 112, 140]. Remission of T2D can also be achieved through lifestyle interventions, where regular physical activity is an integral part [150]. In general, patient benefit from increased insulin sensitivity of several tissues including skeletal muscle, adipose tissue, liver, and brain [10] and improved glycemic control reflected by a decrease in HbA1c by 0.4% to 0.6% [186]. In addition, risk factors for diabetes-related complications such as obesity, blood pressure and blood lipids are reduced. Taken together, exercise is a powerful tool in prevention and therapy of T2D reducing mortality and improving patient's quality of life. According to national guidelines [7, 55, 131], exercise is a key element in lifestyle intervention as part of the non-pharmacological basic therapy recommending to take 150 minutes of moderate-intensity exercise per week, evenly distributed over 3 days of the week. Ideally, a mixture of endurance and resistance training should be carried out.

1.7 The role of skeletal muscle in exercise adaptation processes

Skeletal muscle is a key player during physical activity with great importance for cellular, tissue-specific and whole-body adaptation processes to improve physical performance. This section highlights a few exercise-induced mechanisms in skeletal muscle, that may be responsible for the therapeutic effect of exercise in T2D, as well as potential points of interaction with metformin-induced mechanisms.

Maintaining muscle contraction during physical activity has tremendous consequences for skeletal muscle energy metabolism. Blood flow and glucose uptake are increased nearly 100-fold and both oxidative and glycolytic pathways get activated [201]. Already an acute bout of exercise results in increased insulin-independent glucose uptake and the effect persists up to 48 h into recovery [160, 168] being beneficial for blood glucose regulation even in a state of insulin resistance. Regular exercise training increases skeletal muscle insulin sensitivity in the longer term showing positive effects already after one week [111] while the contrary effect occurs as rapid in a period of detraining [239].

Several mechanisms are discussed to be involved in the exercise-induced increase of GLUT4 translocation thereby increasing glucose uptake [223]. The high demand of energy during exercise leads to the activation of the energy sensor AMPK, which seems to be a major inducer of GLUT4

translocation. Increased intracellular Ca^{2+} during muscle contraction can activate calmodulin and calmodulin-dependent protein kinases (CaMKs) dependent signaling allowing AMPK-independent GLUT4 translocation. In addition, exercise activates downstream targets of the insulin receptor, namely Akt, AS160, and TBC1D1 [154], which activates the Rag proteins required for GLUT4 translocation. In terms of exercise training, enhanced expression of GLUT4 and proteins of the insulin signaling cascade have been demonstrated [186, 201, 223]. The efficacy of glucose utilization is further improved by an increased expression of HK [186, 201] and the increase in mitochondrial volume and function [87, 159]. Moreover, improvements in glucose uptake and insulin sensitivity are associated with increased muscle mass [81, 222]. Induced by mechanical loading mechanistic target of rapamycin complex 1 (mTORC1) is a positive regulator of protein synthesis and is associated with muscle hypertrophy and increases in muscle mass [73]. Furthermore, mTORC1 signaling has been linked to the promotion of mitochondrial biogenesis [166] and changes in lipid metabolism [202].

1.8 Clinical studies on blunted exercise adaptation processes under metformin therapy

Exercise and metformin are both integral parts of the therapy of T2D and are therefore often used in combination [131]. Since both treatment options act on some identical molecular targets and modify similar mechanisms, the question raises whether they cross-react and can influence each other. Clinical studies, that have been performed to address this issue in both exercise training and acute exercise studies, are summarized in Table 2.

Some studies demonstrate that the exercise-induced improvements in cardiorespiratory fitness measured as peak oxygen uptake (VO_{2peak}) are blunted under metformin treatment [24, 152, 151, 165]. Further, the administration of metformin alone reduces VO_{2peak} in insulin-resistant subjects, an effect that is subsequently reversed through additional exercise training [33]. While there is evidence of reduced exercise capacity in the form of a lower respiratory exchange ratio (RER) and increased heart rate (HR) and rate of perceived exertion (RPE) [22, 24, 118] in healthy subjects as well as in metformin-treated patients, metformin treatment does not influence self-selected exercise intensity in a cohort of patients with T2D [192]. In contrast, some other studies do not observe an effect of metformin on the increase in HR during exercise [21, 176, 218].

In addition to fitness-associated parameters, effects on glucose homeostasis were studied. The combination of metformin and exercise shows no superior effect to exercise alone on glycemic control, measured as HbA1c, regardless of the varying exercise intensities used in the study by Boulé et al. [21]. Several studies report no additive effect of metformin on the exercise-induced improvement in whole-body insulin sensitivity [152, 176, 218, 241]. In contrast, Konopka et al. [114] observe an attenuated increase in whole-body insulin sensitivity in a cohort of overweight to obese subjects with metformin treatment. When investigating the effects on postprandial glucose regulation in patients with T2D, Boulé et al. [22] found that an acute bout of exercise attenuates the beneficial effect of metformin on glycemic control after a standardized meal. At the same time no interaction on the response in postprandial glucose was found in subjects with impaired glucose tolerance combining metformin with 12 weeks of exercise training [190].

Only a few studies go beyond the determination of clinical parameters and investigate molecular mechanisms. Kulkarni et al. [120] performed transcriptomic analysis of human muscle biopsies collected within the MASTERS trial [241] revealing a reduced number of differentially regulated genes associated with extracellular matrix (ECM) composition and remodeling when metformin is added to a 14-week resistance exercise intervention. The authors suggest a correlation with the attenuated gain in muscle mass and strength in response to resistance exercise in the metformin-treated group as described in the initial study [241]. In addition, they found increased phosphorylation of

AMPK and blunted ribosomal protein S6 (RPS6) activation in human myotubes after 8 h of electropulse stimulation (EPS) in the presence of 10 mM metformin, which might explain the impaired hypertrophic response to resistance exercise. These results are confirmed in muscle biopsies of the subjects receiving a standard metformin dose of 1 700 mg/day over the study period. Contrasting results are reported after performing an acute bout of exercise. In insulin resistant subjects, AMPK activation is blunted under metformin along with a stronger reduction in muscle glycogen [218], while AMPK activation is unaffected in healthy subjects [118]. A deeper investigation of human muscle biopsies collected within the acute exercise studies performed by Pilmark et al. [192, 190] found no impairment of exercise-induced AMPK activation and alterations in mitochondrial capacity and H_2O_2 emission by metformin treatment [191].

Taken together, the data on the interaction between metformin and exercise adaptation processes is ambiguous, not at least because the studies are poorly comparable in terms of subject characteristics and exercise modalities (Table 2). As some of the studies suggest a negative impact of metformin treatment on the improvement of physical fitness, glucose control and muscle performance, a more precise understanding of this cross-talk on a molecular level is necessary.

Table 2: Overview of clinical studies investigating interactions between metformin treatment and exercise adaptation processes. The table is based on manual review of human clinical studies that were found in the literature search in Pubmed with different combinations of the keywords "metformin", "exercise", "adaptation", "training", "interaction", "muscle", "skeletal muscle", "human", "diabetes", and "insulin resistance".

Subjects	**Study groups**	**Metformin dose [mg/day]**	**Exercise protocol**	**Major findings for combination of Ex + Metf**	**Ref.**
Exercise training					
n=251 (f+m) T2D 47–60 years BMI 26–39	Ex Ex+Metf	1 600*	aerobic (45 min, 70% HR_{max}) and/or resistance (max. weight for 7–9 rep.) partially supervised 22 weeks	beneficial effects of exercise on glycemic control or fitness unaffected by metformin	[21]
n=75 (f+m) IR 35–57 years BMI 25–34	Metf Ex Ex+Metf	1 000 12 weeks	aerobic (30–50 min, 60–80% HRR) supervised 12 weeks	no additive effect on VO_{2peak}; aerobic threshold only improved in Ex	[33]
n=43 (f+m) risk T2D 61–63 years BMI 29–32	Ex+Pla Ex+Metf	2 000 12 weeks	aerobic (15 min, 60% HR_{max}; 30 min, 65–85% HR_{max}) 12 weeks (3 d/w)	blunted increase in skeletal muscle mitochondrial respiration, whole-body insulin sensitivity and VO_{2peak}	[114]
n=32 (f+m) prediabetic 37–60 years BMI 31–34	Pla Metf Ex+Pla Ex+Metf	2 000 12 weeks	aerobic (45 min, 70% HR_{max}) + resistance (15–30 min, 70% 1-RP) supervised 12 weeks (3 d/w)	no additional effect on whole-body insulin sensitivity for combination of Ex + Metf	[152]

continued on next page

Table 2 – *continued from previous page*

Subjects	Study groups	Metformin dose [mg/day]	Exercise protocol	Major findings for combination of Ex + Metf	Ref.
n=16 (f+m) prediabetic 43–51 years BMI 30–35	Ex+Pla Ex+Metf	2 000 10 weeks	aerobic (45 min, 70% HR_{max}) + resistance (15–30 min, 70% 1-RP) supervised 10 weeks (3 d/w)	improvement in VO_{2peak} and fat oxidation unaffected	[151]
n=63 (f+m) metabolic syndrom 46–60 years BMI 28–37	Ex Ex+Metf	1 200*	HIIT (4x4 min, 90% HR_{max}, 3 min, 70% HR_{max} recovery between) supervised 16 weeks (3 d/w)	blunted increase in VO_{2peak}	[165]
n=29 (f+m) IGT 18–70 years BMI 25–42	Ex+Pla Ex+Metf	2 000 15 weeks	interval training (45 min, 55–65% W_{max}) supervised 12 weeks (4 d/w)	no additional effect on post-prandial glucose	[190]
n=36 (f+m) prediabetic 44–54 years obese	Pla Metf Ex+Pla Ex+Metf	2 000 12 weeks	aerobic (135 min, 65% VO_{2peak}) + resistance (45 min, 60–70% 1-RP) supervised 12 weeks (3 d/w)	lower proinsulin concentrations; increased insulin clearance	[238]
n=109 (f+m) healthy 64–91 years BMI 18–34	Ex+Pla Ex+Metf	1 700 14 weeks	resistance (8–12 rep. at 10–RP) supervised 12 weeks (3 d/w)	blunted gains in muscle mass, density and strength; attenuated the shift in fiber type composition toward type 2; increased phosphorylation of AMPK and ACC; reduced RPS6 phosphorylation	[241]
Acute exercise					
n=10 (f+m) T2D 52–64 years BMI 23–33	cross-over Pla Metf Ex+Pla Ex+Metf	2 000 4 weeks	20 leg extensions and flexions 15 min walking, 3.5 km/h 15 min walking <VT 5 min walking >VT	lower RER independent of exercise intensity; increased submaximal HR and lactate concentrations; reduced hypoglycemic effect after exercise	[22]
n=17 (f+m) T2D 24–31 years BMI 21–29	cross-over Ex+Pla Ex+Metf	2 000 7–9 days	incremental treadmill/bicycle test max. 15 min	reduced VO_{2peak}, duration, HR_{max}, VE_{max}, and RER_{max}	[24]

continued on next page

Table 2 – *continued from previous page*

Subjects	Study groups	Metformin dose [mg/day]	Exercise protocol	Major findings for combination of Ex + Metf	Ref.
n=19 (m) healthy 23–25 years BMI 22–25	cross-over Ex+Pla Ex+Metf	acute: 2x 1 500 mg within 2 h short-term: 1 000–2 000 mg for 6 days + 2x 1 500 mg within 2 h acutely	one-legged knee extension (40 min, 80% PWL)	increased perceived exertion and whole-body stress (adrenaline, HR, RPE); no impact on AMPK activation and energy homeostasis	[118]
n=10 (m) healthy, active 20–26 years body fat 11–17%	cross-over Ex+Pla Ex+Metf	500 mg single dose	high intensity test (110% W_{max})	improved performance; no effect on overall anaerobic capacity	[134]
n=10 (f+m) IR 50–55 years BMI 32–38	Ex Metf Ex+Metf	1 100–1 500*	high intensity test 43 min (4x4 min, 90% HR_{peak}; active rest between 70% HR_{peak})	acute insulin-sensitizing effects of a single bout of exercise was not blunted	[176]
n=15 (m) healthy 22–24 years BMI 20–24	cross-over Ex+Pla Ex+Metf	2 000 17 days	45 min aerobic (1x self-selected intensity; 1x 70% VO_{2peak})	increased RPE during fixed intensity exercise bout no impact on self-selected intensity	[192]
n=16 (f+m) IR 23–41 years BMI 26–35	Metf Ex+Metf	2 000 2–3 weeks	aerobic (30 min, 60% VO_{2peak} + 30 min, 65–85% VO_{2peak})	no additive effect on whole-body insulin sensitivity; less AMPK activity	[218]

* average concentration of habitual dose of metformin taken by the patients; 1-RP: one repetition maximum; 10-RP: ten repetition maximum; d/w: days/week; Ex: exercise; f: female; HIIT: high-intensity interval training; HR_{max}: maximal heart rate; HRR: heart rate reserve; IGT: impaired glucose tolerance; IR: insulin resistance; m: male; Metf: metformin; Pla: placebo; PWL: peak work load; RER: respiratory exchange ratio; RPE: rate of perceived exertion; VE_{max}: maximal ventilation; VO_{2peak}: peak oxygen uptake; VT: ventilatory threshold; W_{max}: maximal watt

CHAPTER 2

Aim of the Thesis

Metformin is the first-line oral antidiabetic drug in the treatment of T2D. More than 150 million people worldwide benefit from its efficient glucose lowering effect while keeping the risk for hypoglycemia low. Nonetheless, the exact mechanism of action is still incompletely understood. Organs such as the liver and intestine have been intensively studied in recent decades and reduced hepatic gluconeogenesis is widely accepted as the major mechanism of the blood glucose lowering effect. Although skeletal muscle accounts for up to 40% of the total body mass and plays a central role in insulin-dependent glucose uptake, it has been the subject of comparatively few studies on the mechanisms of action of metformin. This thesis therefore contributes in general to the understanding of metformin effects on human skeletal muscle. In more detail, the project was divided into two parts centering around two more specific questions (Fig. 3):

1. What are the molecular mechanisms by which metformin can induce lactate production in skeletal muscle?

2. Which molecular mechanisms in skeletal muscle can provide an explanation for attenuated health-beneficial adaptations to exercise during metformin therapy?

The first question was raised on the basis, that in rare cases a life-threatening side effect of metabolic acidosis caused by metformin-mediated increased glycolysis and lactate production can occur. In addition, there are reports of slightly elevated plasma lactate levels in a physiological range in patients receiving metformin treatment, which opens the perspective that some of the effects of metformin are mediated via the lactate receptor GPR81 and lactate as alternative energy substrate. The source of the increasing lactate in plasma may originate in the skeletal muscle, which has a high capacity to produce lactate. In order to identify molecular mechanisms that could explain an increase in glycolysis and lactate production, metformin-treated primary human myotubes were investigated. Since the metformin concentrations used for *in vitro* experiments are often well above the pharmacologically achievable concentrations in humans, the dose dependence of the effects was investigated and intracellular concentrations were measured. In addition, plasma lactate levels under metformin were investigated in blood samples from a previous human intervention study and parts of the mechanisms identified *in vitro* were validated in the respective muscle biopsies.

The second question is based on clinical observations reporting of impaired improvement in glucose control, muscle performance and fitness under metformin therapy. As an elementary part of lifestyle intervention as a basic therapy in T2D, exercise is commonly used as a therapeutic option in combination with metformin treatment. As the mechanisms of action overlap to some extent, interactions are likely with potential consequences for the health-promoting effects of exercise. However, mechanistic investigations are limited. In order to investigate contraction-dependent mechanisms, electro-pulse stimulation was applied as *in vitro* exercise model. Further, interactions with the hypertrophic response to mainly resistance exercise was addressed with the focus on mTOR signaling. Again, dose dependency of the effects was investigated.

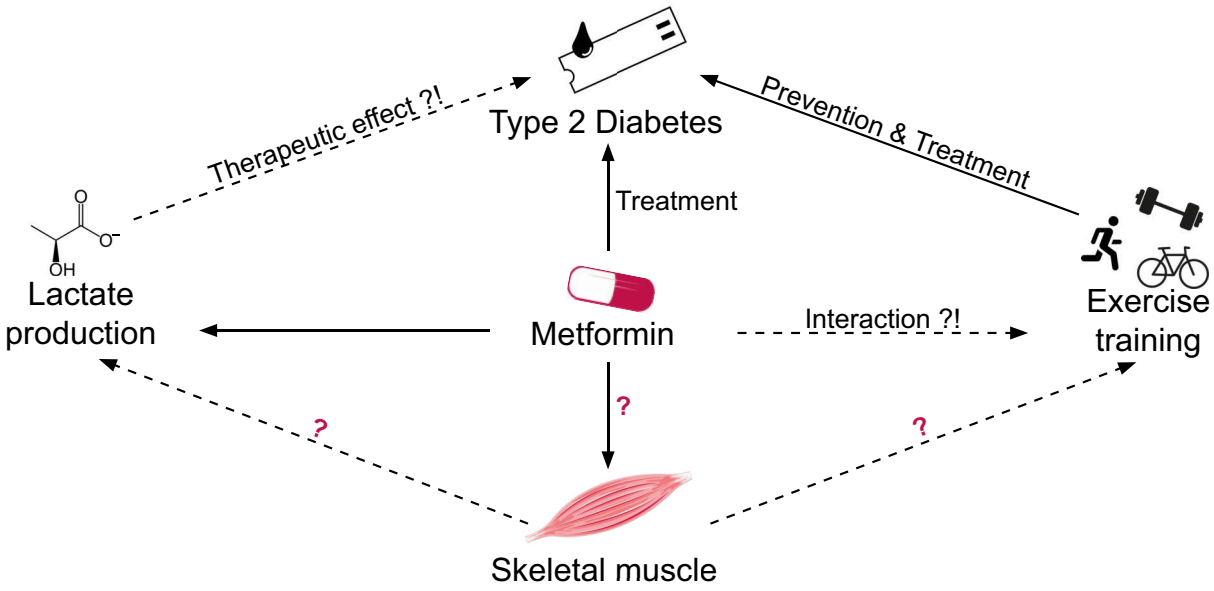

Figure 3: Overview of the project.
The project is divided into two parts and centers around gaining a deeper understanding of metformin effects on human skeletal muscle in the treatment of T2D. The first part addresses the question whether skeletal muscle contributes to the increase in metformin-induced lactate production. The second part investigates interactions between metformin treatment and exercise adaptation processes in skeletal muscle. Most of the experiments were carried out on primary human myotubes, while human biopsies were also used for the investigation of the first question.

CHAPTER 3

Method Descriptions and Materials

3.1 Collection of human skeletal muscle biopsies

3.1.1 Skeletal muscle biopsies for the enrichment of myoblasts

Human muscle biopsies from vastus lateralis were collected as part of a recently published study [87] and an aliquot was used for the isolation of satellite cells and subsequent enrichment of primary myoblasts. The study was registered at Clinicaltrials.gov as trial number *NCT03151590*. All participants gave written informed consent. The study protocol was approved by the ethics committee of the University of Tübingen and was in accordance with the declaration of Helsinki.

For *in vitro* experiments within this work, muscle cells of a total of 27 donors were available. All samples used were collected at the pre-intervention time point and are therefore unaffected by the study intervention itself. Baseline characteristics of all participants are summarized in Table S1.

3.1.2 Skeletal muscle biopsies for *in vivo* studies

Human muscle biopsies from vastus lateralis were collected as part of the study reported in [192]. In a crossover design, 15 healthy young men underwent two treatment periods of 17 day receiving either placebo or metformin (gradually increased over 8 days to a maximum of 2 000 mg per day). Both treatment periods were separated by a 4 day washout phase. At the last day of each treatment period, the subjects underwent an acute bout of exercise (45 min of cycling at 70% VO_2peak) and muscle biopsies were collected before and immediately afterward. Clinical data on the subjects is provided in Table S2. Blood lactate levels were analyzed during the study. Protein lysates of the biopsies were prepared and the immunoblots were performed as described in [80, 192]. Analysis of the proteins reported in the thesis was performed together with Anders Gudiksen in the laboratory of Henriette Pilegaard (Copenhagen, Denmark).

3.2 Myoblast enrichment

3.2.1 Magnetic cell separation

The protocol for myoblast enrichment was adapted based on manufacturer's standard protocol for magnetic cell separation (MACS). Myoblasts passage 0 (P0) were grown on eight 15 cm dishes per donor refreshing cloning medium twice a week until 50% confluence was reached (finally approximately 10–20 million cells). Cells were trypsinated (4 mL trypsin, 5 min) and detachment was stopped by adding 8 mL of pre-warmed cloning medium. Cells from four dishes were pooled and centrifuged at 200g for 4 min. The pellet was carefully resuspended in 1 mL MACS buffer and passed through a 70 µm strainer pooling cells from the same donor. 250 µL was separated as fraction *V* for fluorescence-activated cell sorting (FACS) and the number of cells was counted in 10 µL using a Neubauer chamber. The remaining cell suspension was centrifuged at 200g for 10 min at 4°C. The pellet was resuspended in 120 µL MACS buffer and incubated for 30 min with 30 µL CD56 MicroBeads per 10^7 cells with brief mixing every 10 min. 3 mL MACS buffer was added followed by another centrifugation step at 200g for 10 min at 4°C. The pellet was resuspended in 500 µL MACS buffer, passed through magnet-attached LS columns preconditioned with 5 mL MACS buffer and rinsed with 4 mL MACS buffer. 250 µL of the flow-through was separated as fraction *D* for FACS and the number of cells was counted in 10 µL. The columns were rinsed twice using 3 mL MACS buffer

and the flow-through was discarded. Columns were detached from the magnet and rinsed with 5 mL MACS buffer. 250 µL of the flow-through was separated as fraction *E* for FACS and the number of cells was counted in 10 µL. The remaining cell suspension was centrifuged at 200g for 10 min at 4°C. The pellet was resuspended in cryo medium achieving 500 000 to 1 000 000 cells/mL and frozen 1 mL/cryo tube at -80°C within a freezing container as cells of passage 1 (P1). Afterwards, cells were stored in liquid nitrogen.

3.2.2 Fluorescence-activated cell sorting

FACS was used to check the quality of the MACS process by staining for CD56 as marker for myoblasts and isotype control. 2 mL FACS buffer was added to each of the fractions *V*, *D* and *E* separated during the MACS process. Each fraction was divided into two equal parts containing approximately $1.5 - 2.5 * 10^5$ cells. All samples were washed twice with 500 µL FACS buffer by centrifugation steps (160g, 3 min, 4°C). One part of each fraction was incubated with 100 µL dilution of either CD56 or isotype control antibody for 90–180 min as described in Table 17. 500 µL FACS buffer was added, centrifuged at 160g for 3 min at 4°C, and repeated twice for washing. The pellet was resuspended in 250 µL FACS buffer, 5 000 to 10 000 cells were analyzed using a FACSCalibur flow cytometer and data was evaluated by Flowing Software. An exemplary analysis of data is provided in Figure 4.

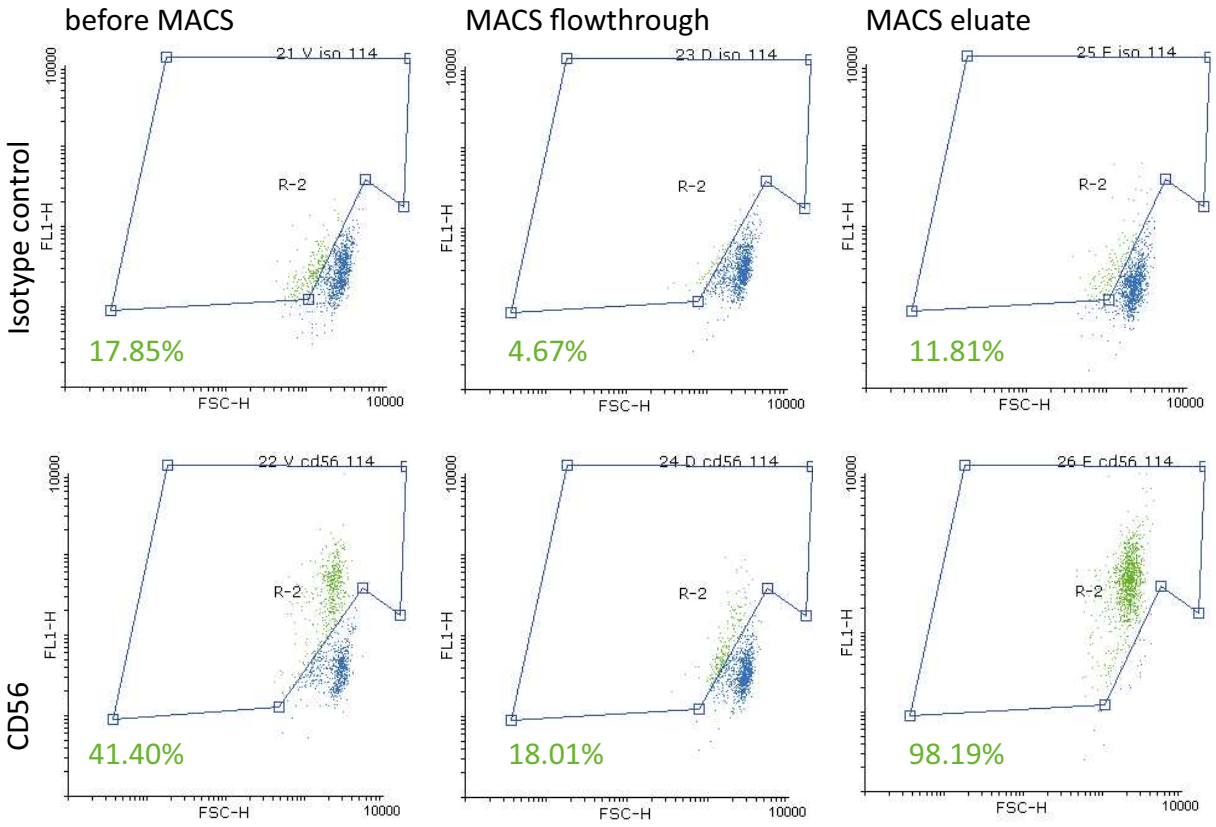

Figure 4: Myoblast enrichment by magnetic cell sorting.
Representative FACS analysis of cell fractions from purification by MACS. The left column shows results before purification (fraction *V*), the middle column shows the flowthrough containing mainly $CD56^-$ fibroblasts (fraction *D*) and the right column shows the eluate containing $CD56^+$ myoblasts (fraction *E*). In the upper row cells were incubated with isotype control antibody while in lower row cells were incubated with antibody against CD56. The percentage value indicates the proportion of $CD56^+$ cells in gate R-2.

3.3 Cell culture protocols

3.3.1 Surface coating

Surface coating was used in dependence of the readout of interest. An overview is provided in Table 3.

Table 3: Overview of cell culture conditions for the experimental readouts.
Type of surface pre-coating, used cell culture plates/dish and number of cells seeded per well/dish in dependence of the readout chosen.

Method / Readout	**Coating**	**Plate (Manufacture)**	**Number of seeded cells**
Capillary electrophoresis	GelTrex	Tissue Culture plate, 6-well (Falcon)	15 000
EPS	GelTrex	Tissue Culture plate, 6-well (Falcon)	15 000
Glucose uptake assay	no	Cell culture plate, 24-well (TPP)	5 000
Immuno blotting	GelTrex	Cell culture plate, 6-well (TPP)	10 000–15 000
Immunohistochemistry	PLL + GelTrex	2-well cell culture slide (Sarstedt)	10 000
LC-MS	GelTrex	Cell culture dish Ø 87 mm (TPP)	100 000
MACS	no	Cell culture dish Ø 137 mm (TPP)	–
NAD^+/NADH Assay	GelTrex	Cell culture plate, 6-well (TPP)	15 000
Oroboros	GelTrex	Cell culture dish Ø 137 mm (TPP)	150 000
RNAsequencing	GelTrex	Cell culture plate, 6-well (TPP)	10 000
Seahorse	no	Seahorse XF24 cell culture microplates (Agilent)	20 000

GelTrex thin layer coating

GelTrex coating was carried out based on manufacturer's protocol for thin layer coating. In brief, GelTrex™ Matrix solution was diluted 1:300 in a 1:1 pre-chilled (4°C) mixture of αMEM:Ham's F-12. Sufficient amount of the dilution to cover the entire growth surface was added, which means 1 mL for 6-well plates, 3 mL for Ø 87 mm dishes and 8 mL for Ø 137 mm dishes. Plates were incubated for 1 h at 37°C followed by another incubation for 1 h at room temperature (RT). The supernatant was removed and cells were seeded immediately.

Poly-L-lysine coating

Poly-L-lysine (PLL) coating was applied for readouts requiring cell culture on slides as an additional pre-coating underneath the GelTrex layer. 5 mg PLL were diluted in 50 mL of sterile water. 1 mL/25 cm^2 of the dilution were used to cover the entire growth surface. After 5 min incubation at RT the remaining supernatant was removed and the surface dried at RT for at least 30 min. The GelTrex layer was applied on top as described in section 3.3.1.

3.3.2 Cultivation of primary human myotubes

Primary human myoblasts (P1) were seeded dependent on the readout as described in Table 3. Myoblast were grown at 37°C, 5% CO_2 in cloning medium until 80% confluence was reached, followed by a change to differentiation medium in order to initiate differentiation at day 0 of differentiation (D0). During the whole time of culturing, medium was refreshed every second to third day. Metformin treatment was performed 48 h before harvest. A 7.8 mM stock solution was prepared by

dissolving 12.85 mg metformin hydrochloride in 10 mL differentiation medium and followed by sterile filtration. The stock solution was diluted with differentiation medium resulting in final concentrations of 16 µM, 39 µM, 78 µM, 338 µM and 776 µM. Culture medium was refreshed using the indicated metformin dilutions. Figure 5 illustrates the two different protocol used within the study, which vary in the composition of the differentiation medium and the duration of the differentiation phase.

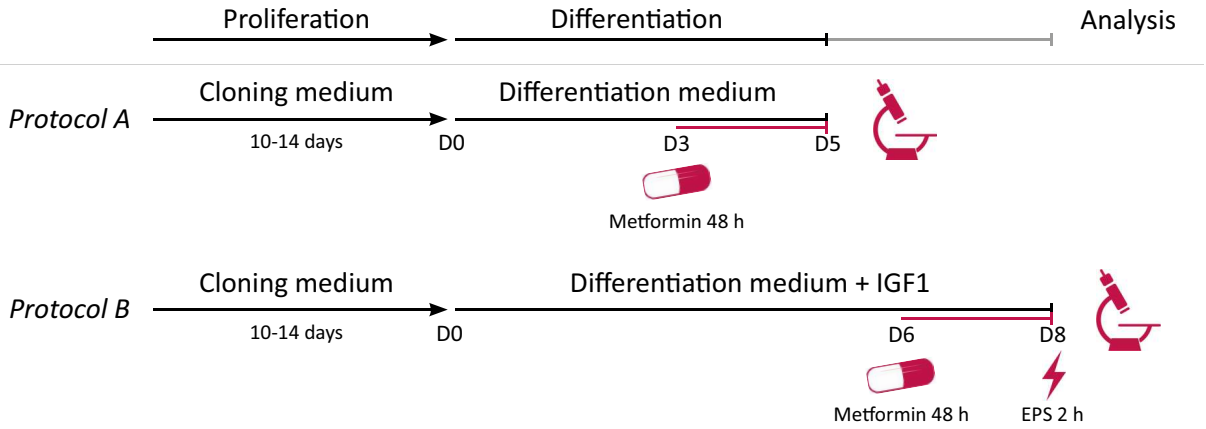

Figure 5: Cell culture protocols for investigation of metformin effects on primary human myotubes. Primary human myotubes were cultured following two different protocols depending on the readout of interest. Both protocols start with a proliferation phase of 10–14 days. *Protocol A* was used to address the question of how metformin enhances lactate production in skeletal muscle and for RNA sequencing analysis. In these cases metformin treatment was performed on day 3 of differentiation (D3) and cells were harvested for analysis at day 5 of differentiation (D5). *Protocol B* was chosen for the second part of the study aiming to investigate metformin effects on exercise adaptation processes. To allow visible contraction under EPS differentiation medium was supplemented with 100 ng/mL IGF1 and differentiation phase was prolonged until day 8 of differentiation (D8). Metformin treatment was again performed 48 h before harvest (D6). For questions in the context of contractility which were investigated without the application of EPS, *protocol B* was selected as well.

3.3.3 Electro-pulse-stimulation as *in vitro* exercise model

EPS was applied as *in vitro* exercise model. Based on the work of Dreher et al. [47], myotubes were cultured according to *protocol B* and stimulation (14 V, 1 Hz, 10 ms) was carried out at D8 for the last 2 h of the 48 h metformin treatment period (Fig. 5). As control, electrodes were installed onto the plate but not connected. 2 h before inserting all electrodes, the medium was refreshed by 3 mL fusion medium. Three videos of 10 s per condition were recorded at x10 magnification on randomly chosen areas of the plate 10 min after starting the stimulation as well as after 1 h and 2 h of stimulation. OpenHeartWare [215, 91] was used for motion analysis, which is based on an optical block-matching algorithm. The calculated area under the curve (AUC) was normalized by the theoretical amount of beats during 10 s.

3.4 Analysis of cell culture supernatant

Immediately before harvesting the cells, the supernatant for each experimental condition was collected and centrifuged at 14 000g for 10 min. The pellet was discarded. 500 µL of the supernatant was used for the determination of glucose and lactate concentrations at the routine site using enzymatic methods (lactate: lactate oxidase; glucose: hexokinase). Since the fusion medium does not contain lactate, the amount of lactate measured corresponds to cellular lactate secretion. To calculate cellular glucose consumption, the amount of glucose detected in the supernatant was subtracted from the glucose concentration of the fusion medium (5.5 mM glucose) given by the

manufacturer. In addition, creatine kinase (CK) and lactate dehydrogenase (LDH) were determined to rule out leakage of lactate caused by cellular damage through the metformin treatment. Both analytes were analyzed by routine methods (CK: modified kinetic method of Szasz; LDH: kinetic enzymatic-based method).

3.5 *In vivo* glucose uptake assay

Cells were cultured until D5 following *protocol A* to determine the cellular glucose uptake using the Glucose Uptake-Glo™ assay and the provided protocol. In brief, metformin was present for a total of 48 h including the 3 h fasting period in glucose-free DMEM media. Incubation with 100 nM insulin was performed for 1 h at 37°C followed by 1 h incubation at RT after the addition of 10 mM 2-deoxyglucose (2-DG). Luminescence was finally measured using the GloMax® Multi Detection System after 1 h incubation at RT with the provided detection reagent. Relative light units (RLUs) were normalized for myotubes derived for the same subject.

3.6 Determination of intracellular metformin concentrations by LC-MS

The quantification of metformin in cell lysates by liquid chromatography-mass spectrometry (LC-MS) was performed at the laboratory of Prof. Guowang Xu (DICP, Dalian, China). The cell lysates were prepared on D5 of cells cultured according to *protocol A*. Cells were washed on ice twice using 5 mL pre-chilled physiological NaCl. 1 mL of cold acetonitril (80%) containing a final concentration of 2 ng metformin-(dimethyl-d6) hydrochloride as internal standard was added and cells were scraped. The received lysate was placed in the TissueLyser for 2 min at 20 Hz and was divided in two equal parts of 450 µL followed by centrifugation for 15 min at 13 000g at 4°C. Both the supernatant and pellet were vacuum dried overnight (20 mbar, 1 500 rpm) for the determination of metformin concentration by LC-MS and total protein content, respectively.

The dried supernatant was dissolved in 50 µL 10% ACN/H_2O. For the quantification of metformin, 0.1 µL was injected in a Shimadzu LCMS-8050 mass spectrometer. The separation was performed on a 5 cm x 2.1 mm Discovery® HS F5 3 µm column. The mobile phase consisted of 0.1% formic acid in H_2O (A) and 0.1% formic acid in ACN (B). The gradient elution was changed from 10% eluent B to 98% eluent B within the first 2 min, then kept for 2 min, and finally returned back to 10% eluent B for another 2 min. Flow rate was set to 0.3 mL/min and the column temperature was kept at 50°C. The limit of detection was 1.4 ng/mL metformin.

The dried pellet was resuspended in 1 mL protein solubilization buffer by placing it into the TissueLyser for 2 min at 30 Hz. After 1:5 dilution with buffer the total protein concentration was determined in duplicates by bradford assay as described in section 3.8.2.

3.7 Analysis on transcript level

The transcriptional data presented within the thesis relies on the RNA sequencing analysis. The application of quantitative real time polymerase chain reaction (qRT-PCR) was used for the collection of data presented as supplementary material and is indicated.

3.7.1 RNA isolation

Isolation of total RNA was carried out using the RNeasy Mini Kit based on the manufacture's protocol. All centrifugation steps were carried out at 15 000g at RT. On the day of harvest, cells were washed with 1 mL cold DPBS and 350 µL RLT buffer was added. The obtained cell lysate was pulled through a QIAshredder spin column by centrifugation for 2 min. The eluate was mixed with 350 µL of 70% (v/v) EtOH, transferred immediately onto a RNeasy spin column and centrifuged

for 20 s. The flowthrough was discarded. 350 µL RW1 buffer was added and centrifuged for 20 s. After discarding the flowthrough, 80 µL DNase dilution (DNase Stock:RDD 1:7) was added onto the column membrane and incubated for 15 min at RT. Again 350 µL RW1 buffer was added and centrifuged for 20 s. The flowthrough was discarded. Two steps of washing were carried out with each 500 µL RPE buffer and centrifugation for 2 min. Total RNA was eluted into a clean collection tube by adding 30 µL RNAse-free H_2O directly onto the column membrane and centrifugation for 1 min. The eluate was once again pipetted onto the column membrane and centrifugation was repeated. The RNA concentration and quality of the eluate were investigated by NanoDrop2000. Isolated RNA was stored at -80°C.

3.7.2 cDNA transcription

For the reverse transcription of RNA into cDNA the Roche Transcriptor First Strand cDNA Synthesis Kit was used. Depending on the yield of RNA isolation 250 or 500 ng of total RNA was transcribed, keeping the amount constant in each series of experiments. According to manufactures protocol, RNA was diluted in 10 µL RNase-free H_2O and denaturated by heating at 65°C for 10 min using the Mastercycler. Next, 10 µL of reverse transcription mastermix (Table 4) was added. The Mastercycler program was continued with the following steps: 25°C for 10 min, 55°C for 30 min and 85°C for 5 min. Finally, cDNA was diluted 1:5 with RNase-free H_2O and stored at -20°C.

Table 4: Composition of reverse transcription mastermix.

Component	Stock concentration	Volume per reaction
Random hexamer primer	600 µM	2 µL
RT reaction buffer	5x conc.	4 µL
Deoxynucleotide mix	10 mM each	2 µL
Anchored-oligo$(dT)_{18}$ primer	50 µM	1 µL
RNase inhibitor	40 U/µL	0.5 µL
Reverse transcriptase	20 U/µL	0.5 µL

3.7.3 Quantitative real time polymerase chain reaction

The qRT-PCR was carried out using the QuantiFast SYBR® Green RT-PCR Kit and the Lightcycler480. 5 µL diluted cDNA was used in a 20 µL qRT-PCR reaction on 96-well microplates. 15 µL PCR mastermix (Table 5) was added. After centrifugation (1 000g, 1 min) of the covered microplate, the qRT-PCR program was started by a 5 min denaturating phase at 95°C. Following, 40 cycling steps of denaturating, annealing and elongation were performed by heating at 95°C for 10 s and 62°C for 30 s. The program was finished by completely denaturating RNA through heating at 95°C for 10 s, 62°C for 5 s and continuous heating up to 98°C with 0.11°C/s and cooling down to 40°C with 2.2°C/s. A standard curve was used for quantification. Therefore, PCR standards were created for each primer by purifying PCR-product with the MinElute PCR Purification Kit. The quality of the PCR product was proven by running 10 µL of the eluate on a 2% agarose gel. Standards were diluted on the day of experiment from a 5 ng/µL stock solution in a 10-fold serial dilution series ranging from 5 pg/µL to 0.5 ag/µL. The acquired data was analyzed with the Lightcycler480 software. An overview of QuantiTect primers used within the study is provided in Table 18.

Table 5: Composition of PCR mastermix.

Component	Stock concentration	Volume per reaction
QuantiFast SYBR Green RT-PCR mastermix	2x	10 µL
QuantiTect primer	10 µM	2 µL
RNase free H_2O	–	3 µL

3.7.4 RNA integrity number

The RNA integrity number (RIN) was required as part of quality control for RNA samples before RNA sequencing analysis using the Agilent RNA 6000 Nano kit. The chip was prepared following manufactures protocol. In brief, 9 µL gel-dye mix and 5 µL RNA ladder were loaded before adding 1 µL RNA sample. The chip was measured on an Agilent 2100 Bioanalyzer and the data was analyzed by Agilent 2100 expert software. The RIN number limit for RNA sequencing was ≥ 7.

3.7.5 RNA sequencing of myotubes

Commercial RNA sequencing was conducted by BGI Tech Solutions and the initial data analysis was performed by Martin Irmler (Helmholtz Munich). A total amount of 300 ng was used and the DNBSEQ Eucaryotic STand-specific Transcriptome Resequencing protocol was applied, resulting in cleaned, adapter-free paired-end data. Reads were aligned to the GRCh38.103 genome (STAR v.2.7.9a) and gene-level read counts were obtained (summarizeOverlaps, mode = 'Union', package GenomicAlignment v.1.30.0). Annotation of Ensemble gene IDs was performed based on the Ensemble database by Biomart (genome version GRCh38.p13). RNA sequencing data have been published at the GEO database at NCBI (GSE229658). No outliers were detected by principle component analysis (Fig. S1). A summary of clinical parameters of subjects donating muscle biopsies used for RNA sequencing analysis is provided in Table S3.

3.7.6 Transcriptomic analysis of muscle tissue

Transcriptomic analysis of human skeletal muscle was performed as part of a recently published study [87]. A methodical description of microarray analysis can be found in [48]. Array data were submitted to the GEO database at NCBI (GSE208032, GSE161750, GSE161749).

3.8 Analysis on protein level

3.8.1 Preparation of protein lysates

For the preparation of cell lysates two wells of fused myotubes (*protocol A*) were pooled in order to receive sufficient amount of protein for further analysis. Using *protocol B* cells of one well were sufficient. At the day of harvest cells were washed with 1 mL cold DPBS followed by the addition of 75 µL RIPA buffer containing both protease and phosphatase inhibitors. Cells were frozen at -80°C for at least 24 h before further processing. After thawing cells on ice, cells were scraped, pooled if required and centrifuged at 15 000g for 15 min at 4°C. The amount of total protein was determined in the supernatant as described in section 3.8.2, while the pellet was discarded. Protein lysates were stored at -80°C.

3.8.2 Determination of total protein content

Total protein content was determined in technical duplicates in a 96-well format. Bicinchonic acid (BCA) assay was first-choice method for the determination of total protein content. The bradford assay was used as indicated whenever BCA assay was inappropriate due to interference with assay material.

BCA assay

Pierce™ BCA protein assay kit was used according to manufacturers protocol. The provided BSA stock (2 mg/mL) was diluted step wise with water for the standard calibration curve (2 mg/mL, 1 mg/mL, 0.5 mg/mL, 0.25 mg/mL, 0.125 mg/mL, 0.063 mg/mL and 0.031 mg/mL). 10 µL of each standard sample was diluted by 10 µL RIPA buffer. 10 µL sample (*protocol A*) or 5 µL sample (*protocol B*) was diluted by H_2O resulting in a final reaction volume of 20 µL. After addition of 200 µL detection reagent, the plate was incubated for 30 min at 37°C. Finally, absorption at 540 nm was measured using the iMark microplate reader.

Bradford assay

Bradford reagent was diluted 1:5 with H_2O and filtrated through a MN 615 filter. The standard calibration curve starting with 0.5 mg/mL as highest concentration was generated similar to BCA assay except that protein solubilization buffer was used for the final dilution of the standard samples. 5 µL of sample material was diluted by 15 µL H_2O. After addition of 200 µL bradford reagent, the plate was incubated for 5 min at RT. Finally, absorption at 595 nm was measured using the iMark microplate reader.

3.8.3 Immuno blotting

For analysis of cell lysates 40 µL sample per lane was prepared containing 12–15 µg of protein. To that end sufficient amount of protein lysate was heated in Laemmli sample buffer for 5 min at 95°C or 50°C in case of the detection of mitochondrial proteins. Samples and 3 µL of Liqor Chameleon® Duo ladder were loaded on sodium dodecyl sulfate polyacrylamide gel (fix: 12.5%; gradient: 15–5%, see Table 6) for electrophoresis (150 V) followed by semidry electroblotting on MeOH-activated PVDF membranes (0.8 mA/cm^2). The efficiency of protein transfer was controlled by Ponceau S solution. The membrane was blocked in Net-G buffer for 10 min at RT. Primary antibodies were incubated at 4°C over night. After 3 steps of 10 min washing with TBS-T buffer, fluorescence-labeled secondary antibodies were incubated for 2 h at RT. Following further washing steps of 2x 5 min TBS-T buffer and 2x 5 min TBS buffer were performed. Odyssey scanner was used for the detection and the collected data was analyzed using ImageLab software. Detailed information on the antibodies used is provided in Table 17.

Immuno blotting of muscle tissue was performed in the laboratory of Henriette Pilegaard (Copenhagen, Denmark) according to the description in [156].

Table 6: Composition of electrophoresis gels.

Gradient gel 15–5%			
Component	**Separation gel 15%**	**Separation gel 5%**	**Stacking gel 3%**
H_2O	1.37 mL	5.7 mL	3.18 mL
Separation gel buffer	2.5 mL	2.5 mL	–
Stacking gel buffer	–	–	1.25 mL
Glycerol	1.0 mL	–	–
Acrylamide	5.0 mL	1.67 mL	0.5 mL
Temed	17 µL	17 µL	8 µL
APS	67 µL	67 µL	33 µL
Fixed gel 12.5%			
Component	**Separation gel 12.5%**	**Stacking gel 5%**	
H_2O	6.4 mL	2.85 mL	
Separation gel buffer	5.0 mL	–	
Stacking gel buffer	–	1.25 mL	
Acrylamide	8.33 mL	0.8 mL	
Temed	33 µL	8 µL	
APS	133 µL	33 µL	

3.9 Analysis of mitochondrial respiration and cellular redox state

Substrate stock solutions were prepared and stored at -20°C in aliquots, while dilutions were prepared freshly on the day of the experiment.

3.9.1 Seahorse system

The Seahorse system was used to determine respiratory states (*protocol A*, D5) and ATP production rate (*protocol B*, D8). The assays were performed based on manufactures protocols for Seahorse XF Cell Mito Stress Test and Seahorse XF Real-Time ATP Rate Assay. Cells were washed twice using 900 µL and 400 µL freshly prepared, pre-warmed (37°C) seahorse assay medium (SA medium) and a final volume of 500 µL SA medium was added to each well. After performing the calibration of the Seahorse XFe24 Analyzer, the assay was started using the substrates listed in Table 7. When finished, SA medium was removed and 50 µL RIPA buffer was added to each well before freezing the plate at -20°C for at least 24 h. 10 µL of the lysate was used for the determination of total protein content by BCA assay in duplicates for normalization.

Table 7: Substrates loaded into the assay plate ports for the Seahorse XF Cell Mito Stress Test and the Seahorse XF Real-Time ATP Rate Assay.

Port	Substrate	Concentration of stock solution [mM]	Solvent of stock solution	Concentration in port [µM]	Final concentration in well [µM]
Seahorse XF Cell Mito Stress Test					
A	Oligomycin	5	DMSO	10	1
B	FCCP	1	DMSO	20	2
C	Rotenone	1	EtOH	5	0.5
C	Antimycin A	5	EtOH	5	0.5
Seahorse XF Real-Time ATP Rate Assay					
A	Oligomycin	5	DMSO	10	1
B	Rotenone	1	EtOH	5	0.5
B	Antimycin A	5	EtOH	5	0.5

3.9.2 Oroboros system

Respiratory measurements using the Oroboros system were performed on D5 of cells cultured following *protocol A*. Cells were washed twice with 10 mL DPBS. 1 mL of Mir05 buffer was added and following the cells were kept on ice. Cells were carefully scraped and collected in an Eppendorf tube. The cell suspension from each dish was divided into two equal samples for duplicate measurement. 100 µL of each duplicate were separated for determination of protein content by BCA assay for normalization of O_2 flux. Remaining 400 µL of the samples were pelleted (13 000g, 5 min, 4°C) and supernatant was removed. The pellet was resuspended in 100 µL Mir05 buffer and was injected into the measurement chamber of an Oxygraph-2k, which has been pre-equilibrated with 2 mL Mir05 at 37°C. After forming a plateau, 3 µL digitonin was injected for cell permeabilization. In the following, stepwise injection of the substrates as listed in Table 8 was performed always waiting for a plateau in between. Reoxygenation was performed before O_2 < 120 µmol, which occurred usually during FCCP titration.

Table 8: Substrates injected during Oroboros measurement.

Order	Substrate	Concentration of stock solution [mM]	Solvent of stock solution	Injected volume [µL]	Final concentration in chamber [mM]
0	Digitionin	8.1	DMSO	3	0.012
1	Malate	800	H_2O	3.2	1.28
2	ADP	500	H_2O	10	2.5
3	Octanoylcarnitine	100	H_2O	10	0.5
4	Pyruvate	1 000	H_2O	10	5
5	Glutamate	2 000	H_2O	10	10
6	Succinate	1 000	H_2O	20	10
7	Cytochrome C	4	H_2O	5	0.01
8	FCCP	1	DMSO	steps of 1	0.001
9	Rotenone	1	EtOH	1	0.001
10	Antimycin A	5	EtOH	2	0.005

3.9.3 Luciferase assay for the determination of NAD^+:NADH ratio

The NAD/NADH-Glo™ assay was used to determine intracellular concentrations of NAD^+ and NADH on D5 (*protocol A*). For this purpose, the provided protocol for measuring NAD^+ and NADH individually was carried out. In brief, cells were washed with 1 mL DPBS, 100 µL DPBS was added and cells were scraped. Each 10 µL of the cell suspension was transferred into a white 96-well microplate for the following acidic (NAD^+) or basic (NADH) treatment for separate determination of both analytes. Luminescence was measured by the GloMax®Multi Detection System after 30 min incubation at RT. RLUs were normalized to the amount of total protein, which was determined in again 10 µL of the cell suspension by BCA assay.

3.10 Immunohistochemistry

Staining for immunohistochemical analysis was conducted on D8 of myotubes cultured following *protocol B* on 2-well slides. For fixation, cells were washed twice with DPBS (w/ Ca^{2+}, Mg^{2+}) followed by 20 min incubation in 1 mL RotiHistofix and three further washing steps. Blocking was performed by 30 min incubation in 500 µL IHC blocking solution. Primary antibodies were incubated overnight at 4°C and after washing the slides three times with DPBS, incubation with fluorescence-labeled secondary antibodies, DAPI (1:500) and Phalloidin (1:500) was carried out for 2 h at RT. Detailed information on antibodies used is provided in Table 17. Further three washing steps with DPBS were executed, the frame was removed and the slides were covered using PermaFlour Mounting. Images were recorded using the Aviovert Observer Z.1 microscope in the indicated magnification and post-processing was performed using ZEN software.

3.11 Determination of adenylate energy charge by capillary electrophoresis

Nucleotides were quantified in myotubes cultured following *protocol B* at D8 by capillary electrophoresis (CE). Cells were harvested immediately after finishing EPS as described in section 3.3.3. After washing the cells on ice with 1 mL cold DPBS, 100 µL CE lysis buffer containing 8-bromoguanosine as internal standard and 200 µL ACN were added. The lysate of three identical treated wells was pooled, intensively vortexed and divided into two aliquots of each 450 µL. A centrifugation step of 15 min at 14 000g at 4°C was performed. Both the supernatant and pellet were vacuum dried overnight (20 mbar, 1 500 rpm) for the determination of nucleotides by CE and total protein content, respectively.

The method for the CE measurement was based on the description of Friess et al. [62]. The measurements were performed in collaboration with Nadja Kalinke and Carolin Huhn (Institute of Physical and Theoretical Chemistry, University Tuebingen). The analysis was performed on an Agilent7100 using a bare fused silica capillary (90 cm x 50 µm, +30 kV). The system was equipped with a DAD (260 nm) and an autosampler which kept 15°C continuously. The capillary was preconditioned by rinsing with CE running buffer for 120 s and regenerated by rinsing with 90 s 0.1 M NaOH, 90 s H_2O and 30 s CE running buffer after each run. The sample was resuspended in 25 µL H_2O and was injected applying 100 mbar for 20 s. A representative electropherogram is provided as Figure S4.

The dried pellet was resuspended in 0.5 mL protein solubilization buffer by placing it into the TissueLyser for 2 min at 30 Hz. After 1:2 dilution with buffer the total protein concentration was determined in duplicates by bradford assay as described in section 3.8.2.

Adenylate energy charge (AEC) was calculated using the formula 3.1 described by Atkinson [11]:

$$\mathrm{AEC} = \frac{[\mathrm{ATP}] + 0.5 * [\mathrm{ADP}]}{[\mathrm{ATP}] + [\mathrm{ADP}] + [\mathrm{AMP}]} \tag{3.1}$$

3.12 Data analysis and statistics

For initial data collection software provided by the manufactures was used and is listed in Table 19. Merging of the data was performed with Microsoft Excel. If indicated, raw data of myotubes of each individual donor were normalized. Statistical analyses and plotting of graphics were performed using R/RStudio [197, 208]. An overview of relevant packages can be found in Table 20. Dose-dependent effects of metformin were analyzed by t-tests against the control group and spearman rank correlation was used for correlation analysis. Multiple pairwise-comparison analysis was conducted by ANOVA and following Tukey HSD test. A p-value < 0.05 was considered statistically significant. Statistical parameters, significance levels as well as number of replicates are provided in the figure legends. The n-number reports the number of biopsies derived from individual donors included in the experiment. Data are presented as mean ± standard deviation (sd).

For RNA sequencing analysis low expressed genes across all samples were removed if the sum of total counts < 60. A gene-level differential expression analysis was performed using DESeq2. The p-values were adjusted using the Benjamini and Hochberg method for the correction for multiple testing. An adjusted p-value < 0.1 was considered statistically significant. Gene sets were filtered for average counts > 5 in at least one group per comparison. g:Profiler [199] was used for the functional enrichment analysis using g:SCS multiple testing correction method applying a significance threshold of 0.05.

3.13 Materials

3.13.1 Chemicals

Table 9: Chemicals.

Reagent	Short	Identifier	Supplier
1,4-dithiothreitol	DTT	38225821	Roche Diagnostics
4-(2-hydroxyethyl)piperazine-1-ethanesulfonic acid	HEPES	6763,1	Carl Roth GmbH + Co. KG
4',6-diamidino-2-Phenylindole, Dilactate	DAPI	D3571	Thermo Fisher Scientific
8-bromoguanosine	8-BG	Cay18152-1	Cayman Chemical
Acetonitrile	ACN	100029	Merck Millipore
Adenosine 5'-diphosphate monopotassium salt dihydrate	ADP	A5285	Sigma-Aldrich
Adenosine 5'-diphosphate potassium salt	ADP	117105-1GM	Merck Millipore
Adenosine 5'-monophosphate sodium salt	AMP	A1752	Sigma-Aldrich
Adenosine 5'-triphosphate disodium salt hydrate	ATP	A7699	Sigma-Aldrich
Agarose		35-1020	Peqlab Biotechnologie GmbH
Ammonium persulfate	APS	A3678	Sigma-Aldrich
Amphotericin B solution		A2942	Sigma-Aldrich
Antimycin A from streptomyces sp.	AmA	A8674	Sigma-Aldrich
Bio-Rad Protein Assay Dye Reagent Concentrate		500-0006	Bio-Rad Laboratories GmbH
Bovine serum albumin	BSA	A6003	Sigma-Aldrich
Bovine serum albumin solution, 10% in DPBS		A1595	Sigma-Aldrich
Bromophenol blue solution		318744	Sigma-Aldrich
Carbonyl-cyanide-4-(trifluoro-methoxy)phenylhydrazone	FCCP	C2920	Sigma-Aldrich
CD56 MicroBeads, human		130-050-401	Miltenyi Biotec B.V. & Co. KG
CHAPS hydrate	CHAPS	C9426	Sigma-Aldrich
Chick Embryo Extract		MDL-004E-UK	Life Science Group Ltd.
cOmplete™ protease inhibitor cocktail		11836153001	Roche Diagnostics
Cytochrome C from equine heart	CyC	C7752	Sigma-Aldrich
Digitonin	Dig	D5628	Sigma-Aldrich
Dimethyl sulfoxide	DMSO	A994.1	Carl Roth GmbH + Co. KG
DL-octanoyl-carnitine-HCL	Oct	0605	Tocris Bioscience
D-sucrose		1,07687	Merck Millipore
Dulbecco's Balanced Salt Solution, w/ Ca^{2+}, Mg^{2+}	DPBS	14040133	Thermo Fisher Scientific

continued on next page

Table 9 – *continued from previous page*

Reagent	Short	Identifier	Supplier
Dulbecco's Balanced Salt Solution, w/o Ca^{2+}, Mg^{2+}	DPBS	14190250	Thermo Fisher Scientific
Dulbecco's Modified Eagle Medium	DMEM	A1443001	Thermo Fisher Scientific
Ethanol, p.A.	EtOH	100983	Merck Millipore
Ethylene diaminetetraacetic acid	EDTA	324503	Sigma-Aldrich
Ethylene glycol-bis(β-aminoethyl ether)-N,N,N',N'-tetraacetic acid	EGTA	3054.2	Carl Roth GmbH + Co. KG
FACSclean		340345	BD Bioscience
FACSrinse		340346	BD Bioscience
Fetal bovine serum Superior	FBS	S0615	Sigma-Aldrich
Formic acid		5438040250	Merck Millipore
Gelatine		1.04070	Merck Millipore
GelRed Nucleic Acid Stain	GelRed	SCT123	Merck Millipore
GelTrex		A1413302	Thermo Fisher Scientific
Glycerine		G5516	Sigma-Aldrich
Glycine		G8898	Sigma-Aldrich
H_2O HPLC grade		115333	Merck Millipore
Ham's F-12 Nutrient Mix	Ham's F-12	21765	Thermo Fisher Scientific
Immersol 518F		444960-0000-000	Carl Zeiss Microscopy GmbH
Insulin, human recombinant		I9278	Sigma-Aldrich
Lactobionic acid		153516	Sigma-Aldrich
L-carnitine hydrochloride		C0283	Sigma-Aldrich
L-glutamic acid monosodium salt hydrate	Glut	G1626	Sigma-Aldrich
L-glutamine solution, 200 mM		G7513	Sigma-Aldrich
L-malic acid	Mal	M1000	Sigma-Aldrich
Magnesium chloride hexahydrate	$MgCl_2 \cdot {}_6(H_2O)$	M2670	Sigma-Aldrich
Metformin hydrochloride		Cay13118	Cayman Chemical
Metformin-(dimethyl-d6)-hydrochloride		53183	Merck Millipore
Methanol	MeOH	20847	VWR International GmbH
Minimum Essential Medium Eagle, alpha modification	αMEM	M4526	Sigma-Aldrich
N,N,N',N'-tetramethyl ethylenediamine	TEMED	2367.1	Carl Roth GmbH + Co. KG
Oleic acid		O1008	Sigma-Aldrich
Oligomycin from streptomyces diastatochromogenes		O4876	Sigma-Aldrich
Palmitic acid		P0500	Sigma-Aldrich
Penicillin-Streptomycin Mixture		P4333	Sigma-Aldrich

continued on next page

Table 9 – *continued from previous page*

Reagent	Short	Identifier	Supplier
PermaFluor Mounting		TA-030-FM	Epredia Netherlands B.V.
physiological NaCl solution, 0.9%		B230422	Fresenius Kabi Deutschland GmbH
Poly-L-lysine	PLL	P7890	Sigma-Aldrich
Ponceau S-solution		A2935	AppliChem GmbH
Potassium hydroxide	KOH	5658,1	Carl Roth GmbH + Co. KG
Potassium phosphate monobasic	KH_2PO_4	1,04873	Merck Millipore
Pyruvic acid sodium salt	Pyr	P2256	Sigma-Aldrich
recombinant human insulin like growth factor 1	rhIGF1	291-G1-01M	R&D Systems, Inc.
Rhodamin-Phalloidin		R415	Thermo Fisher Scientific
Rotenone	Rot	R8875	Sigma-Aldrich
Roti®Histofix 4% Formaldehyde		P087.6	Carl Roth GmbH + Co. KG
Rotiphorese Gel 30 (37.5 :1)	AA	3029.2	Carl Roth GmbH + Co. KG
Seahorse XF 1.0 M glucose solution		103577	Agilent Technologies
Seahorse XF 100 mM pyruvate solution		103578	Agilent Technologies
Seahorse XF 200 mM glutamine solution		103579	Agilent Technologies
Seahorse XF DMEM assay medium		103575	Agilent Technologies
Sodium chloride	NaCl	106404	Merck Millipore
Sodium deoxycholate	NaDOC	D6750	Sigma-Aldrich
Sodium dodecyl sulfate	SDS	1610302	Bio-Rad Laboratories GmbH
Sodium fluoride	NaF	S6776	Sigma-Aldrich
Sodium hydroxide, 0.1 M	NaOH	AP181693.1211	AppliChem Panreac
Sodium orthovanadate		S6508	Sigma-Aldrich
Succinate disodium salt hexahydrate		S2378	Sigma-Aldrich
Taurine		T0625	Sigma-Aldrich
TE buffer solution, pH 8.0		93283	Sigma-Aldrich
Tetrasodium pyrophosphate decahydrate	$Na_4P_2O_7$	221368	Sigma-Aldrich
Thiourea		T7875	Sigma-Aldrich
Tris(hydroxymethyl)aminomethane	Tris	T1503	Sigma-Aldrich
TRIS-HCl		T3253	Sigma-Aldrich
Triton-X-100		X100	Sigma-Aldrich
Trypsin		T1426	Sigma-Aldrich
Tween-20		P9416	Sigma-Aldrich
Ultra-pure water (prepared by a Milli-Q system)			
Urea		U5378	Sigma-Aldrich
β-glycerolphosphate		50020	Sigma-Aldrich

continued on next page

Table 9 – *continued from previous page*

Reagent	Short	Identifier	Supplier
β-mercatoethanol		M3148	Sigma-Aldrich

Table 10: Commercial kits.

Commercial kit	Identifier	Supplier
Agilent RNA 6000 Nano Kit	5067-1511	Agilent Technologies
Glucose Uptake-Glo™ Assay	J1341	Promega Corporation
MinElute PCR purification kit	28004	Qiagen
NAD/NADH-Glo™ Assay	G9071	Promega Corporation
Pierce™ BCA Protein Assay Kit	23227	Thermo Fisher Scientific
QuantiFast SYBR® Green RT-PCR Kit	1044154	Qiagen
RNase-Free DNase Set	79254	Qiagen
RNeasy Mini Kit	74104	Qiagen
Seahorse XF DMEM assay medium pack	103680-100	Agilent Technologies
Seahorse XFe24 FluxPak	102340-100	Agilent Technologies
Transcriptor First Strand cDNA Synthesis Kit	04897030001	Roche Diagnostics

Table 11: Ladders.

Ladder	Identifier	Supplier
Chameleon® Duo Pre-stained Protein Ladder	978-16526	LI-COR Biosciences
Quickload 1 kb DNA ladder	N0468L	New England Biolabs GmbH
Quickload 100 bp DNA ladder	N0467L	New England Biolabs GmbH

3.13.2 Buffers and solutions

Unless otherwise stated all buffers and solutions were prepared with ultra-pure water.

Table 12: Buffers and solutions.

Components	Final concentration	Storage
Agarose gel (2%)		fresh
TAE buffer (x50) Agarose	1x 2% (m/v)	
CE lysis buffer		fresh
Triton X-100 8-bromoguanosine	0.5% (V/V) 40 nM	
CE running buffer (pH 9.0)		RT
Sodium tetra borate EDTA	30 mM 1 mM	

continued on next page

Table 12 – *continued from previous page*

Components	**Final concentration**	**Storage**
Cryo medium		fresh
FBS Superior	90% (V/V)	
DMSO	10% (V/V)	
Electrophoresis buffer (x10; pH 8.3)		RT
Tris base	250 mM	
Glycine	1.92 M	
SDS	1% (w/V)	
Diluted with H_2O for use x1.		
FACS buffer		4°C
DPBS (w/o Ca^{2+} and Mg^{2+})	–	
FBS Superior	2% (V/V)	
IHC blocking solution		4°C
DPBS (w/ Ca^{2+} and Mg^{2+})	–	
BSA	3.0% (V/V)	
Digitonin	0.1% (V/V)	
Laemmli buffer (x5; pH 6.8)		-20°C
Tris-HCl	60 mM	
Glycerine	12.5% (V/V)	
SDS	1% (w/V)	
β-mercaptoethanol	5% (V/V)	
Bromophenol blue	0.1% (w/V)	
MACS buffer		4°C
DPBS (w/o Ca^{2+} and Mg^{2+})	–	
Na_2EDTA	2 mM	
BSA	0.5% (m/V)	
Sterile filtrated before use.		
MirO5 buffer (pH 7.1)		-20°C
EGTA	0.5 mM	
$MgCl_2$	3 mM	
Lactobionic acid	60 mM	
Taurine	20 mM	
KH_2PO_4	10 mM	
HEPES	20 mM	
D-Sucorse	110 mM	
BSA	1 g/L	
pH was adjusted to 7.1 using KOH.		
Net-G buffer (x10; pH 7.4)		4°C
Gelatine	2.5% (w/V)	
NaCl	1.5 M	
EDTA	50 mM	

continued on next page

Table 12 – *continued from previous page*

Components	**Final concentration**	**Storage**
Tris-HCl	500 mM	
Triton-X-100	0.5% (V/V)	
Diluted with H_2O for use x1.		
Protein solubilization buffer		4°C
Urea	5 M	
Thiourea	2 mM	
DTT	15 mM	
CHAPS	2% (m/V)	
Phosphatase inhibitors (x10)		-20°C
NaF	10 mM	
Na-pyrophosphate	5 mM	
Na-orthovanadate	10 mM	
β-glycerolphosphate	10 mM	
RIPA lysis buffer		4°C
Tris, pH 7.6	25 mM	
NaCl	150 mM	
SDS	0.1% (w/V)	
NaDOC	0.5% (w/V)	
Triton-X-100	1% (V/V)	
Phosphatase inhibitors (x10)	x1	
cOmplet™ protease inhibitor cocktail (25x)	x1	
Addition of phosphatase inhibitors and cOmplete™ protease inhibitor cocktail immediately before use.		
Seahorse assay medium		fresh
Seahorse DMEM	–	
Glucose	10 mM	
L-Glutamine	2 mM	
Pyruvate	1 mM	
Separation gel buffer		RT
Tris-HCl	1.5 M	
SDS	2% (w/V)	
Stacking gel buffer		RT
Tris-HCl	0.5 M	
SDS	2% (w/V)	
TAE buffer (x50; pH 8.0)		RT
TRIS	1.25 M	
Acetic acid	625 mM	
EDTA	50 mM	

continued on next page

Table 12 – *continued from previous page*

Components	Final concentration	Storage
TBS buffer (x10)		RT
NaCl	1.5 M	
Tris	250 mM	
Diluted with H_2O for use x1.		
TBS-T buffer		RT
TBS buffer (x10)	x1	
Tween-20	0.1% (V/V)	
Transfer buffer (x10)		RT
Tris base	480 mM	
Glycine	390 mM	
SDS	0.4% (w/V)	
Transfer buffer (x1)		RT
Transfer buffer (x10)	10% (V/V)	
MeOH	20% (V/V)	
H_2O	70% (V/V)	

3.13.3 Cell culture media

Table 13: Cell culture media for cultivation of primary human myotubes.

Components	Final concentration	Storage
Cloning medium		4°C
αMEM	38% (V/V)	
Ham's F-12	38% (V/V)	
FBS	20% (V/V)	
Chicken extract	1% (V/V)	
L-Glutamine solution	2 mM	
Penicillin-Streptomycin mixture	100 U; 100 µg/mL	
Amphotericin B	0.2% (V/V)	
Chicken extract was resuspended in 1:1 mixture of αMEM:Ham's F-12 and centrifuged for 10 min at 3 200g. Supernatant was used.		
Differentiation medium (*protocol A*)		4°C
αMEM	96% (V/V)	
L-Glutamine solution	2 mM	
Penicillin-Streptomycin mixture	100 U; 100 µg/mL	
Amphotericin B	0.2% (V/V)	
Palmitate, coupled to BSA	50 µM	
Oleate, coupled to BSA	50 µM	
L-Carnitine, 500 mM in H_20	100 µM	

continued on next page

Table 13 – *continued from previous page*

Components	Final concentration	Storage
Differentiation medium (*protocol B*)		4°C
αMEM	96% (V/V)	
L-Glutamine solution	2 mM	
Penicillin-Streptomycin Mixture	100 U; 100 µg/mL	
Amphotericin B	0.2% (V/V)	
Palmitate, coupled to BSA	50 µM	
Oleate, coupled to BSA	50 µM	
L-Carnitine, 500 mM in H20	100 µM	
rhIGF1	100 ng/mL	
BSA-coupled fatty acids		-20°C
Fatty acid, 200 mM in EtOH	6 mM	
BSA in PBS	10% (w/V)	

3.13.4 Consumables

Table 14: Consumables.

Resource	Identifier	Supplier
96 well opticl Btm Plt PolymerBase White w/Lid	165306	Thermo Fisher Scientific
Ampliseal™ transparent microplate sealer	676040	Greiner bio-one
Cell culture dish Ø 137 mm	93150	TPP Techno Plastic Products AG
Cell culture dish Ø 87 mm	93100	TPP Techno Plastic Products AG
Cell culture plate, 24-well	92024	TPP Techno Plastic Products AG
Cell culture plate, 6-well	92006	TPP Techno Plastic Products AG
Cell scraper	83,1831	SARSTEDT AG & Co. KG
Cell scraper, 1.8 mm	3010	Corning Incorporated
CellStar Tubes, 15mL, PP, conical bottom	188271	Greiner bio-one
CellStar Tubes, 50mL, PP, conical bottom with support skirt	210261	Greiner bio-one
Combitips® advanced 0.5 mL	0030089634	Eppendorf SE
Combitips® advanced 2.5 mL	0030089650	Eppendorf SE
Combitips® advanced 5.0 mL	0030089669	Eppendorf SE
Crimp vial, 1.5mL	548-0003	VWR International GmbH
Cryo tubes vials 1.8 mL	368632	Thermo Fisher Scientific
Discovery® HS F5 HPLC Column, 3 µm	567503-U	Merck Millipore
epT.I.P.S. Reloads 0.1 - 10 µL	0030073371	Eppendorf SE
epT.I.P.S. Reloads 2 - 200 µL	0030073436	Eppendorf SE
epT.I.P.S. Reloads 50 - 1000 µL	0030073479	Eppendorf SE
Falcon round bottom polystyrene tube 5 mL	352053	Thermo Fisher Scientific

continued on next page

Table 14 – *continued from previous page*

Resource	Identifier	Supplier
Folded filters MN615	531018	Machery-Nagel GmbH & Co. KG
Immobilon-P membrane, PVDF, 0.45 µm	IPVH00010	Merck Millipore
LS Columns	130-042-401	Miltenyi Biotec B.V. & Co. KG
MACS SmartStrainer (70 µm)	130-098-462	Miltenyi Biotec B.V. & Co. KG
Micro inserts, 0.05 mL	548-0021	VWR International GmbH
Microplate, 96 well, PS, F-bottom, clear	655101	Greiner bio-one
Microscope Cover glasses 24x60mm	01-2460/S	R. Langenbrinck GmbH
Millex-GP, 0.22 µm	SLGPM33RS	Merck Millipore
MultiFlex Round Tips, 200 µL	13790	Sorenson BioScience Inc.
PARAFILM® M	PM-999	Bemis Company, Inc.
Pasteur capillary pipettes, 230 mm	4522.1	Carl Roth GmbH + Co. KG
PCR SingleCap 8er-SoftStrips 0.2 mL	710980	Biozym Scientific GmbH
Polyproplyene Conical tube 50 mL	352070	Corning Incorporated
QIAshredder	79654	Qiagen
Safe-Lock tubes 0.5 mL	30121023	Eppendorf SE
Safe-Lock tubes 1.5 mL	30120086	Eppendorf SE
Safe-Lock tubes 2.0 mL	30120094	Eppendorf SE
Sample Cups	10309450	Siemens Healthcare GmbH
Sample Cups, 3 mL	10309545	Siemens Healthcare GmbH
Sapphire microplate, 96 well, for Rt PCr	669285	Greiner bio-one
Serological pipette 10 mL	CLS4488	Greiner bio-one
Serological pipette 25 mL	CLS4489	Greiner bio-one
Serological pipette 5 mL	CLS4487	Greiner bio-one
Serological pipette 50 mL	CLS4490	Greiner bio-one
Silverseal Sealer, aluminium	676090	Greiner bio-one
Snap Caps	5181-1513	Agilent Technologies
Stericup 1000ml Millipore Express PLUS 0.22 µm PES	SCGPU10RE	Merck Millipore
TipOne Filter Tip, graduated, 0.1 µL – 10 µL	S1121-3810-C	STARLAB GmbH
TipOne Filter Tip, graduated, 10 µL	S1123-1810-C	STARLAB GmbH
TipOne Filter Tip, graduated, 100 µL	S1123-1840-C	STARLAB GmbH
TipOne Filter Tip, graduated, 1000 µL	S1126-7810-C	STARLAB GmbH
Tissue Culture Plate, 6-well	353046	Corning Incorporated
TSP Standard FS Tubing, 50 µM ID	TSP-050375	BGB Analytik Vertrieb GmbH
Whatman GB 005 Gel Blotting Papaer	10426994	GE Healthcare UK Limited
x-well cell culture chamber, 2-well, on PCA slide, removable frame	94.6140.202	SARSTEDT AG & Co. KG

3.13.5 Instruments and hardware

Table 15: Laboratory equipment.

Instrument	Supplier
Agarose gel chamber midi	Harnischmacher Labortechnik
Alpha 2-4 Cold Trap	Martin Christ Gefriertrocknungsanlagen GmbH

continued on next page

Table 15 – *continued from previous page*

Instrument	Supplier
Alpha RVC 2-33 Rotational Vacuum Concentrator	Martin Christ Gefriertrocknungsanlagen GmbH
Alpha RVC Rotational Vacuum Concentrator	Martin Christ Gefriertrocknungsanlagen GmbH
Apotome 2	Carl Zeiss Microscopy GmbH
Axio Observer A1	Carl Zeiss Microscopy GmbH
Axio Observer Z1	Carl Zeiss Microscopy GmbH
AxioCam ICc1	Carl Zeiss Microscopy GmbH
Axiovert 40 C	Carl Zeiss Microscopy GmbH
Bergström needle	Pelomi Medical equipment
Centrifuge 5417R	Eppendorf SE
Centrifuge 5425 R	Eppendorf SE
Centrifuge 5804 R	Eppendorf SE
Centrifuge 5810	Eppendorf SE
Circulator	Scientific Industries
Color Sprout Plus Mini	Biozym Scientific GmbH
CoolCel™ FTS30 freezing container	Corning Incorporated
Easypet 3	Eppendorf SE
Flexacam C3	Leica Camera AG
Gradient maker	Hoefer Inc
Hamilton syringe 10 µL	Hamilton Bonaduz AG
Hamilton syringe 25 µL	Hamilton Bonaduz AG
Hamilton syringe 50 µL	Hamilton Bonaduz AG
Hamilton syringe 500 µL	Hamilton Bonaduz AG
Heating block Thermostat Plus	Eppendorf SE
Hera Safe hood	Heraeus Holding
HXP 120 V	Carl Zeiss Microscopy GmbH
Incubator Binder C150	Binder GmbH
Incubator Binder CB210	Binder GmbH
Incubator for cells BBD6220	Binder GmbH
Incubator for cells Cytoperm	Heraeus Holding
Incubator Function line	Heraeus Holding
Laboratory balance ALJ160-4NM	Kern & Sohn GmbH
Laboratory balance BL1500	Sartorius AG
Laboratory balance RC210-D	Sartorius AG
Magnetic stirrer MH15	Carl Roth GmbH + Co. KG
Mikro 220 R	Andreas Hettich GmbH & Co. KG
Milli-Q Gradient A10	Merck Millipore
Multipette E3	Eppendorf SE
Multipette plus	Eppendorf SE
Neubauer chamber	Paul Marienfeld GmbH & Co.KG
PCR -cooler, 0.2 mL	Eppendorf SE
Pipetus	Hirschmann Laborgeräte GmbH & Co. KG
Power supply 232	Carl Zeiss Microscopy GmbH
Power supply Consort E802	Consort N.V.
Power supply E42/1	Behringwerke AG
Rainin EDP3-plus multichannel pipette	Mettler Toledo

continued on next page

Table 15 – *continued from previous page*

Instrument	Supplier
Research Pro 5 - 100 µL	Eppendorf SE
Research Single 0.1 - 2.5 µL	Eppendorf SE
Research Single 0.5 - 10 µL	Eppendorf SE
Research Single 10 - 100 µL	Eppendorf SE
Research Single 100 - 1000 µL	Eppendorf SE
Research Single 20 - 200 µL	Eppendorf SE
Safe Imager 2.0	Thermo Fisher Scientific
Semi dry blotting chamber	H.Hölzel GmbH
Shaker ST5	Glaswarenfabrik Karl Hecht GmbH & Co KG
ThermoPlate	Tokai Hit., Co, Ltd.
TissueLyser II	Qiagen
Water Bath GFL 1003	LAUDA DR. R. WOBSER GMBH & CO. KG
Water Bath MP-7A Typ	JULABO GmbH

Table 16: Special laboratory instruments.

Instrument	Supplier
ADVIA Chemistry XPT System	Siemens Healthcare GmbH
Agarose gel chamber midi	Harnischmacher Labortechnik
Agilent 2100 Bioanalyzer	Agilent Technologies
Agilent7100 CE system	Agilent Technologies
C-dish, 6-well	IonOptix LLC
C-PACE EP	IonOptix LLC
FACSCalibur flow cytometer	BD Science
GloMax® Multi Detection system	Promega Corporation
iMark microplate reader	Bio-Rad Laboratories GmbH
LCMS-8050	Shimadzu Corporation
Lightcycler 480	Roche Diagnostics
Mastercycler	Eppendorf SE
NanoDrop2000	Thermo Fisher Scientific
Odyssey infrared scanner	LI-COR Biosciences
Oxygraph-2k	Oroboros Instruments
quadroMACS	Miltenyi Biotec B.V. & Co. KG
Seahorse XFe24 Analyzer	Agilent Technologies

3.13.6 Antibodies

Table 17: Overview of antibodies used for the application in FACS, immuno blotting (WB) and immunohistochemistry (IHC). Antibodies for FACS were directly pipetted into the cell suspension. Antibodies for immuno blotting were diluted in Net-G buffer and for the use in IHC the dilution was made in 1:10 IHC blocking solution in DPBS.

Target	Clone	Identifier	Supplier	Application	Dilution	Host
Labeled antibodies						
Anti-CD56, Alexa Fluor™ 488	B159	557699	BD Bioscience	FACS	1:100	mouse IgG1
Anti-IgG1 Isotype control, Alexa Fluor™ 488	MOPC-21	557702	BD Bioscience	FACS	1:100	mouse IgG1
Primary antibodies						
ABRA	polyclonal	PA5-69859	Invitrogen	WB	1:1000	rabbit
Acetyl-CoA-Carboxylase	polyclonal	3662	Cell signaling	WB	1:1000	rabbit
Acetyl-CoA-Carboxylase (pSer-79)	D7D11	118189	Cell signaling	WB	1:500	rabbit
AMPKα	D5A2	5831	Cell signaling	WB	1:1000	rabbit
AMPK (pThr-172)	polyclonal	2531	Cell signaling	WB	1:1000	rabbit
Citrat Synthase	polyclonal	ab96600	abcam	WB	1:1000	rabbit
GAPDH	6C5	ab8245	abcam	WB	1:20 000	mouse IgG1
MHC-fast	MY-32	M4276	Sigma-Aldrich	IHC	1:2000	mouse IgG1
MHC-fast	MY-32	M4276	Sigma-Aldrich	WB	1:1000	mouse IgG1
MHC-slow	NOQ7.5.4D	M8421	Sigma-Aldrich	IHC	1:4000	mouse IgG1
MHC-slow	NOQ7.5.4D	M8421	Sigma-Aldrich	WB	1:1000	mouse IgG1
mTOR (pSer-2448)	polyclonal	2971	Cell signaling	WB	1:1000	rabbit
OXPHOS cocktail		MS604	abcam	WB	1:1000	mouse
PDH (pSer-232)	polyclonal	AP1063	Calbiochem	WB	1:500	rabbit
PDH (pSer-293)	polyclonal	ab92696	abcam	WB	1:400	rabbit
PDH (pSer-300)	polyclonal	AP1064	Merck	WB	1:500	rabbit
PDH-E1α	D-6	sc-377092	santa cruz	WB	1:1000	mouse

continued on next page

Table 17 – *continued from previous page*

Target	Clone	Identifier	Supplier	Application	Dilution	Host
S6 Ribosomal Protein	5G10	2217	Cell signaling	WB	1:1000	rabbit
S6 Ribosomal Protein (pSer-235/236)	91B2	4857	Cell signaling	WB	1:1000	rabbit
Secondary antibodies						
Goat anti-Mouse IgG1, Alexa Fluor™ 488		A21121	Invitrogen	IHC	1:2000	goat
IRDye® Donkey@Mouse 680LT		p26-68022	LI-COR Biosciences	WB	1:20000	donkey
IRDye® Donkey@Rabbit 800CW		925-32213	LI-COR Biosciences	WB	1:10000	donkey
IRDye® Goat@Mouse 680RD		926-32280	LI-COR Biosciences	WB	1:10000	goat

3.13.7 Primers for qRT-PCR

All primers used were provided by Qiagen.

Table 18: QuantiTect primers.

Primer	Species	Identifier
RPS28	human	QT02310203
SLC19A3	human	QT00043225
SLC22A1	human	QT00019572
SLC22A2	human	QT00056987
SLC22A3	human	QT00039578
SLC22A4	human	QT00047824
SLC29A4	human	QT00002135
SLC47A1	human	QT00033054
SLC47A2	human	QT00021525
SLC6A4	human	QT00058380
TBP	human	QT00000721

3.13.8 Software and algorithms

Table 19: Software used for inital data collection and post-processing.

Software	Version	Supplier
Adobe Illustrator 2023	27.0.1	Adobe Systems Software Ireland Limited
Adobe InDesign 2023	18.0	Adobe Systems Software Ireland Limited
Agilent 2100 expert software	B.02.11.SI811	Agilent Technologies
DatLab	7.4.0.4	Oroboros Instruments
Endnote20	20.2.1	ClavivateAnalytics
Flowing Software	2.5.1	Turku Bioscience
ImageStudio Lite	5.2.5	LI-COR Biosciences
Lightcycler480 software	1.5.0.39	Roche Diagnostics
Microplate Manager	6.3	Bio-Rad Laboratories GmbH
Microsoft Excel 2019	1808	Microsoft Corporation
miKTeX	23.4	Christian Schenk
NanoDrop2000	1.5	Thermo Fisher Scientific
NAS UniChrom	5.0.19.1178	New Analytical Systems Ltd
OpenHeartWare	1.3.0	Loskill Lab
OpenLAB CDS	A.02.10	Agilent Technologies
Origin 2020	9.7.0.185	Origin Lab Corporation
R	4.2.1	R Core Team
Rstudio	2022.02.3	RStudio Team
TEXMAKER	5.1.3	Pascal Brachet
Wave	2.6.3	Agilent Technologies
ZEN blue edition	2.6	Carl Zeiss Microscopy GmbH

Table 20: R packages used for data analysis and statistics.

Package	Version	Package	Version
base	4.2.1	magrittr	2.0.3
ComplexHeatmap	2.14.0	methods	4.2.1
corrplot	0.92	openxlsx	4.2.5.1
datasets	4.2.1	plotly	4.10.1
DescTools	0.99.47	plyr	1.8.8
DESeq2	1.32.0	PMCMRplus	1.9.6
dplyr	1.0.10	purrr	0.3.5
factoextra	1.0.7	RColorBrewer	1.1-3
forcats	0.5.2	readr	2.1.3
ggplot2	3.4.0	renv	1.0.2
ggprism	1.0.4	rstatix	0.7.1
ggpubr	0.4.0	scales	1.2.1
ggrepel	0.9.2	stats	4.2.1
ggsignif	0.6.4	stringr	1.4.1
graphics	4.2.1	tibble	3.1.8
grDevices	4.2.1	tidyverse	1.2.1
grid	4.2.1	utils	4.2.1
gridExtra	2.3		

CHAPTER 4

Metformin forces lactate production through alterations in cellular redox state and pyruvate metabolism

This chapter focuses on the investigation of mechanisms by which metformin increases lactate production in the human skeletal muscle. Large parts of the data shown within this chapter have already been published [156] and are marked accordingly. In addition, the declaration of contribution can be found attached.

Primary human myotubes were used as a model to address the research question. Unless otherwise stated, cell culture *protocol A* (Fig. 5) was used.

4.1 Cellular uptake of metformin in human myotubes

First, the expression levels of reported metformin transporters [139] in human skeletal muscle tissue (Fig. 6A) and primary human myotubes (Fig. 6B) were investigated. All nine transporters were detected by microarray analysis in skeletal muscle biopsies with *SLC22A3* and *SLC47A1* being the most abundant. In contrast, *SLC47A2* and *SLC29A4* have the highest abundance of all described transporters in myotubes based on RNA sequencing (Chapter 4.4). Except *SLC22A4*, all other transporters were below 0.05 transcripts per million, so a negligible amount of transcripts can be assumed here.

Next, cellular uptake of metformin in myotubes was determined by LC-MS based quantification of metformin in cell lysates. Based on reported *in vivo* plasma concentrations [128, 246], low metformin concentrations (16–78 µM) were chosen for the treatment referred to as pharmacological concentrations. Supra-pharmacological concentrations (388–776 µM) were also included well in line with concentrations frequently used in *in vitro* studies [128]. The treatment time was set to 48 h to mimic a long-term treatment better reflecting the *in vivo* situation. Metformin was not detectable in the control group, while for the increasing treatment concentrations, the metformin measured intracellularly likewise increased. Using pharmacological metformin concentrations of 16, 39, and 78 µM resulted in intracellular concentrations of 0.66$\pm$0.21 nmol/mg protein, 1.65$\pm$0.22 nmol/mg protein, and 4.17$\pm$1.40 nmol/mg protein, respectively (Fig. 6C). The highest intracellular concentration reached was 32.38$\pm$8.46 nmol/mg protein at a treatment dose of 776 µM metformin. Analyzing the relative uptake of metformin based on the treatment dose, intracellular metformin uptake ranges within 0.43$\pm$0.06% to 0.74$\pm$0.08% (Fig. 6D). A significantly reduced percentual uptake ($p < 0.05$) observed for the highest treatment dose suggests that intracellular saturation was reached.

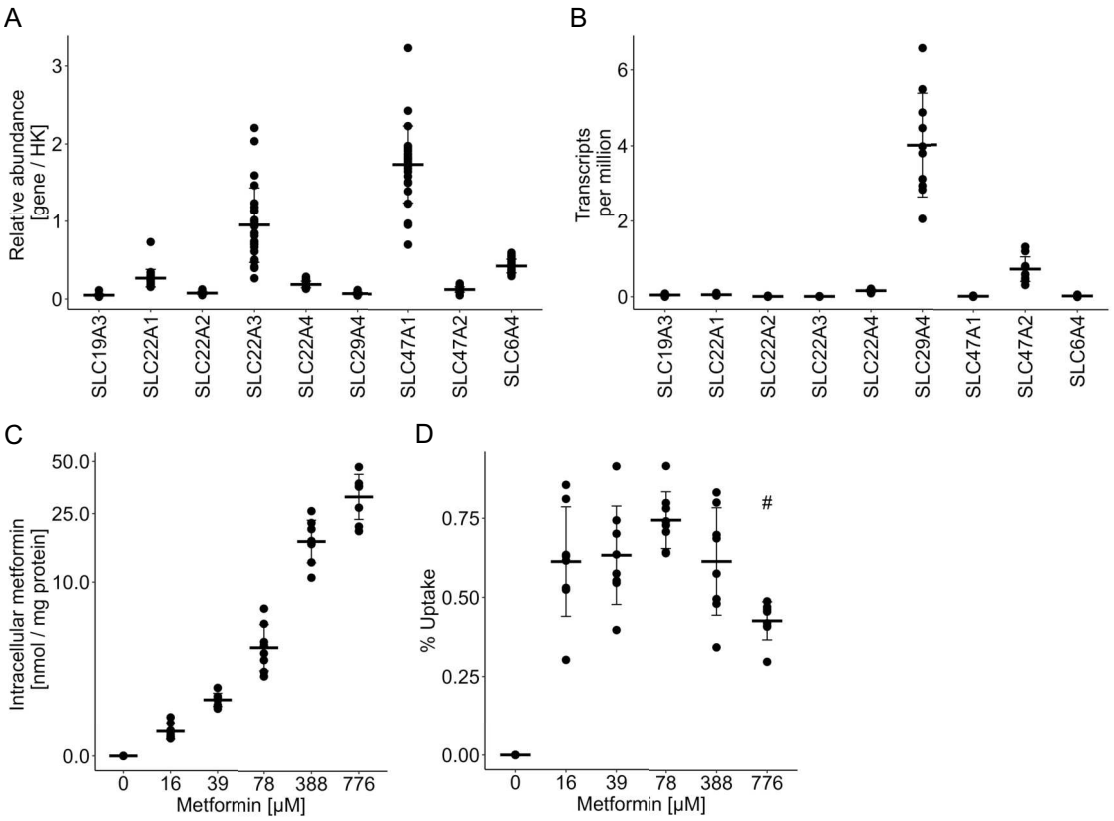

Figure 6: Metformin is taken up into human myotubes.
Basal expression of reported metformin transporters in (A) human skeletal muscle tissue (n = 25 donors) and (B) cultured primary human myotubes (n = 10 donors) were analyzed by micro array and RNA sequencing, respectively. LC-MS was used to quantify intracellular concentrations of metformin measured in cell lysates of primary human myotubes. The values were normalized to the total protein content of the lysate and are expressed as (C) absolute values and (D) relative to the treatment concentration (n = 8 donors). All individual data points are displayed; bars represent means ± SD; t-test between groups: # different from all other metformin treated groups $p < 0.05$. – *Figure adapted from [156].*

4.2 Metformin enhances lactate production and induces a shift toward glycolytic phenotype

The initial question was whether primary human myotubes showed metformin-induced lactate production. Analyzing the supernatant after 48 h treatment with metformin, a significant dose-dependent increase in lactate production and secretion was observed ($\geq$ 78 µM, $p < 0.01$, Fig. 7A). At the same time, glucose consumption increased ($\geq$ 78 µM, $p < 0.05$, Fig. 7B). The metformin-induced increase in both lactate production and glucose consumption showed a positive correlation (Fig. 7C). For the control group as well as for the metformin concentrations up to 388 µM, a stoichiometric ratio of glucose:lactate in a range between 0.61 and 0.68 was observed (Fig. 7D). This suggests that glycolysis is driving the increase in lactate production while the deviation from the theoretical ratio of 1:2 leaves room for the oxidation of pyruvate and lactate. Using 776 µM metformin, the ratio declines to an almost 1:2 ratio (0.53, $p < 0.0001$), which can be interpreted as a nearly complete conversion of glucose to lactate, which is secreted from the cells.

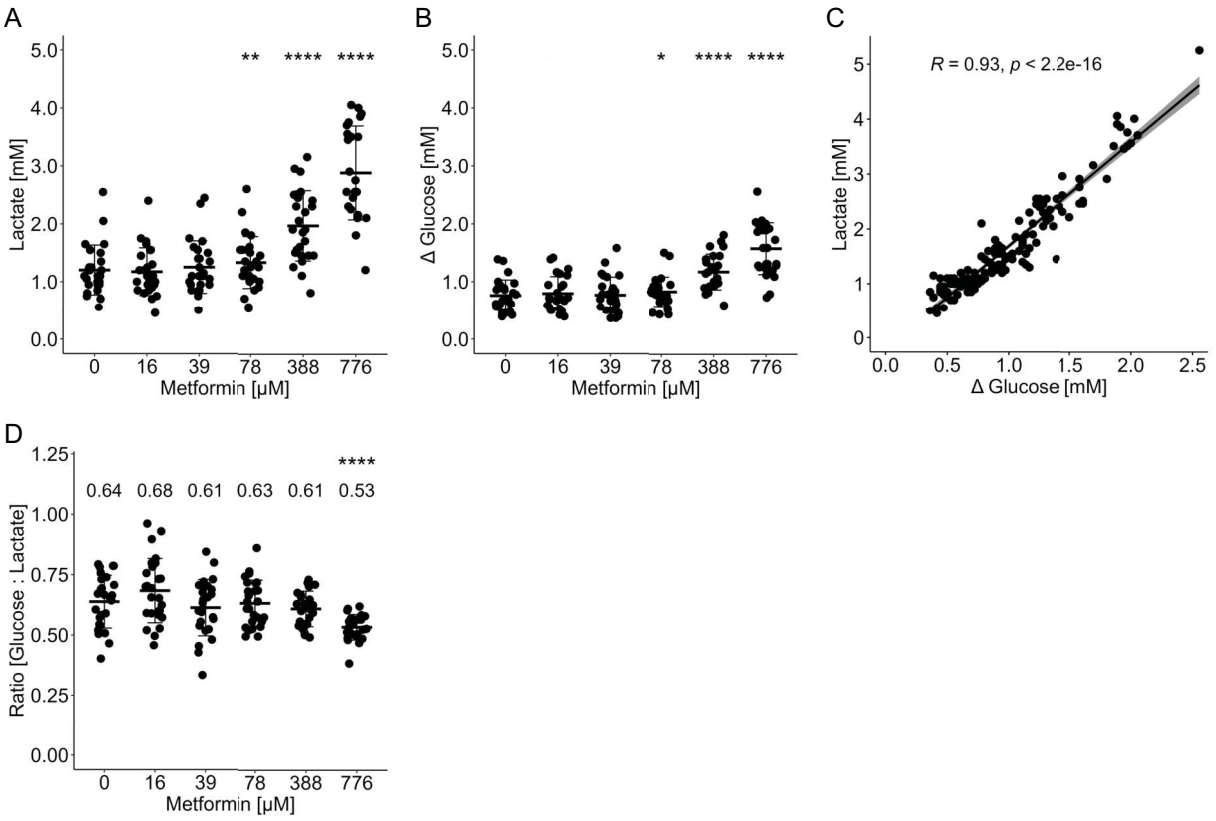

Figure 7: Lactate production is heightened in human myotubes in response to metformin.
The supernatant obtained immediately before myotube harvest after 48 h of metformin treatment at indicated doses was analyzed for lactate and glucose. (A) Cellular lactate production was considered to be the measured concentration in the supernatant, given that the medium does not contain any lactate. (B) The difference between the measured glucose in supernatant and the glucose present in the medium represents cellular glucose consumption. (C) Spearman correlation of cellular lactate production and glucose consumption. (D) Ratio between glucose consumption and lactate production. All data points represent the mean value of technical duplicates (n = 26 donors); bars represent means ± SD; paired t-test against 0 µM metformin: ns p > 0.05, * p < 0.05, ** p < 0.01, **** p < 0.0001. – *Figure adapted from [156].*

In the following, to confirm that the increased lactate concentration in the supernatant of metformin-treated cells is not due to cellular damage, CK and LDH were determined as markers of cellular damage in the supernatant collected immediately before harvesting myotubes after 48 h treatment with metformin. Both analytes were unaffected by the treatment (Fig. 8), indicating that the observed increase in lactate secretion is not caused by leakage due to treatment-induced cell damage.

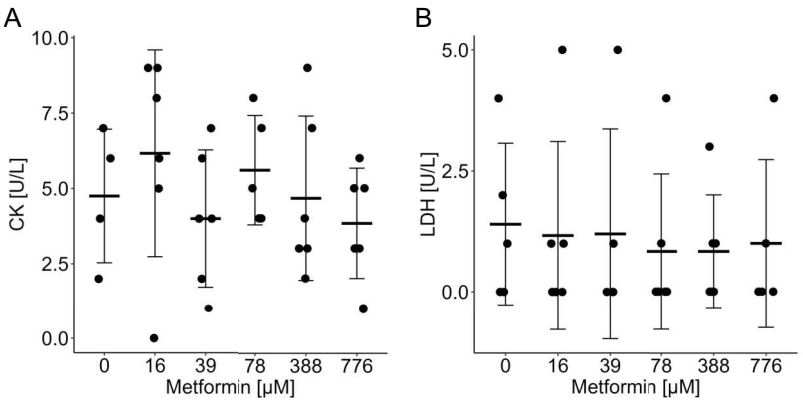

Figure 8: Lactate secretion is not increased due to cell damage by metformin treatment.
(A) Creatine kinase (CK) and (B) lactate dehydrogenase (LDH) were determined in the supernatant collected immediately before harvesting myotubes after 48 h treatment with metformin doses as indicated. All individual data points are displayed (n = 6 donors); bars represent means ± SD; paired t-test against 0 µM metformin: ns p > 0.05 – *Figure from [156].*

The assumption of increased glycolysis was further supported by increased glucose uptake assessed as uptake of 2-DG over 60 min ($\geq$ 388 µM, $p < 0.01$, Fig. 9A). The RNA sequencing data (Chapter 4.4) suggested that the increased glucose consumption may be covered by increased expression of glucose transporter *SLC2A4* (GLUT4) (776 µM, $p < 0.01$, Fig. 9C), while *SLC4A1* (GLUT1) slightly decreased (776 µM, $p < 0.1$, Fig. 9B). To prove whether the regulatory effect of metformin is preserved on protein level, cell lysates cultured according *protocol B* were investigated as it has been shown that expression of GLUT4 is low without the supplementation of insulin-like growth factor 1 (IGF1) [47]. However, the changes observed on transcriptional level could not be confirmed on protein level (Fig. 9D–F). Bioenergetic phenotyping based on the basal normalized oxygen consumption rate (OCR) and extracellular acidification rate (ECAR) determined during seahorse measurements, revealed a shift from an aerobic to a more glycolytic phenotype with increasing concentrations of metformin (Fig. 9G). This is also represented by the decrease in the OCR:ECAR ratio ($\geq$ 388 µM, $p < 0.01$, Fig. 9H). Together, metformin increased glucose uptake and glycolysis without affecting GLUT1 and GLUT4 protein levels.

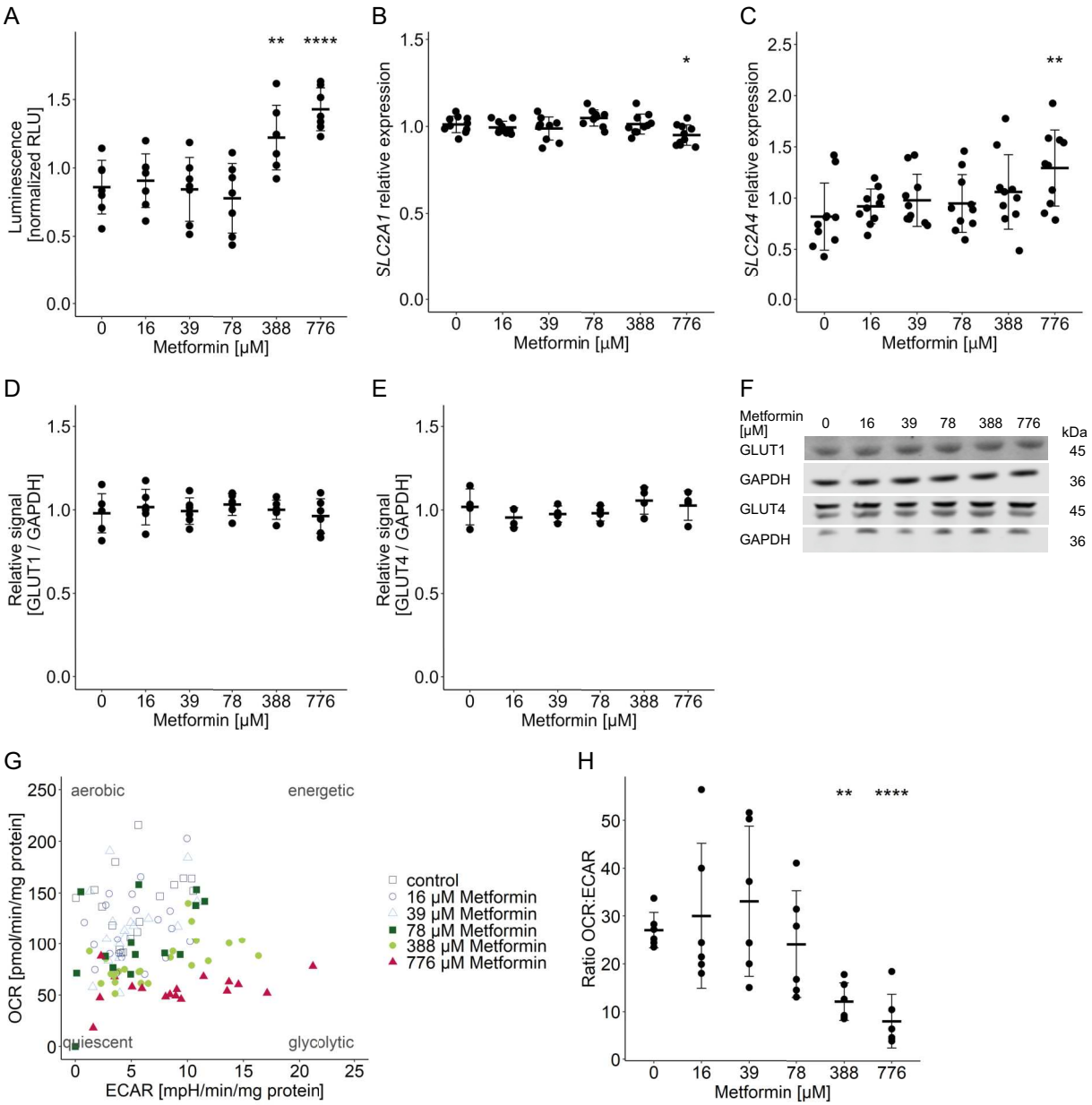

Figure 9: Metformin augments glucose uptake and promotes a transition toward a glycolytic phenotype.

(A) Cellular glucose uptake was assessed by a bioluminescent assay as uptake of 2-deoxyglucose (2-DG) over 60 min. All data points represent the mean value of technical duplicates after donor normalization (n = 7 donors); bars represent means ± SD; paired t-test against 0 µM metformin: ns $p > 0.05$, ** $p < 0.01$, **** $p < 0.0001$. The influence of metformin on transcriptional expression of (B) *SLC2A1* and (C) *SLC2A4* was investigated based on RNA sequencing data. All individual data points are displayed (n = 10 donors); bars represent means ± SD; adjusted p values (Benjamini-Hochberg): ns $p > 0.1$,* $p < 0.1$, ** $p < 0.01$. Quantification of signal intensity of immunoblots using antibodies against (D) GLUT1 and (E) GLUT4 related to GAPDH. Cell lysates were obtained following *protocol B*. All individual data points are displayed (n = 4–6 donors); t-test against 0 µM metformin: ns $p > 0.05$. (F) Representative immunoblot of one individual donor. For the quantification of GLUT4, both bands were analyzed. (G) The energy map based on the Seahorse XF Mito Stress Test Assay visualizes the dose-dependent influence of metformin on the metabolic phenotype. The relation between basal normalized OCR and ECAR reflects the four phenotypes: aerobic (predominantly mitochondrial respiration), glycolytic (predominantly glycolysis), energetic (both pathways), and quiescent (low activity via either metabolic pathway). All data points represent the mean value of technical replicates of 3–4 (n = 6 donors). (H) Ratio of basal normalized OCR to ECAR in dependence of indicated metformin dose. All data points represent the mean value of technical replicates of 3–4 (n = 6 donors); bars represent means ± SD; paired t-test against 0 µM metformin: ns $p > 0.05$, ** $p < 0.01$, **** $p < 0.0001$.
– *Figure adapted from [156].*

4.3 Metformin alters cellular redox state by inhibition of mitochondrial complex I respiration

The metformin-induced increase in lactate production can be caused by shifting the equilibrium of the LDH reaction (Equ. 4.1) through mechanisms enhancing either intracellular pyruvate or NADH concentrations.

$$\text{Pyruvate} + \text{NADH} + \text{H}^+ \overset{\text{LDH}}{\rightleftharpoons} \text{Lactate} + \text{NAD}^+ \tag{4.1}$$

Therefore, mitochondrial respiration was investigated as a mechanism that affects the cellular redox state and thus NADH concentration. First, dose-dependent effects on overall respiration were analyzed using the Seahorse system (Fig. 10). While maximal respiration (Fig. 10D) after uncoupling with FCCP was unaffected, basal respiration (776 µM, $p < 0.01$, Fig. 10B), ATP production ($\geq$ 388 µM, $p < 0.05$, Fig. 10C) and non-mitochondrial respiration ($\geq$ 388 µM, $p < 0.05$, Fig. 10E) were reduced using supra-pharmacological concentrations of metformin.

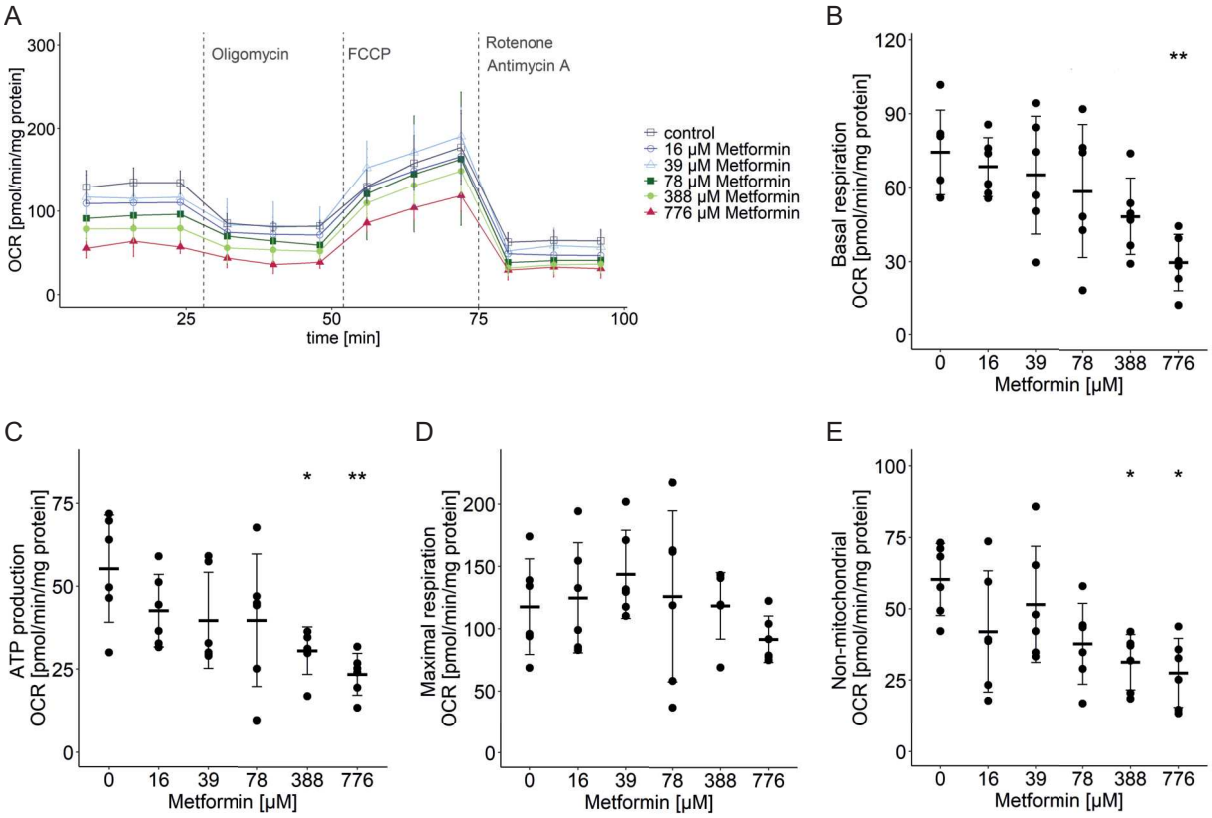

Figure 10: Metformin blunts mitochondrial respiration.
(A) Determination of dose-dependent metformin effect on mitochondrial respiration using Seahorse XF Mito Stress Test assay. Quantification of respiratory states: OCR at the beginning of the measurement represents (B) basal respiration, (C) ATP production is determined after the addition of oligomycin, (D) maximal respiration is measured after uncoupling by FCCP, and (E) non-mitochondrial respiration is determined after the addition of rotenone and antimycin A. All data points represent the mean value of technical replicates of 3–4 (n = 6 donors); bars represent means ± SD; multiple pairwise-comparison between the means of groups by ANOVA and Tukey HSD test: ns $p > 0.05$, * $p < 0.05$, ** $p < 0.01$. – *Figure adapted from [156].*

For resting skeletal muscle, the lactate to pyruvate ratio is approximately 10:1 [209], which was affected by the metformin-induced increase in lactate production. The medium used for the Seahorse assay contains 1 mM pyruvate in addition to glucose and L-glutamine. This raises the question

of whether the observed effect of metformin on mitochondrial respiration is influenced by changes in the lactate:pyruvate ratio through the supply of extracellular pyruvate or lactate. Therefore, untreated control and metformin-treated myotubes (776 µM) were investigated providing either 1 mM pyruvate (GGP) or 1 mM lactate (GGL) in addition to glucose and L-glutamine (Fig. 11). For all four investigated respiratory states, no influence of the provided assay medium was found and the metformin-induced effects could be confirmed (Fig. 11B–E).

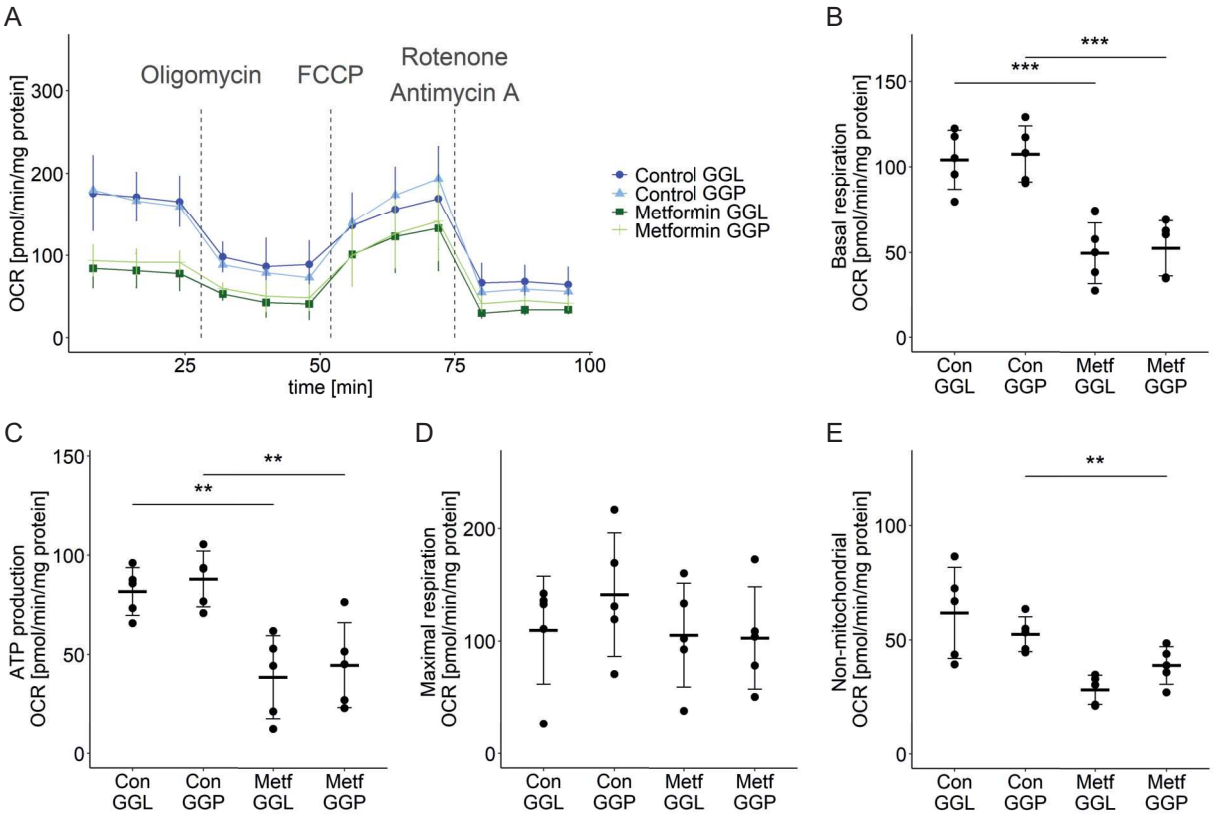

Figure 11: Metformin effect on mitochondrial respiration is unaffected of substrates provided during measurement.
(A) Determination of the effect of provided substrates during Seahorse XF Mito Stress Test assay on metformin effect on mitochondrial respiration. The assay was performed using two different assay media (GGL: glucose, L-glutamine, lactate; GGP: glucose, L-glutamine, pyruvate) in untreated control and metformin-treated (776 µM) myotubes. Quantification of respiratory states: OCR at the beginning of the measurement represents basal respiration (B), ATP production is determined after the addition of oligomycin (C), maximal respiration is measured after uncoupling by FCCP (D), and non-mitochondrial respiration is determined after the addition of rotenone and antimycin A (E). All data points represent the mean value of technical replicates of 5 (n = 5 donors); bars represent means ± SD; multiple pairwise-comparison between the means of groups by ANOVA and Tukey HSD test: ns $p > 0.05$, ** $p < 0.01$, *** $p < 0.001$. – *Figure adapted from [156].*

Next, high-resolution respirometry was carried out using the Oroboros system. By step wise providing multiple substrates, inhibitors and uncouplers, it allows to gain more precise insights into the inhibitory mechanism of metformin on mitochondrial respiration. Metformin-treated myotubes using 39 and 776 µM were compared with untreated control myotubes (Fig. 12A, B) applying a substrate-uncoupler-inhibitor-titration (SUIT) protocol after cell permeabilization with digitonin. Consistent with the data from the Seahorse measurements, there was no difference between control and the low dose of metformin (Fig. 12A). For the high metformin dose, a decrease in oxygen flux was observed after step wise injection of ADP, octanoylcarnitine, and complex I substrates pyruvate and glutamate ($p < 0.01$, Fig. 12B). Adding the sole complex II substrate succinate, the difference disappeared. Further, maximal uncoupled respiration investigated by the titration of FCCP was unaffected

by metformin as expected from the data obtained by Seahorse. The small increase in oxygen flux observed by the injection of malate at the beginning of the protocol can be explained by the activity of malic enzyme 2 (ME2) in myotubes which generates pyruvate [86]. Mitochondrial protein markers NADH:ubiquinone oxidoreductase subunit B8 (NDUFB8) for complex I and citrate synthase (CS) for mitochondrial content were analyzed by immunoblotting to study whether the observed reduction in complex I respiration is due to changes in activity and not reduced mitochondrial mass or complex I abundance (Fig. 12C–E). NDUFB8 showed a slight increase ($\geq$ 388 µM, $p < 0.05$) while CS was unaffected by metformin treatment.

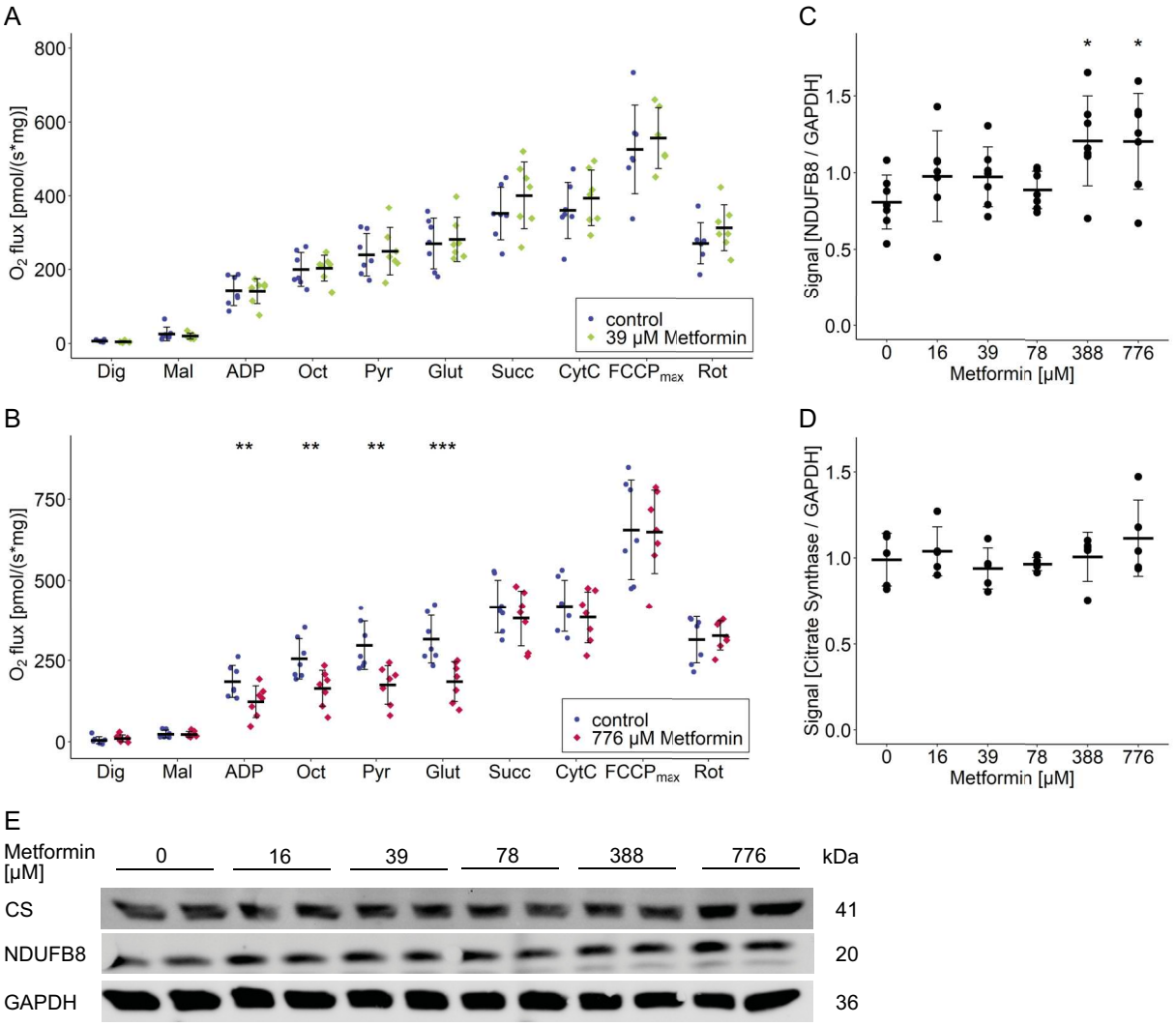

Figure 12: Reduced mitochondrial respiration is caused by inhibition of complex I.
Oroboros measurement of permeabilized myotubes comparing untreated control myotubes with metformin-treated myotubes using either (A) 39 µM or (B) 776 µM. Step wise injection of malate, ADP, octanoylcarnitine, pyruvate and glutamate allows the investigation of complex I respiration. By the addition of succinate complex II respiration is initiated. Titration of FCCP is used to analyze maximal uncoupled respiration. Oxygen flux was normalized to mg protein lysate. All data points represent the mean value of technical duplicates (n = 7 donors); bars represent means $\pm$ SD; paired t-test between both groups: ns $p > 0.05$, ** $p < 0.01$, *** $p < 0.001$. Quantification of signal intensity of immunoblots using antibodies against (C) NDUFB8 and (D) citrate synthase related to GAPDH. All individual data points are displayed (n = 5–7 donors); bars represent means $\pm$ SD; t-test against 0 µM metformin: ns $p > 0.05$, * $p < 0.05$. (E) Representative immunoblot of one individual donor. – *Figure adapted from [156].*

The findings of reduced mitochondrial complex I respiration are further supported by the observation, that metformin induced an increase in NADH and thereby reduced the NAD^+:NADH ratio (Fig. 13).

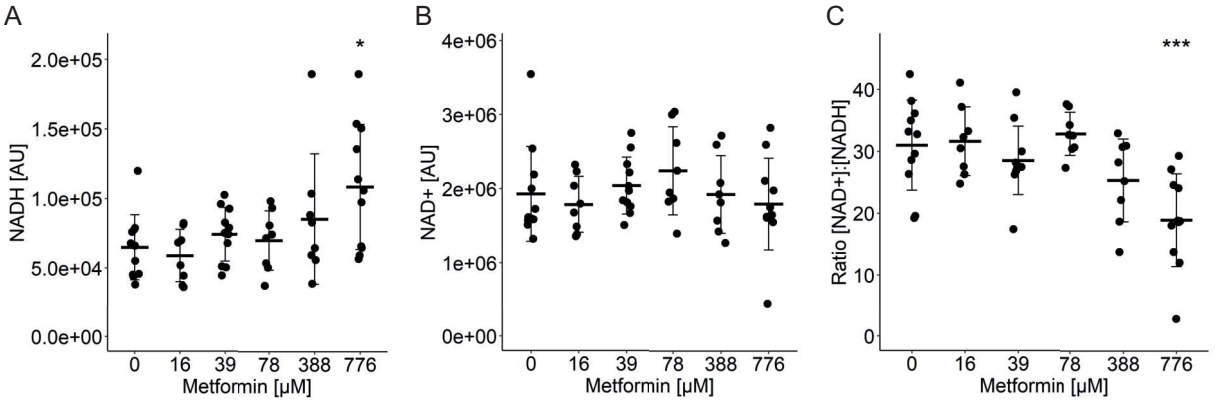

Figure 13: Impaired mitochondrial respiration shifts cellular redox state.
Simultaneous determination of (A) NADH and (B) NAD^+ using a luciferase assay. (C) Calculation of NAD^+:NADH ratio. All individual data points are displayed (n = 11 donors); bars represent means ± SD; paired t-test against 0 µM metformin: ns p > 0.05, * p < 0.05, *** p < 0.001. – *Figure adapted from [156].*

Taken together, these data show that metformin inhibits mitochondrial complex I respiration and thereby shifts cellular redox state. The induced increase in cellular NADH can contribute to force lactate production. However, comparing metformin doses necessary to inhibit complex I and to increase lactate production, it has to be stated that lactate production is already induced at lower concentrations. Therefore, this is not the sole mechanism.

4.4 Metformin induces the inhibition of pyruvate oxidation through phosphorylation of pyruvate dehydrogenase

Searching for an explanation of metformin-induced lactate production at lower concentrations of 78 or 388 µM, the focus was on mechanisms inducing pyruvate accumulation. RNA sequencing analysis was performed to gain a deeper understanding of dose-dependent metabolic changes ongoing in myotubes under metformin treatment (16–776 µM). A number of 17 683 transcripts was detected of which 7 208 were differentially regulated by 776 µM metformin (adj.p < 0.1, Suppl. Table S4). A global analysis did not find an enrichment in transcripts associated with glucose or pyruvate metabolism as might have been expected from the previous results. In a more detailed analysis, regulated transcripts (776 µM) were investigated that are involved in pyruvate conversion based on the GO terms *pyruvate transport* (GO:0006848), *pyruvate dehydrogenase activity* (GO:0004738), *pyruvate dehydrogenase complex* (GO:0045254) and Mitocarta3.0 pathway *pyruvate metabolism* (Table 21).

Table 21: Dose-dependent regulatory effect of metformin on transcripts annotated for GO terms associated with pyruvate metabolism. *Pyruvate transport* (GO:0006848), *pyruvate dehydrogenase activity* (GO:0004738), *pyruvate dehydrogenase complex* (GO:0045254) and Mitocarta3.0 pathway *pyruvate metabolism* were analyzed and changes are expressed as fold-change (adjusted p-value (Benjamini-Hochberg), ns p > 0.1) – *Table adapted from [156].*

Gene symbol	Description	Metformin				
		16 µM	**39 µM**	**78 µM**	**388 µM**	**776 µM**
DLAT	dihydrolipoamide S-acetyltransferase	1.01 (ns)	-1.02 (ns)	-1.02 (ns)	-1.06 (0.092)	-1.08 (0.007)
DLD	dihydrolipoamide dehydrogenase	-1.05 (ns)	-1.06 (ns)	-1.07 (ns)	-1.09 (0.014)	-1.14 (<0.001)
MPC1	mitochondrial pyruvate carrier 1	1.03 (ns)	1.00 (ns)	-1.03 (ns)	-1.05 (ns)	-1.07 (ns)
MPC2	mitochondrial pyruvate carrier 2	-1.02 (ns)	-1.07 (ns)	-1.03 (ns)	-1.10 (ns)	-1.10 (0.065)
PDHA1	pyruvate dehydrogenase E1 subunit alpha 1	1.00 (ns)	-1.02 (ns)	-1.02 (ns)	-1.00 (ns)	-1.00 (ns)
PDHB	pyruvate dehydrogenase E1 subunit beta	-1.01 (ns)	-1.03 (ns)	-1.02 (ns)	-1.03 (ns)	-1.08 (0.028)
PDHX	pyruvate dehydrogenase complex component X	-1.02 (ns)	-1.00 (ns)	1.00 (ns)	-1.06 (ns)	-1.06 (ns)
PDK1	pyruvate dehydrogenase kinase 1	1.01 (ns)	1.03 (ns)	1.04 (ns)	1.05 (ns)	-1.03 (ns)
PDK2	pyruvate dehydrogenase kinase 2	1.01 (ns)	1.03 (ns)	-1.02 (ns)	1.06 (ns)	1.04 (ns)
PDK3	pyruvate dehydrogenase kinase 3	-1.06 (ns)	-1.04 (ns)	1.04 (ns)	-1.01 (ns)	1.09 (ns)
PDK4	pyruvate dehydrogenase kinase 4	-1.02 (ns)	1.06 (ns)	-1.02 (ns)	1.33 (<0.001)	1.66 (<0.001)
PDP1	pyruvate dehyrogenase phosphatase catalytic subunit 1	1.00 (ns)	-1.03 (ns)	-1.00 (ns)	-1.01 (ns)	-1.00 (ns)
PDP2	pyruvate dehyrogenase phosphatase catalytic subunit 2	1.09 (ns)	1.00 (ns)	1.05 (ns)	1.11 (ns)	1.18 (0.007)
PDPR	pyruvate dehydrogenase phosphatase regulatory subunit	1.00 (ns)	-1.02 (ns)	-1.02 (ns)	-1.00 (ns)	-1.03 (ns)
SLC16A1	solute carrier family 16 member 1	-1.05 (ns)	-1.05 (ns)	-1.03 (ns)	-1.06 (ns)	-1.07 (0.050)

continued on next page

Table 21 – *continued from previous page*

		16 µM	**39 µM**	**78 µM**	**388 µM**	**776 µM**
SLC16A3	solute carrier family 16 member 3	-1.06 (ns)	-1.06 (ns)	1.00 (ns)	-1.06 (ns)	-1.12 (0.061)
SLC16A7	solute carrier family 16 member 7	-1.06 (ns)	-1.05 (ns)	-1.02 (ns)	-1.08 (ns)	-1.04 (ns)

Among the 17 related transcripts, sole *PDK4* showed a significant regulation with a fold-change > 1.2 ($\geq$ 388 µM, $p < 0.001$, Fig. 14A). Pyruvate dehydrogenase kinases (PDKs) are involved in the regulation of PDH complex activity and PDK4 is a highly abundant isoform in both skeletal muscle and myotubes [23, 79, 207]. Through PDK-dependent phosphorylation of at least one of multiple serine sites at the E1α subunit the PDH complex gets inactivated and the oxidation of pyruvate is blocked. Therefore, the metformin effect on the phosphorylation pattern at the three serine sites 232, 293, and 300 was analyzed. For all three sites, an up-regulation in phosphorylation was found ($\geq$ 39 µM, $p < 0.01$, Fig. 14B–D) indicating an inhibitory effect of metformin on PDH complex activity. In addition, serine 232 showed a dose-dependent increase in phosphorylation correlated with the amount of produced lactate (Fig. 14F).

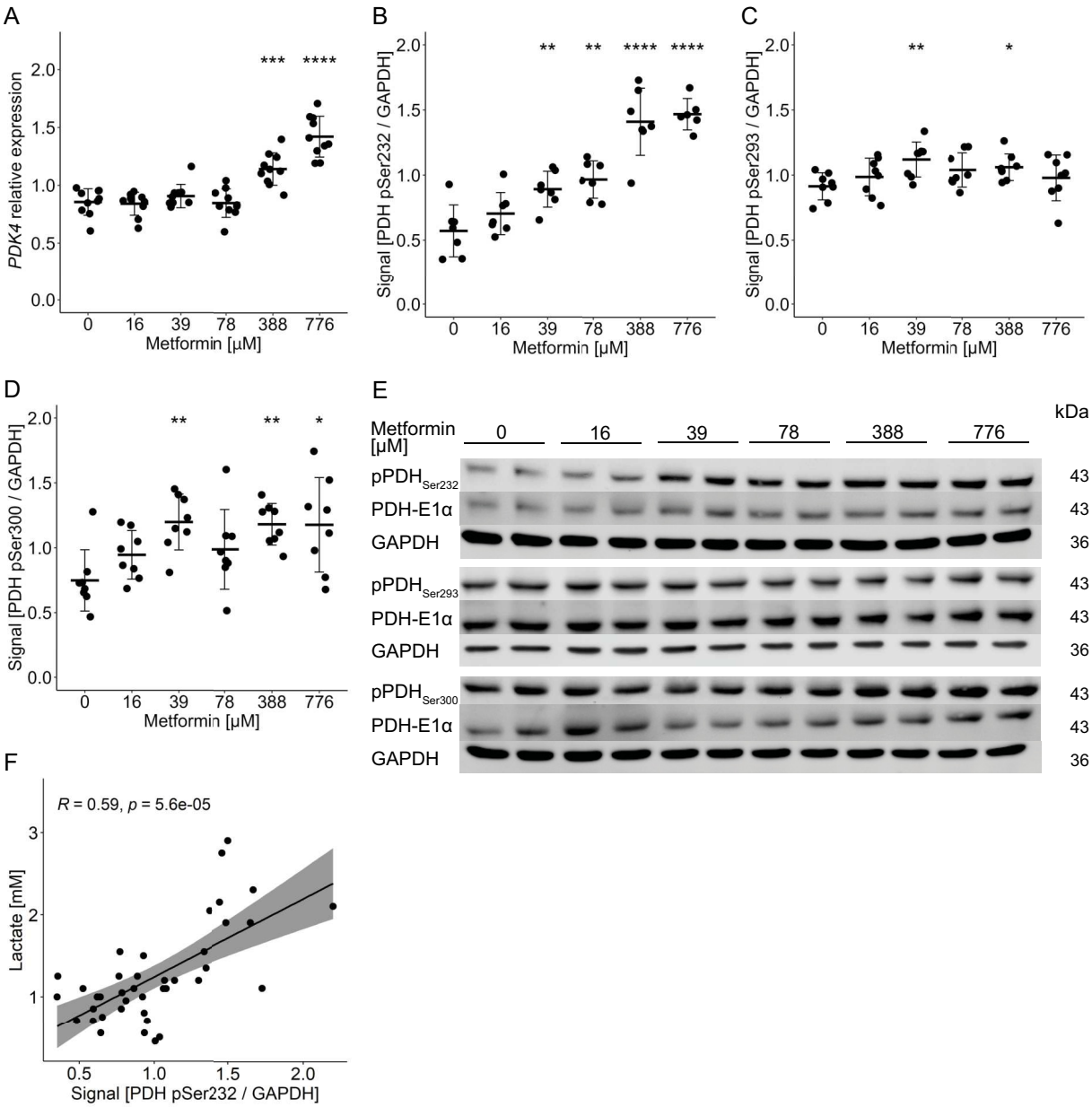

Figure 14: Metformin induces inactivating phosphorylation of the PDH complex.
(A) Metformin effect on the relative expression of *PDK4* was assessed by RNA sequencing (n = 10 donors). All individual data points are displayed; bars represent means ± SD; adjusted p values (Benjamini-Hochberg): ns p > 0.1 , *** p < 0.001, **** p < 0.0001. Quantification of signal intensity of immunoblots using antibodies against phosphorylation sites (B) Ser232, (C) Ser293, and (D) Ser300 of PDH-E1α related to glyceraldehyde-3-phosphate dehydrogenase (GAPDH). All data points represent the mean value of technical duplicates after donor normalization (n = 8 donors); bars represent means ± SD; t-test against 0 µM metformin: ns p > 0.05, * p < 0.05, ** p < 0.01, **** p < 0.0001. (E) Representative immunoblot of one individual donor. (F) Spearman correlation of phosphorylation at Ser232 of the PDH-E1α and cellular lactate production. – *Figure from [156].*

4.5 Metformin administration and acute exercise separately increase human blood lactate levels

Lastly, the question arises as to whether metformin induces lactate production in human and whether the identified metformin effect on pyruvate metabolism can also be confirmed *in vivo*. For this purpose, human blood samples and skeletal muscle biopsies from a recently published study [192] were investigated. In brief, 15 healthy young men received a 17 day metformin treatment in a placebo-controlled cross-over study design with a 4 day washout period in between. The metformin dose was titrated over 8 days until a final concentration of 2 000 mg/day was reached. At the last day of each treatment period, an acute bout of exercise consisting of 45 min cycling at 70% VO_2max was performed. The blood and tissue samples were collected immediately before and after exercise. Analyzing blood lactate levels, a slight increase was observed in the metformin-treated arm at the pre-exercise time point ($p < 0.05$, Fig. 15A). Comparing values at the post-exercise time point, the difference disappeared (ns > 0.05, Fig. 15A), while a more pronounced increase in blood lactate levels was found after completing the acute bout of exercise independently of the drug treatment ($p < 0.0001$, Fig. 15A). Exercise is a strong stimulus of lactate production in human skeletal muscle, suggesting that a potentially preserved metformin-induced increase in blood lactate levels after completion of acute exercise was overwritten by the exercise effect. The metformin effect on pyruvate metabolism was again investigated based on the phosphorylation pattern of PDH complex subunit PDH-E1α by immunoblotting. For all three phosphorylation sites, a reduction in signal intensity was found in the post-exercise samples regardless of placebo or metformin group ($p < 0.01$, Fig. 15B–E). Thus, metformin resulted in no effect on the phosphorylation pattern independent of the sampling time point (ns > 0.05, Fig. 15B–E). These results show that increased blood lactate levels can occur *in vivo* during pharmacological therapy with metformin. Nevertheless, the mechanism described *in vitro* via the inhibition of pyruvate oxidation cannot be transferred to *in vivo* based on these data.

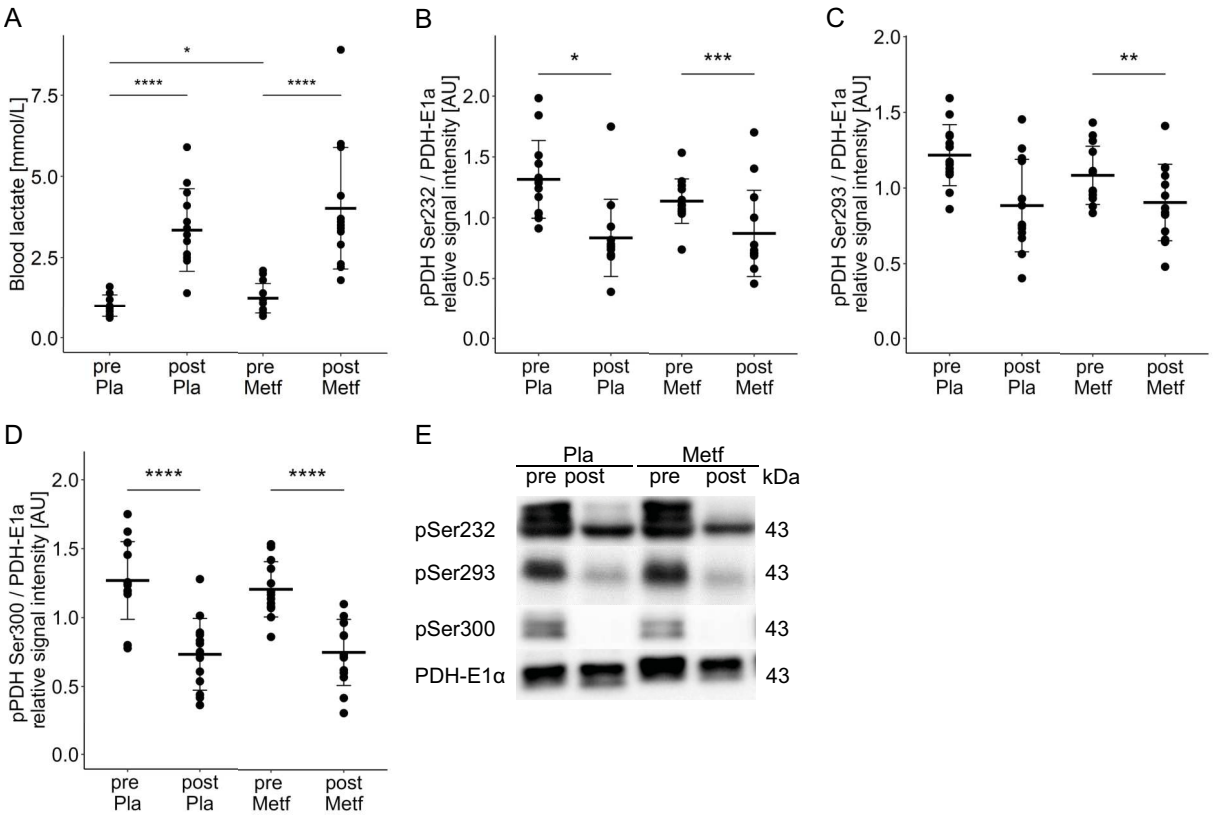

Figure 15: Metformin and acute exercise increase blood lactate levels in human.
(A) Lactate levels were analyzed in blood samples drawn immediately before and after an acute bout of exercise in both placebo and metformin arm (n = 14 donors). All individual data points are displayed; bars represent means ± SD; t-test between groups: ns $p > 0.05$, * $p < 0.05$, **** $p < 0.0001$. Protein lysates from biopsies collected at matching time points were investigated. Quantification of signal intensity of immunoblots using antibodies against phosphorylation sites (B) Ser232, (C) Ser293, and (D) Ser300 of PDH-E1α related to the total amount of PDH-E1α (n = 14 donors). All individual data points are displayed; bars represent means ± SD; t-test between groups: ns $p > 0.05$, * $p < 0.05$, ** $p < 0.01$, *** $p < 0.001$, **** $p < 0.0001$. (E) Representative immunoblot of one individual donor. – *Figure from [156].*

4.6 Summary

The aim of the first part of the thesis was to identify molecular mechanisms that explain how metformin contributes to an increase in lactate production in human skeletal muscle. Primary human myotubes were used as a model to answer the research question. It was shown that there is an increase in lactate production and secretion after intracellular uptake of metformin and that this effect is dose-dependent (Fig. 16). The data indicate that heightened glycolysis covers lactate production. Two mechanisms were identified which contribute to force lactate production through a shift in the equilibrium of LDH reaction (Equ. 4.1):

- Metformin inhibits mitochondrial complex I respiration leading to the accumulation of NADH and thereby shifting the cellular redox state.
- Metformin induces the inhibition of the PDH complex, possibly through an up-regulation of PDK4, resulting in pyruvate accumulation.

Assessing the relevance of the second mechanism *in vivo*, no metformin effect on the phosphorylation of the PDH complex and thereby pyruvate oxidation was found. However, blood lactate levels were increased after 17 days of metformin treatment in healthy young men.

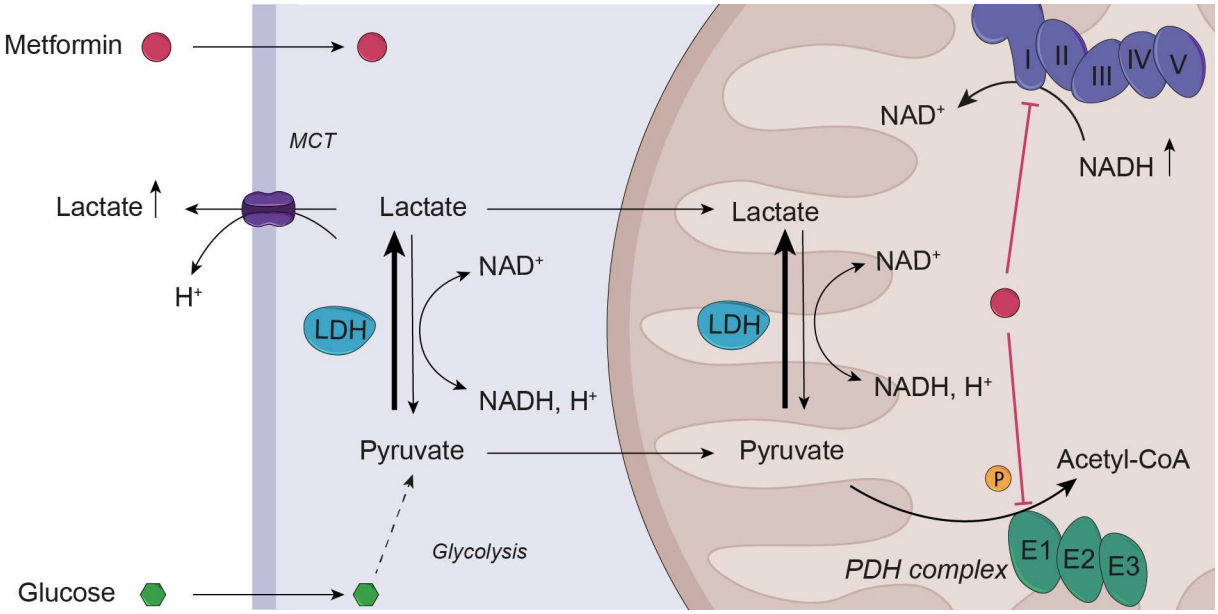

Figure 16: Metformin induces lactate production in human myotubes.
Metformin treatment of primary human myotubes results in increased lactate production and secretion. Two mechanisms were identified which contribute to a shift in LDH reaction toward lactate production. At pharmacological concentrations, metformin induces phosphorylation of the PDH complex resulting in inhibited pyruvate oxidation. At supra-pharmacological concentrations, metformin additionally inhibits mitochondrial complex I respiration leading to an accumulation of NADH.
– *Figure from [156].*

CHAPTER 5

Hypertrophic response and contractility are blunted under metformin treatment in human myotubes

Within this chapter, molecular mechanisms are investigated which may support the clinical observations of negative interactions between metformin therapy and health benefits of exercise, as elucidated in the introduction. As an *in vitro* exercise model, electro-pulse stimulation (EPS) was chosen to address this question. Based on earlier work [47], the cell culture protocol used in the previous chapter (*protocol A*) had to be modified by providing 100 ng/mL IGF1 during a prolonged cell differentiation phase (Fig. 5). This results in visible contracting myotubes under EPS. Unless otherwise stated, the data presented in this chapter was collected using this modified protocol (*protocol B*).

5.1 Metformin-induced down-regulation of transcripts in skeletal muscle is linked to hypertrophy and muscle contraction

In an initial analysis, the RNA sequencing data introduced in the previous chapter (*protocol A*) was examined with regard to metformin-induced muscle-specific changes. A relevant number of 3 049 and 7 208 regulated transcripts was detected for the treatment doses of 388 and 776 µM metformin, respectively (adj.p < 0.1, Fig 17A, upper circle). The data set was filtered for transcripts that are annotated for *skeletal muscle* according to the Human Protein Atlas (Fig. 17A, lower circle). Of the transcripts regulated by 388 and 776 µM metformin 452 and 967 transcripts were skeletal muscle transcripts. Considering a fold-change of $\pm$1.2 as up or down-regulation slightly more transcripts were down-regulated by the high doses of metformin as indicated by the arrows. A gene enrichment analysis of down-regulated skeletal muscle transcripts by 776 µM metformin pointed toward an association with muscle hypertrophy and contractility (Fig. 17B). The transcripts regulated by 776 µM metformin and annotated in the GO term *striated muscle contraction* are shown in the heatmap (Fig. 17C). These data, together with the evidence of weakened hypertrophic response to resistance exercise under metformin treatment [241] suggests an effect of metformin on hypertrophy and contractility, which was examined in more detail.

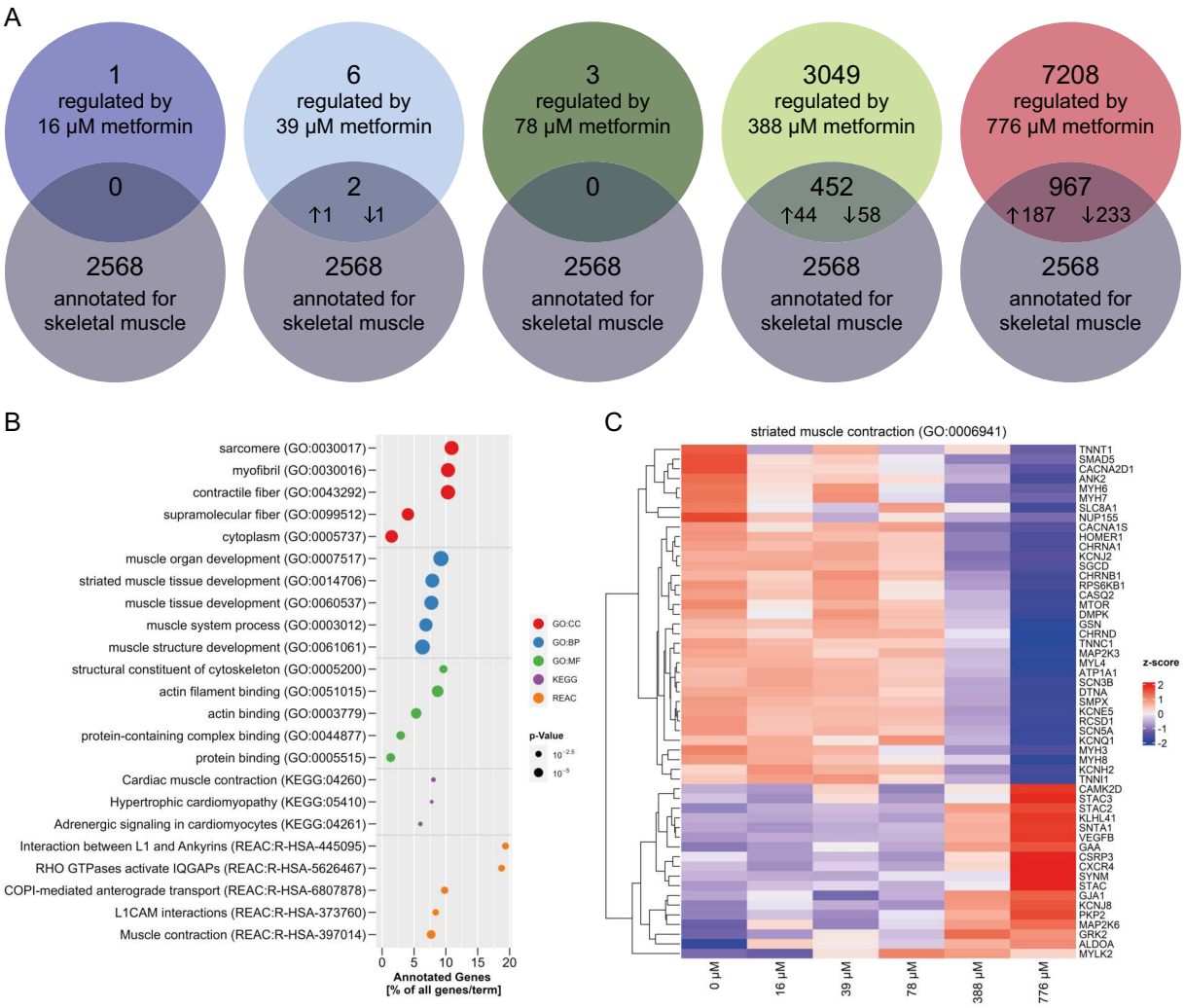

Figure 17: Down-regulation of skeletal muscle transcripts is associated with hypertrophy and muscle contraction.
Analysis of RNA sequencing data of metformin-treated myotubes based on *protocol A* (n = 10 donors). (A) Overlap of regulated transcripts by the indicated treatment dose of metformin with transcripts which are annotated for *skeletal muscle* according to Human Protein Atlas (displayed in the lower circle). The upper circle shows the number of transcripts regulated by the indicated dose of metformin with adj.p < 0.1 (Benjamini-Hochberg). In the overlapping part the number of transcripts found is both data sets is shown and the arrow indicate the number of up and down regulated transcripts by a fold-change of at least ±1.2. (B) GO-term analysis of skeletal muscle transcripts which were down-regulated by 776 µM metformin was performed using gProfiler. The x-axis represents the percentage of regulated transcripts in the total number of transcripts annotated for the corresponding term. A maximum of top five terms by percentage is displayed for each source if a significance level of p < 0.05 was reached. (C) Heatmap showing dose-dependent regulation of transcripts by fold-change (adj.p < 0.1, Benjamini-Hochberg) annotated for the GO-term *striated muscle contraction* (GO:0006941).

5.2 Blunted hypertrophic response under metformin treatment may be mediated by decreased mTOR-S6K1 signaling

Muscle mass homeostasis is maintained by a tight interplay between regulatory pathways of protein synthesis and protein degradation. The Akt/mTORC1 pathway is considered to be the major positive regulator and plays a crucial role in muscle hypertrophy [73, 214]. Metformin decreased the mechanistic target of rapamycin (mTOR) phosphorylation at Ser2448 (776 µM, p < 0.05, Fig. 18A), a site which is associated with mTORC1 and is suggested to be regulated by S6K [40]. In addition,

phosphorylation of the downstream target RPS6 at Ser235/235 was reduced ($\geq$ 338 µM, $p < 0.05$, Fig. 18B) indicating a reduction of mTORC1 activity. Together, these findings suggest, that a blunted hypertrophic response under metformin treatment may be mediated by reduced mTORC1/S6K1 signaling.

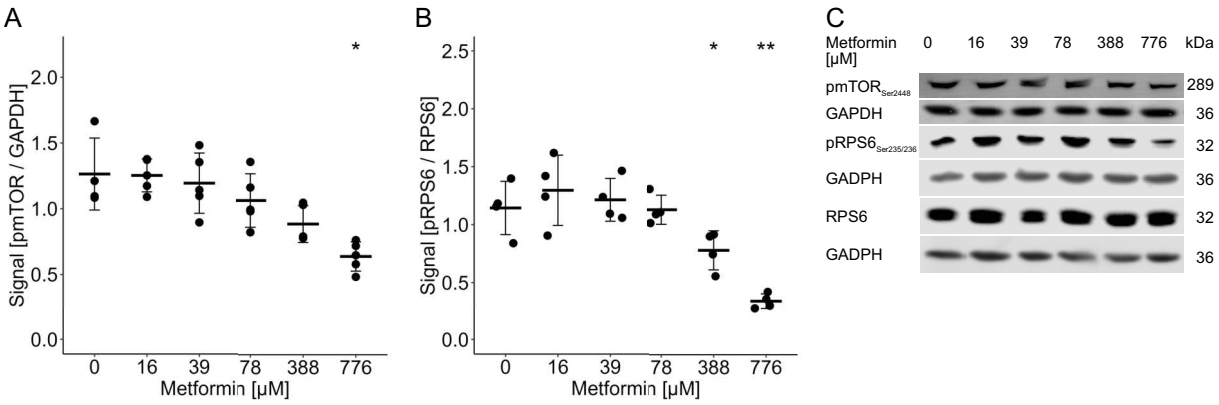

Figure 18: Metformin decreases phosphorylation of mTORC1 and its downstream target RPS6.
Quantification of signal intensity of immunoblots using antibodies against the phosphorylation sites (A) mTOR-Ser2448 (n = 6 donors) and (B) RPS6-Ser235/236 (n = 4 donors) related to GAPDH and RPS6, respectively. (C) Representative immunoblot of one individual donor. All individual data points are displayed; bars represent means $\pm$ SD; t-test against 0 µM metformin: ns $p > 0.05$, * $p < 0.05$, ** $p < 0.01$.

5.3 Metformin interferes with the EPS-induced contraction of primary human myotubes

The influence of metformin on myotube contractility was investigated by applying EPS. A illustrative representation of the experimental setting is shown in Fig. 19A. In brief, differentiated primary human myotubes were treated for 48 h with the indicated doses of metformin. For the last 2 h, EPS was applied. After 10 min, 1 h, and 2 h of stimulation, 3 videos per condition and donor were recorded in randomly selected areas. Visual microscopic observations showed impaired contraction of myotubes treated with high doses of metformin. Quantification of myotube contractility based on an optical block-matching algorithm using OpenHeartWare [91, 215] confirmed a metformin-induced impairment of myotube contraction ($\geq$ 39 µM, $p < 0.05$, Fig. 19B–D). As shown in the upper panel of the representative analysis of untreated control myotubes (Fig. 19E) and 776 µM metformin-treated myotubes (Fig. 19F), in both conditions myotubes visual appear to be normally differentiated. The motion arrows in the quiver plot prove that recognized movement in the control group was detected in areas where myotubes had grown. In contrast, the few arrows in the metformin-treated group were in regions without fully fused myotubes, suggesting the software detected floating particles or air bubbles above the background noise. Furthermore, the motion curve in the lower panel of the control group showed a rhythmic peak pattern matching the stimulation frequency. The left column shows a fully relaxed state with no movement, the middle column shows maximal movement during contraction, and the right column shows movement during relaxation. A similar pattern was missing in the metformin-treated group (Fig. 19F).

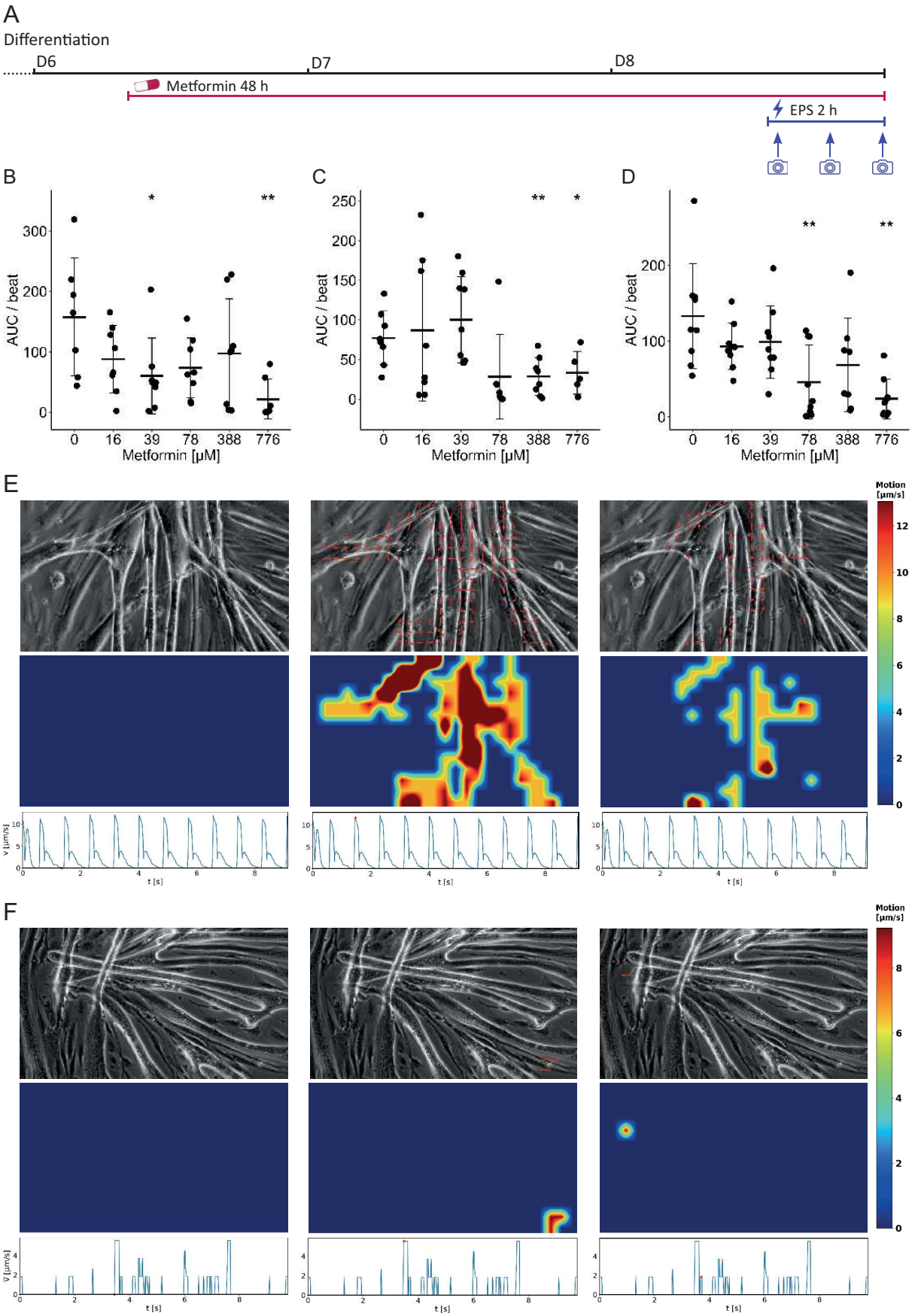

Figure 19: *– continued on next page*

– continued from previous page

Figure 19: Metformin attenuates the contraction induced by EPS in primary human myotubes.
(A) Schematic representation of the chronological sequence of the electro-pulse stimulation (EPS) experiment carried out: EPS was applied to differentiated myotubes for the last 2 h of the 48 h metformin treatment period. Videos were recorded 10 min, 1 h, and 2 h after the beginning of stimulation and were analyzed using OpenHeartWare software. Quantification of myotube contractility after (B) 10 min, (C) 1 h, and (D) 2 h EPS based on an optical block-matching algorithm (n = 4 donors). All individual data points are displayed; bars represent means ± SD; t-test against 0 µM metformin: ns p > 0.05,* p < 0.05, ** p < 0.01). Representative analysis of (E) untreated control cells and (F) 776 µM metformin-treated myotubes of one individual donor after 2 h EPS. The quiver plots in the upper panel show the microscopic view of the selected area with the red arrows indicating the direction of movement detected in the specific frame. The heatmaps in the middle panel illustrate the intensity of movement in the detected areas of the matching frame. The motion curves in the bottom panel express the detected motion over time. The red dot marks the time point of the analyzed frame. The left column shows a frame with no movement detected, the middle column shows a frame with maximal movement, and the right column shows a frame with less movement.

Application of EPS for 10 min prior to metformin administration and visual observation demonstrated that the myotubes were able to contract before starting with metformin treatment (Fig. 20A). Further this short stimulus did not have an impact on the finding that 48 h of metformin treatment impairs myotube contractility (Fig. 20B–D), confirming the previous results.

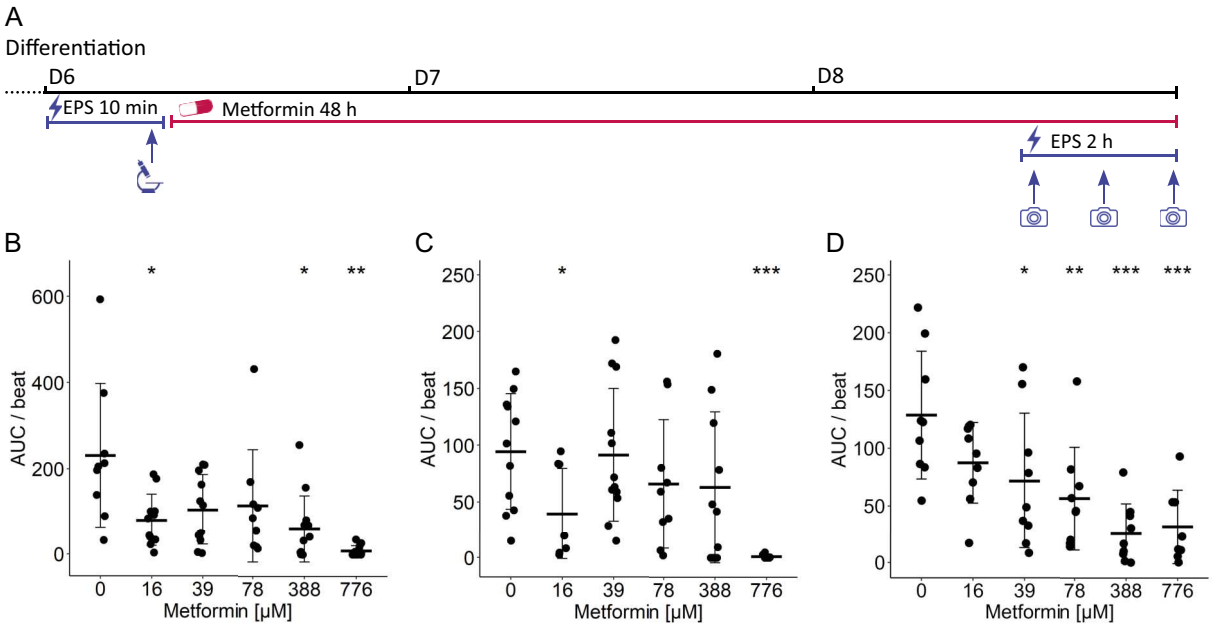

Figure 20: EPS induces myotube contraction prior metformin administration, which impairs contraction.
(A) Schematic representation of a modification of the electro-pulse stimulation (EPS) experiment: before the administration of metformin, EPS was applied for 10 min to control for visual contractility of the myotubes. 2 h EPS was carried out at the end of the 48 h treatment period and videos were recorded as in the previous experiment. Quantification of myotube contractility after (B) 10 min, (C) 1 h, and (D) 2 h stimulation (n = 4 donors). All individual data points are displayed; bars represent means ± SD; t-test against 0 µM metformin: ns p > 0.05, * p < 0.05, ** p < 0.01, *** p < 0.001.

5.4 No evidence of metformin-induced structural changes associated with contractility

The finding that metformin affects myotube contractility raises the question of how this observation can be explained mechanistically. RNA sequencing analysis has shown that the down-regulated

transcripts include several transcripts relevant for structural proteins, like myosin heavy chains and subunits of the troponin complex (Fig. 17C). This leads to the hypothesis that metformin-induced structural changes in the contractile units of human myotubes lead to the impairment in contractility. *Actin binding Rho activating protein (ABRA)* was found to be strongly regulated on transcriptional level by metformin showing a dose-dependent decrease ($\geq$ 388 µM, adj.p < 0.0001, Fig. 21A). The muscle-specific protein located to the I-band of the sarcomere has been reported to regulate actin polymerization involving RhoA-signaling as well as being involved in exercise adaptation, regeneration, and muscle repair [8, 130]. Furthermore, the myosin heavy chains *MHY1*, *MHY2* and *MHY7* were decreased by metformin ($\geq$ 388 µM, adj.p < 0.1, Fig. 21B–D). However, the observed metformin effects on transcriptional level were not confirmed on protein level for ABRA, fast type myosin heavy chain (MHfast) representing MYH1 and MYH2 , and slow type myosin heavy chain (MHslow) representing MYH7 (adj.p > 0.1, Fig. 21E–H). In addition, the immunohistochemical stainings against MHfast and MHslow provided no further evidence of visible structural changes, as the striated pattern appeared undisturbed for all conditions (Fig. 21I,J). Taken together, there was no evidence of metformin-induced changes in structural proteins of contractile units of human myotubes that can be associated with the impaired contractility under EPS.

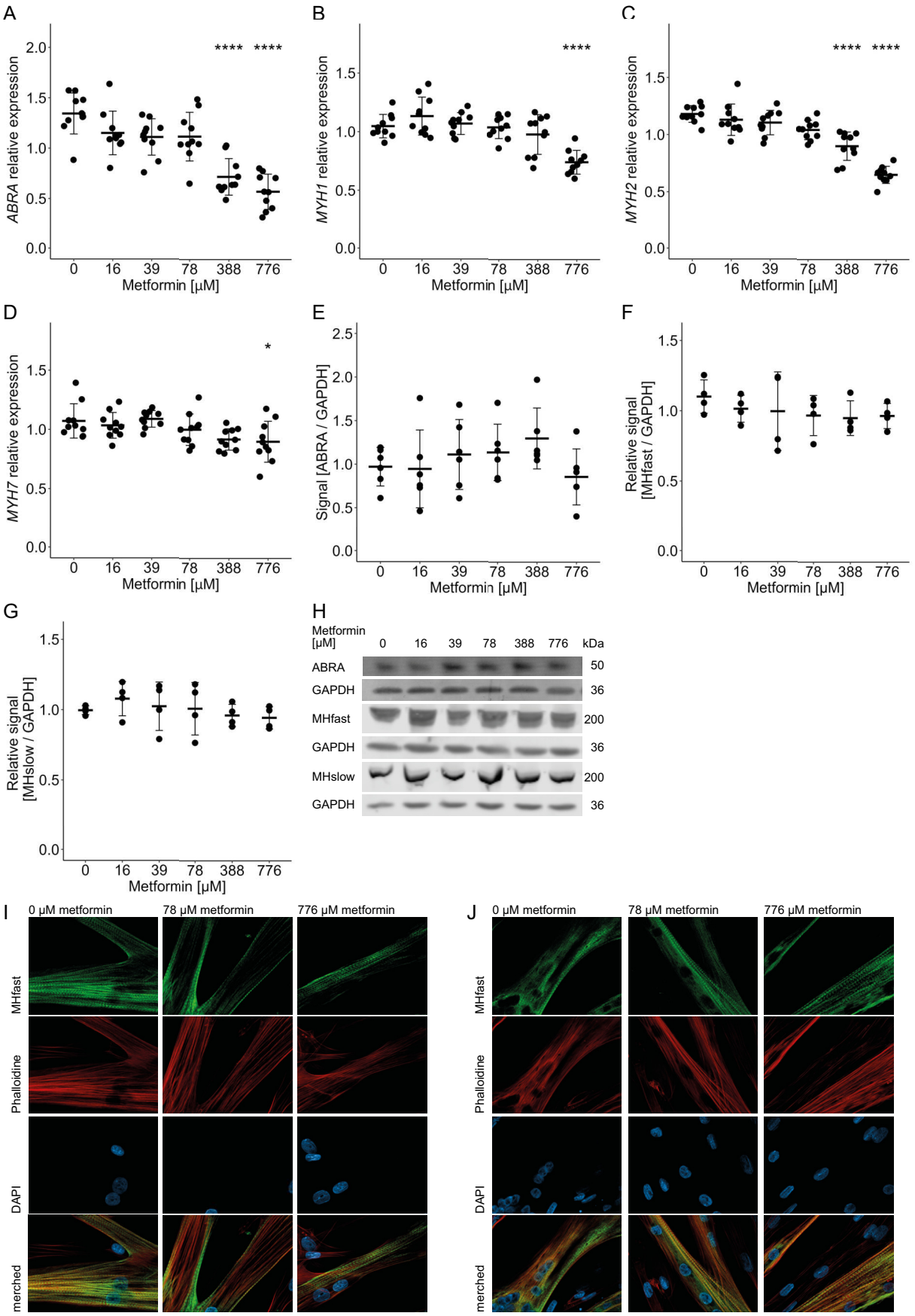

Figure 21: *– continued on next page*

– continued from previous page

Figure 21: No evidence of structural changes associated with contractility.
The metformin effect on selected structural targets was assessed by RNA sequencing. Relative transcriptional expression of (A) *ABRA*, (B) *MYH1*, (C) *MYH2*, (D) *MYH7* are shown (n = 10 donors). All individual data points are displayed; bars represent means ± SD; adjusted p values (Benjamini-Hochberg): ns $p > 0.1$, * $p < 0.1$, **** $p < 0.0001$. Quantification of signal intensity of immunoblots using antibodies against (E) ABRA (n = 6 donors), (F) MHfast (n = 4 donors), and (G) MHslow (n = 4 donors) related to GAPDH. All individual data points are displayed; bars represent means ± SD; t-test against 0 µM metformin: ns $p > 0.05$. (H) Representative immunoblot of one individual donor. Representative images of immunohistochemical staining using antibodies against (I) MHfast and (J) MHslow of one individual donor; x40 magnitude.

5.5 Metformin-induced metabolic changes may lead to cellular lack of energy

In the first part of the thesis it was shown that metformin inhibits mitochondrial complex I respiration, resulting in reduced ATP production and thereby forcing a compensatory increase of glycolysis in order to cover cellular energy demand. Under conditions of heightened energy consumption, as it is the case during EPS, the amount of available ATP might not be sufficient to ensure full functionality of the myotubes. Hence, it is hypothesized that metformin induces a lack of cellular energy causing impaired myotube contractility under EPS. The cellular energy sensor AMPK was activated due to metformin treatment ($\geq$ 388 µM, $p < 0.5$, Fig. 22A,C), suggesting an increase in [AMP]:[ATP] ratio. Further, the phosphorylation of the downstream target ACC increased following metformin treatment ($\geq$ 16 µM, $p < 0.5$, Fig. 22B,C), providing further evidence for the compensation for energy deficiency, in this case by enhancing fatty acid oxidation (FAO). A further Seahorse assay confirmed that metformin also negatively affects ATP production rate in myotubes cultured according to the IGF1-supplemented *protocol B* (Fig. 22D). It was demonstrated that with increasing metformin doses there was not only a shift from mitochondrial to glycolytic ATP production ($\geq$ 16 µM, $p < 0.5$), but also a decrease in the overall ATP production rate ($\geq$ 16 µM, $p < 0.5$). In order to investigate changes in the cellular energy status due to EPS, the adenosine nucleotides AMP, ADP, and ATP were quantified using CE. Based on preliminary results, cell culture medium had to be refreshed two hours before EPS in order to ensure appropriate nutrient supply. Otherwise the AEC was already low in the control group, which did not allow to detect any metformin or EPS-induced changes. Refreshment of medium did not abrogate the impact of metformin on contractility (Suppl. Fig. S3). Using this experimental setup, no changes by both metformin treatment and EPS were found in the concentrations of the three nucleotides in cell lysates (ns > 0.5, Fig. 22E–G). Hence, AEC was not altered and averaged 0.74 ± 0.08 (ns > 0.5, Fig. 22H), indicating a healthy energy status of the myotubes. To conclude, insufficient acute energy supply does not explain the inhibitory effect of metformin on EPS-induced contractility. However, the observed activation of AMPK and reduced ATP production measured in the seahorse assay leave room to debate a long-term effect of metformin on energy homeostasis of the myotubes.

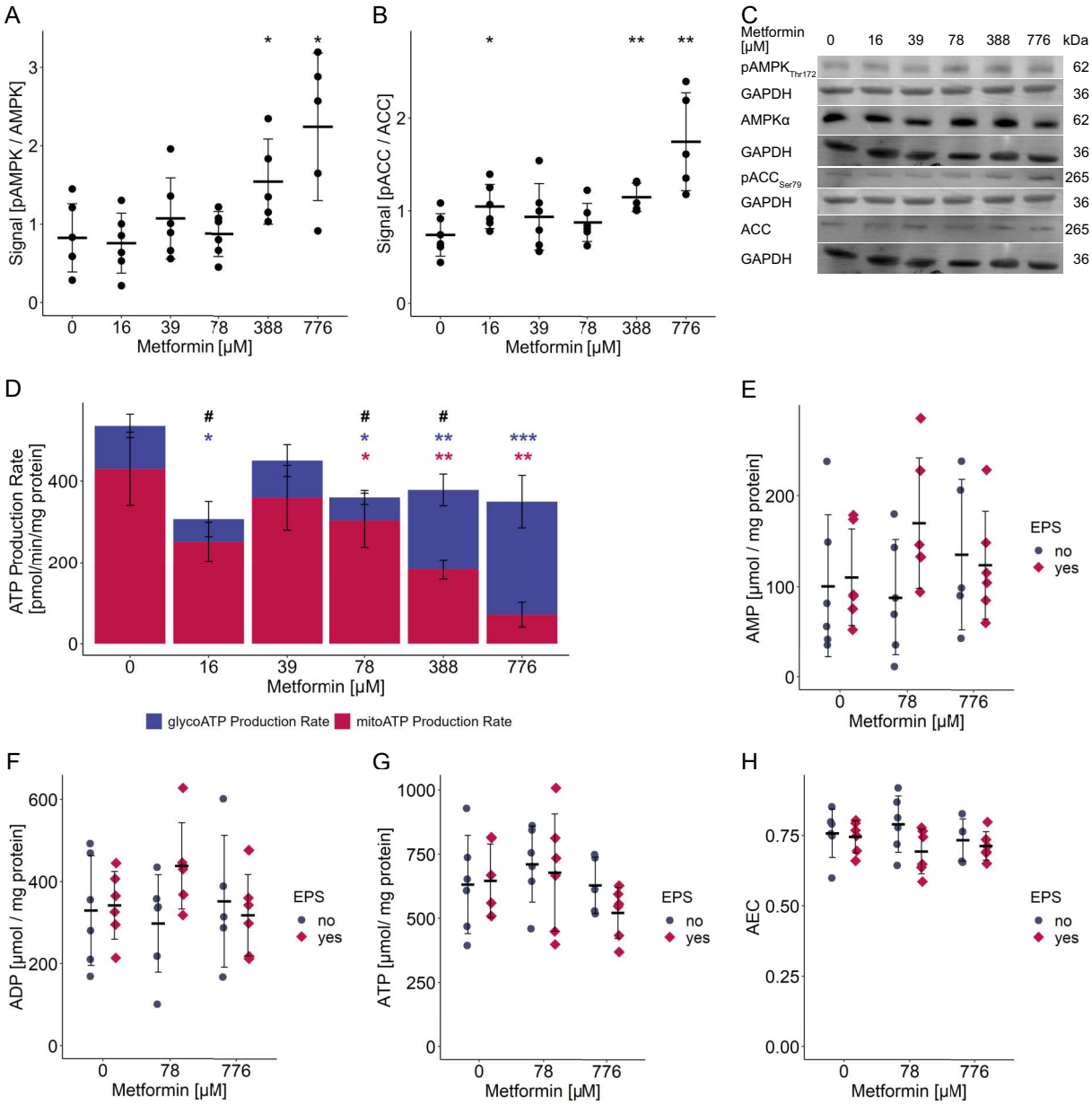

Figure 22: Cellular energy stress is reflected by metformin-induced AMPK activation and reduced ATP production.

Quantification of signal intensity of immunoblots using antibodies against the phosphorylation sites (A) AMPK-Thr172 (n = 6 donors) and (B) ACC-Ser79 (n = 6 donors) related to total AMPK and ACC, respectively. (C) Representative immunoblot of one individual donor. All individual data points are displayed; bars represent means ± SD; t-test against 0 µM metformin: ns $p > 0.05$, * $p < 0.05$, ** $p < 0.01$. (D) ATP production rate was determined using the Seahorse XF Real-Time ATP Rate assay. The step wise addition of oligomycin and a mixture of rotenone and antimycin A allows the distinction between ATP produced via glycolysis (blue) and mitochondrial produced ATP (red) (n = 6 donors). Bars represent means ± SD; paired t-test against 0 µM metformin for each ATP source (*) and total ATP (#): ns $p > 0.05$, * $p < 0.05$, ** $p < 0.01$, *** $p < 0.001$. Quantification of single nucleotides (E) AMP, (F) ADP, and (G) ATP by capillary electrophoresis in metformin-treated myotubes after 2 h of EPS. Values were normalized to total amount of protein in cell lysate (n = 6 donors). All individual data points are displayed; bars represent means ± SD; t-test against 0 µM metformin: ns $p > 0.05$. (H) Calculation of adenylate energy charge (AEC) based on nucleotide determination by capillary electrophoresis. All individual data points are displayed; bars represent means ± SD; t-test against 0 µM metformin: ns $p > 0.05$.

5.6 Summary

The second part of the thesis aimed to identify molecular mechanisms that contribute to clinically described negative interactions between metformin therapy and exercise adaptation processes. It was shown that metformin decreases mTORC1/S6K1 signaling in primary human myotubes, which may result in a reduced hypertrophic response. Further, metformin-impaired EPS-induced contraction of myotubes (Fig. 23). Based on the data shown, there is no evidence that metformin leads to structural changes that affect the functionality of the myotubes. Metformin-induced metabolic changes provide initial evidence that cellular energy stress occurs, which is reflected by the activation of AMPK. Whether reduced ATP production is causing the impairment in contractility could not be conclusively answered from the available data.

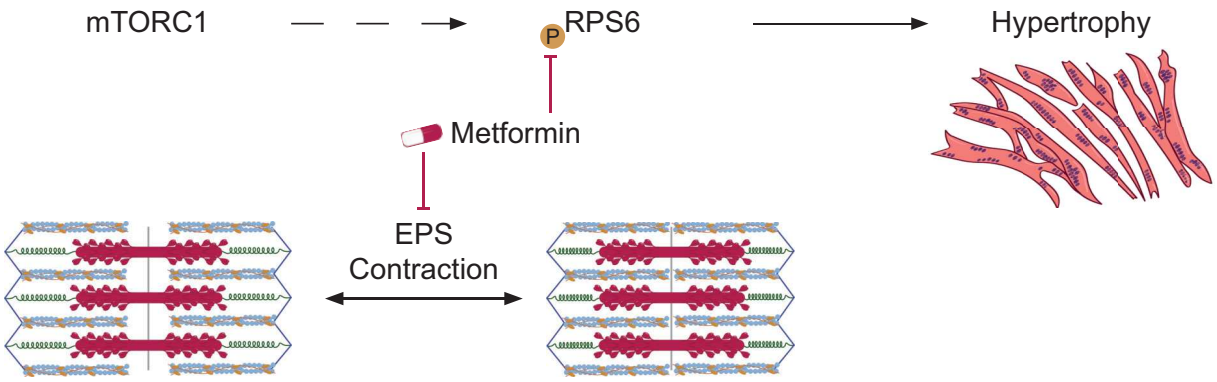

Figure 23: Metformin blunts hypertrophic response and contractility.
48 h treatment of primary human myotubes attenuates mTORC1/S6K1 signaling, which potentially blunts hypertrophic response to exercise. In addition, EPS-induced contraction of myotubes is impaired under metformin treatment.

CHAPTER 6

Discussion

6.1 Experimental vs pharmacological metformin concentrations

Several experimental parameters have to be considered, when interpreting outcomes of *in vitro* studies using chemical compounds as therapeutics with regard to its *in vivo* transferability. These comprise the drug dosage and duration, the route of administration and the model. In the field of metformin research, there is a heated debate ongoing about the experimental metformin concentrations used and the associated transferability and relevance in clinical application.

A systematic literature review by Kajbaf and colleagues [101] on measured metformin concentrations in humans demonstrates that the individually reported plasma concentrations show a large inter-individual variation (1–700 µM), with the high concentrations often associated with hyperlactatemia. LaMoia and Shulman [128] conclude in their work, that the therapeutic plasma concentrations of metformin should be in a range between 10 and 40 µM taking strong individual outliers into account. Comparing the reported human plasma concentrations with the treatment concentrations used in the experiments in this thesis, we assume that 78 µM metformin is in a high but still pharmacological range and therefore might be of clinical relevance.

In addition to the plasma concentrations, however, the biodistribution of the drug must also be considered allowing tissue-specific investigations. For organs such as the liver, where access to biopsy material is challenging, the use of labeled metformin is a good alternative and additionally enables a whole-body assessment of the biodistribution. Oral administration of ^{11}C-metformin in humans reveals pronounced tracer uptake in liver, kidneys and bladder, while low uptake is detectable in the intestine and skeletal muscle [75]. Investigating the tracer activity over time, skeletal muscle shows a gradual increase in activity suggesting a slow uptake and accumulation of the tracer [75]. Consistent with this, a human physiologically based pharmacokinetic (PBPK) model demonstrates that the maximum metformin levels in muscle are reached approximately 2 h later compared to plasma, liver, and intestine (t_{max} = 1.2–2.0 h), as well as that the half-life is prolonged [258].

Patients with T2D receive a therapeutic maximum daily oral dose of 2 000 mg metformin [131], which corresponds to a dose of 25 mg/kg body weight for an average body weight of 80 kg. In comparison, preclinical studies in rodents administrate doses of 200–400 mg/kg body weight [59]. An effective single oral dose in terms of the blood glucose-lowering effect of metformin has been estimated in mice to be approximately 200–250 mg/kg body weight [60, 64, 93, 161]. This discrepancy may in parts be due to a shorter half-life of metformin in mice (1–3 h) compared to human (4–9 h) [39, 100, 212, 257] and underlines that the transferability of results in animal models must always be considered carefully.

The experimental metformin concentrations, which are used *in vitro* range from 0.01 to 200 mM [128]. Assuming metformin added to cell culture medium to represent human plasma levels of metformin, many studies are above pharmacological concentrations with treatment concentrations of $\geq$ 1 mM. With the liver as a major target of metformin, many studies have been conducted in hepatocytes. It should be noted that higher concentrations in this context may still be clinically relevant, as 2 to 3-fold higher concentrations in the portal vein and intracellular accumulation are known to occur *in vivo* [59, 84, 246]. The same could apply to mitochondrial effects of metformin, as it is hypothesized that metformin also accumulates within the mitochondria due to its positive charge under physiological conditions [25, 58, 180].

Regardless whether studies are performed *in vitro* or in animal models, best practice would be to report the intracellular concentrations and plasma and tissue concentrations of metformin, respectively. Therefore, we quantified metformin in the lysates of metformin-treated myotubes and report an increase in the concentrations from 0.66±0.21 to 32.38±8.46 nmol/mg protein corresponding to the amount of administrated metformin. Reference values are provided by ^{14}C-metformin determination in rodent hepatocytes after an incubation time of 2 h to 4 h [4, 164]. Treatment doses of 100 and 200 µM metformin achieved intracellular concentrations of 1–2 ng/mg protein, while a high dose of 1 mM resulted in > 10 ng/mg protein. Hence, the values measured here are in a comparable range suggesting that primary myotubes have a similar metformin uptake rate as primary hepatocytes. Although the slight upward deviations in myotubes may be due to intracellular metformin accumulation during the substantially longer treatment period of 48 h. In relation to the treatment concentration of metformin provided in the cell culture medium, the intracellular uptake was at most 0.82%, well in line with the PBPK model, predicting a maximum uptake of 2% of the administrated metformin dose into any of the tissue compartments including skeletal muscle [258]. Nevertheless, a comparison with intramuscular concentrations would be beneficial. These data are rarely available. Kristensen et al. [118] report intramuscular concentrations in healthy young man after acute treatment (2x 1 500 mg within 4.5 h) of 4.5 µmol/L muscle volume and 9 µmol/L muscle volume after short-term intervention (daily 1 500–2 000 mg over 4 days). The expression of the values in relation to muscle volume allows only a very crude estimation of the exact amount of metformin in relation to muscle protein, which would be necessary for a meaningful comparison with the values measured in primary human myotubes.

Based on these circumstances, the dose-dependent effects of metformin in primary human myotubes were investigated in this thesis. The pharmacological (16–78 µM) as well as the supra-pharmacological range (388–776 µM) was covered in order to be able to estimate the clinical relevance and to include toxic metformin effects in the investigations. A treatment duration of 48 h was chosen to allow for the intracellular accumulation of metformin, as this must not be neglected in view of the long-term medication of patients with T2D.

6.2 Global metformin effects on primary human myotubes

Despite the important role of skeletal muscle in whole-body glucose homeostasis, skeletal muscle has been subject of comparatively few metformin studies. In order to gain a deeper understanding of metformin's effect on skeletal muscle, the dose-dependent transcriptional response in myotubes to metformin treatment was investigated by RNA sequencing analysis. Differentially regulated transcripts were observed at most for the treatment concentrations that we had previously defined as supra-pharmacological (Suppl. Table S4). This contrasts with our observations of increased lactate production and glucose uptake, PDH complex inhibition and impairment of contractility, all of which occurred at treatment concentrations of 38 or 78 µM metformin. Thus, pharmacological doses of metformin interfere with cellular signaling, as evidenced by changes in the phosphorylation pattern of proteins and affects metabolic fluxes represented by the more glycolytic cellular phenotype and increased lactate production. At the same time, these low concentrations were not sufficient to induce transcriptional changes in the myotubes. Previous global investigations of metformin-induced transcriptional changes have been performed in fibroblasts, hepatocytes and intestinal cells using concentrations of 0.5 mM and higher [68, 143, 252], so we are not aware of comparable data at similarly low concentrations as in our approach. Therefore, it can only be speculated that the transcriptional changes observed at high concentrations are of a compensatory origin. This hypothesis is supported by the enrichment analysis carried out (Suppl. Fig. S5), which revealed predominantly rather unspecific terms, such as *cytosol*, *protein metabolic process*, and *enzyme binding*. We found no evidence suggesting a cellular stress response or apoptotic processes induced by the supra-pharmacological metformin concentrations. This is consistent with the observations that the treated

myotubes did not show visible changes in morphology with any of the doses used and appeared to tolerate them well. In support, studies using up to 10-fold higher concentrations of metformin [52, 189, 185] report no tremendous toxic effects on the cells either.

6.3 Increased lactate production under metformin: toxic or therapeutic?

The first part of the thesis provides evidence for dose-dependent metformin-induced lactate production of primary human myotubes along with a shift toward a glycolytic phenotype. Of note, we determined secreted lactate in the supernatant, but the metformin-induced increases in glucose consumption and glycolysis, as well as the slight drop in the glucose:lactate ratio, point to an increase in lactate production as the driver for the increased lactate secretion. While other studies reporting increased lactate production in myotubes used metformin concentrations of 2–10 mM [179, 251], the effect was observed at concentrations 20- to 100-fold lower ($\geq$ 78 µM) within this work. In line, Brunmair et al. [28] achieved an increase in lactate production in isolated rat soleus muscle by using similar low concentrations of 90 µM. Metformin-induced lactate production does not appear to be a muscle-specific effect, as comparable increases in lactate production have also been described for hepatocytes [52, 180, 251], adipocytes [167] and human platelets [189, 195]. Again, the effective concentrations were in the millimolar range, indicating that *in vivo* it may be primarily organs that reach high intracellular metformin levels, such as the liver and intestine, that play a role in increased lactate production. This assumption is supported by a 16-week study in patients with T2D, which shows no increased release of lactate from the skeletal muscle after metformin administration [224]. Nevertheless, Protti et al. [196] aimed to investigate toxic metformin effects and measured increased lactate concentrations in the muscle interstitium of pigs infused with high concentrations of metformin (300 nmol/min). It is interesting to note that the plasma lactate levels hardly changed in the animals, which leads to the speculation that lactate either has a local function or that a high lactate clearance rate counteracts an increase in plasma.

Apart from the toxic effects of metformin leading to hyperlactatemia and metabolic acidosis, data on physiologically elevated plasma lactate levels in humans under metformin treatment remain controversial. Multiple studies report no effects of metformin on plasma lactate levels in patients with T2D [42, 46, 224]. Huang et al. [90] conclude in their review article that plasma lactate levels of patients showing no comorbidities are at most slightly elevated. At the same time, a community-based study found modest heightened plasma lactate levels by an average of 0.28 mmol/L in patients with T2D [44]. In line, we report a metformin-induced increase in plasma lactate levels by an average of 0.21 mmol/L (placebo: 1.10 mmol/L, metformin: 1.31 mmol/L) in a cohort of healthy young men. Although the values under metformin were elevated, they are still within a range considered physiological of 0.5 to 1.5 mmol/L lactate under resting conditions [2, 255]. During exercise, lactate levels can increase significantly, with studies showing that lactate concentrations in plasma can reach up to 25 mmol/L during intense physical activity [30, 74], mainly released from skeletal muscle [99, 235]. In our human intervention study, the metformin-mediated difference in plasma lactate levels was equalized after an acute bout of exercise. We attribute this to the fact that exercise strongly stimulates lactate production in skeletal muscle and overrides the metformin effect. In summary, while there is some evidence suggesting a potential increase in plasma lactate levels in a physiological range with metformin use, the overall impact of metformin on plasma lactate levels in patients with T2D remains inconclusive.

Regardless the source of lactate, the slight chronic increase in plasma lactate levels has been discussed as mediator of some of the pleiotropic effects of metformin *in vivo* [67]. Many of the mechanisms of metformin described so far are related to energetic changes in the cells. Lactate in its role as an energy precursor might help to compensate for the deficits caused by metformin

or under conditions of high energy demand. The direct uptake of circulating lactate and subsequent oxidation allows organs like the heart, kidneys and brain to be rapidly supplied with energy, bypassing glycolysis and avoiding potential harmful byproducts. Thereby lactate could contribute to the cardio-, reno-, and neuroprotective effects of metformin [67]. Lactate may in addition act as a signaling molecule activating the GPR81. Physiological lactate concentrations are sufficient to partially activate the receptor [226], thus chronically elevated plasma lactate levels under metformin could enhance the activation. In a study demonstrating the involvement of GPR81 in hepatic lipid homeostasis, metformin has been shown to up-regulate GPR81 expression in hepatocytes and to rescue obesity-induced suppression of the receptor [248]. The authors link these effects to the lactate accumulation they observed.

Although elevated plasma lactate concentrations may be therapeutic, they are at most negatively associated with metformin therapy and the occurrence of life-threatening hyperlactatemia and metabolic acidosis. Of note, this side effect is not exclusively mediated by metformin, but also by other substances of the biguanide class, like phenformin [124]. Comparing both biguanides, studies demonstrated increased lactate production as a response to mitochondrial dysfunction in hepatocytes [50, 96]. Phenformin has been withdrawn from market due to its higher risk for developing severe hyperlactatemia and metabolic acidosis. Unlike metformin, phenformin undergoes liver metabolism primarily by CYP2D6, leading to accumulation in poor CYP2D6 metabolizers and subsequent toxic effects [254]. In comparison, accumulation of metformin causing clinically relevant hyperlactatemia and metabolic acidosis under metformin usually occurs in the presence of comorbidities or is due to an overdose [126, 234]. In particular, impaired kidney function is associated with an increased risk of hyperlactatemia and metabolic acidosis [54], suggesting that impaired metformin clearance causes high drug concentrations, which are required *in vivo* to induce a relevant increase in lactate production. Toxic metformin concentrations in plasma are determined to be up to 650 µM [126], which is in a range where we also observe increased lactate production in human myotubes.

Finally, to our knowledge it is still unclear, which tissues contribute to metformin-induced lactate production in a toxic scenario. The current data suggests that the skeletal muscle can contribute to enhanced lactate production at high, mostly toxic metformin concentrations *in vivo*. At pharmacological concentrations, recent *in vivo* studies demonstrated that metformin induces intestinal lactate production [203, 228] suggesting the gut to be a source of the slightly elevated plasma lactate levels. Nevertheless, further investigations are required.

6.4 The glycolytic phenotype of metformin-treated myotubes

An increase in skeletal muscle glucose uptake might contribute to the hypoglycemic effect of metformin. Enhanced glucose uptake by metformin treatment is described in various muscle cell lines [43, 121, 163, 210, 211], which in C2C12 cells affects basal glucose uptake but not insulin-stimulated glucose uptake with comparatively low concentrations around 500 µM [43, 121]. In line, we report an increased glucose uptake of metformin-treated myotubes measured as 2-DG uptake at 388 µM or higher. The positive correlation with the secreted lactate in combination with a nearly 1:2 stoichiometric ratio of glucose:lactate, suggests that the increased lactate production was driven by an increased glycolytic flux. In metformin-treated macrophages, lactate is produced via glycolysis from ^{13}C-glucose, which is then further converted to lactoyl-phenylalanine (Lac-Phe) [250], previously known to be exercise-induced and recently shown to be increased in plasma of humans after metformin administration [216, 250]. Even though little is known about the physiological role of Lac-Phe in the human body, the authors provide initial insights into a possible connection with the weight-reducing effect of metformin [250] and present another example of positively associated metformin-induced lactate production.

An increase in cellular glucose uptake may suggest, that there is an altered abundance of the

major muscular glucose transporters GLUT1 and GLUT4. The RNA sequencing data suggest that the expression of the two transporters is slightly affected by high concentrations of metformin, but this effect is not reflected at the protein level. Of note, a limitation of the myotube fusion *protocol A* is a low ratio of GLUT4 to GLUT1 protein levels, which does not reflect the *in vivo* situation correctly [1]. Based on this fact, the insulin-dependent uptake of 2-DG was not investigated. Consequently, protein levels of the glucose transporters were investigated in fused myotubes according to *protocol B*, where it was recently demonstrated that supplementing IGF1 during differentiation enhances GLUT4 abundance [47]. Since there are indications from studies with *ex vivo* metformin-treated muscle strips from human subjects, that insulin-dependent glucose uptake can also be influenced by metformin [66, 65], it is of interest to follow up this topic by using our improved fusion protocol.

6.5 Mechanisms of metformin-induced lactate production

Having demonstrated that metformin enhances lactate production in human myotubes in a dose-dependent manner, the question arises as to which molecular mechanisms can explain this observation. Increased lactate production in myotubes could be mechanistically linked to a dual mechanism involving inhibition of complex I respiration, resulting in increased NADH levels, and reduced PDH complex activity, leading to elevated intracellular pyruvate levels, collectively driving a shift in the LDH reaction toward lactate production.

Since the inhibitory effect of metformin on mitochondrial complex I respiration was demonstrated for the first time in two independent research groups [52, 180], the effect has been confirmed in several species, tissues and cell lines [25, 28, 189]. Again, studies using human samples are rare, but concentrations above 3 mM metformin in an *ex vivo* titration experiment of permeabilized muscle fibers from healthy subjects confirm the dose-dependent inhibitory effect on complex I respiration [132]. However, the clinical relevance of complex I inhibition is debated based on the fact that supra-pharmacological concentrations were used in the respective *in vitro* studies [57, 237]. Contrasting findings are reported in hepatocytes where low micromolar concentrations exhibit an opposing effect [243], albeit not consistently observed in C2C12 myoblasts [185]. Further, the clinical relevance is challenged by the finding that human muscle fibers from chronically metformin-treated (2 000 mg/day) patients with T2D show comparable mitochondrial respiration as the healthy control group [132]. In accordance with most of the literature, we observed inhibition of complex I respiration in human myotubes after treatment with supra-pharmacological 776 µM metformin. Additionally, we confirmed the findings that metformin does not diminish mitochondrial protein abundance [117, 244], thus indicating that the attenuation of complex I respiration is not attributable to alterations in mitochondrial content or reduction in complex I protein levels. An argument that supports the relevance of the high metformin concentration in relation to complex I inhibition is the demonstration that metformin accumulates in the mitochondria [25]. This may explain why higher inhibitory concentrations tend to be required when studying metformin effects on complex I in isolated mitochondria compared to studies using intact cells. It has not yet been conclusively investigated how complex I is inhibited by metformin, but Bridges at al. [25] describe the binding of metformin to the amphipathic region of the complex, which in turn suggests that intramitochondrial metformin levels would be critical for the effect. It would therefore also be valuable here to determine not only the intracellular but also the intramitochondrial concentrations. In hepatocytes, this determination was carried out after treatment with 500 µM metformin, but the cytosolic fraction shows the largest proportion of metformin [243]. Nevertheless, they demonstrated inhibition of complex I respiration and are thus in comparable concentration ranges as in this work.

It has been recently demonstrated in hepatocytes and C2C12 cells, that the inhibition of mitochondrial complex I by rotenone decreases the cellular NAD^+/NADH ratio and this effect is associated with increased lactate production [88]. In line, we observed a dose-dependent decrease in the

NAD^+/NADH ratio of metformin-treated myotubes in support of complex I inhibition. The influence on the ratio was driven by the increase in cellular NADH. We attribute the fact that we were unable to measure an effect on the NAD^+ concentration to technical limitations of the assay used. The physiological ratio of NAD^+ to NADH is a factor 10–20 in skeletal muscle [245], and was in case of the investigated myotubes a factor of 20–30, so that the assay sensitivity might be insufficient to detect minor changes in the NAD^+ levels.

Although we provide evidence that metformin mediates its effect on lactate production by inhibiting mitochondrial complex I, the discrepancy remains that we observe increased lactate production already at 78 µM metformin, whereas complex I inhibition only occurs at 776 µM. If clinically relevant, this mechanism will probably only play a role in terms of toxic metformin effects.

At lower metformin concentrations increased lactate production can be caused by the second mechanism we describe, which is the inhibition of the PDH complex. The PDH complex serves as a central metabolic node that governs pyruvate oxidation and plays a critical role in cellular energy metabolism [182]. The activity is finely regulated through posttranslational modifications, including phosphorylation and dephosphorylation of its subunits, primarily the E1α subunit [198]. We report enhanced phosphorylation of the three serine sites 232, 293 and 300 of the PDH-E1α subunit using pharmacological concentrations of metformin ($\geq$ 39 µM). In addition, the degree of phosphorylation at the Ser232 site showed a positive correlation with the amount of lactate secreted by the myotubes.

There is *in vivo* evidence for metformin-induced changes in pyruvate metabolism on transcriptional level from a human placebo-controlled study [119]. Here, muscle biopsies from older subjects with impaired glucose tolerance (mean age 71 years; IGT based on oGTT) were analyzed by RNA sequencing after a 6-week treatment period with 2 000 mg/day metformin. Differentially regulated genes were associated with pyruvate metabolism based on an enrichment analysis. In line, we found not only *PDK4* up-regulated in human myotubes, which is a prevalent isoform of PDKs in myotubes and skeletal muscle [23, 79, 207], but also increased phosphorylation at the three regulatory serine sites of the PDH complex subunit E1α. Different from human myotubes, we observed no effect of metformin on the phosphorylation pattern in human muscle biopsies obtained from healthy young men, albeit these subjects showed slightly elevated lactate levels under metformin treatment. The subjects performed in addition an acute bout of exercise at the end of the 17 day metformin intervention. Exercise is a known physiological stimulator of the PDH complex, which is due to an increased activation of PDH dephosphatases by increased Ca^{2+}, free ADP, and pyruvate concentrations [221], and is associated with diminished PDH phosphorylation [115]. In line, we found a reduction of the phosphorylation at all three serine sites in the muscle biopsies collected post-exercise, regardless of previous metformin treatment. Taken together, there is contrasting data with regard to the involvement of pyruvate metabolism in metformin-induced lactate production in human skeletal muscle. Whether the metformin-induced transcriptional changes observed in human myotubes and *in vivo* [119] affect post-translational modifications like protein phosphorylation *in vivo* remains unknown. Therefore, further studies are warranted to clarify whether the novel described mechanism of metformin-induced inhibition of the PDH complex is of pharmacological relevance in human skeletal muscle.

6.6 Further development of the cell culture protocol: are metformin effects influenced by IGF1?

Human myotubes differentiated in serum-free cell culture medium according to *protocol A* show a decisive limitation. They do not reach full functionality with regard to visible contraction during EPS. However, to investigate interactions between metformin and exercise adaptation processes *in vitro* in the second part of the thesis a model of contractile human myotubes must be used. At the time of the first part of the thesis, *protocol B* was established in our laboratory, where the addition of

100 ng/mL IGF1 during differentiation resulted among other improvements toward a striated muscle phenotype in visible contracting myotubes [47]. Except RNA sequencing data, which were already collected within the the first part of the thesis, all measurements aiming to investigate interactions between metformin and exercise adaptation processes are relied on *protocol B*.

IGF1 is a key regulator of muscle growth and maintenance [256] and exercise is a potent stimulus of muscular IGF1 expression and increases circulating IGF1 levels [108, 116, 261]. Physiological human plasma levels are in a range of 100–150 ng/mL [5, 236], comparable to the amount of IGF1 we supplied in cell culture. The addition of the growth factor with the differentiation medium goes along with some cellular changes of the myotubes [47]. First, expression of GLUT4 is increased, allowing higher insulin-dependent glucose uptake. Second, oxidative phosphorylation contributes stronger to ATP production and in line the abundance of proteins typically higher expressed in oxidative muscle fibers is increased. Third, proteins of the contractile apparatus, sarcoplasmic Ca^{2+} release and energy supply are enhanced, laying the groundwork for contractility in response to electrical pulses.

IGF1-induced changes may interfere with metformin effects on the myotubes. Based on our visual observations, the IGF1-differentiated myotubes tolerated all the metformin doses we used equally well and comparable with *protocol A*. Comparing the basal expression of potential metformin transporters, IGF1-differentiated myotubes show a higher abundance in transcripts of most of the transporters (Suppl. Fig S6A) in line with overall heightened translational activity in IGF1-differentiated myotubes (unpublished data). In both protocols, *SLC29A4* and *SLC47A2* are the most abundant transporters for cellular uptake and release, respectively. The dose-dependent increase in lactate production and glucose consumption by metformin in both protocols is highly comparable reaching extracellular lactate concentrations of 2.97 and 2.82 mM, respectively (Suppl. Fig S6B,C). In untreated myotubes, the basal ratio of glucose:lactate is slightly higher with 0.74 vs 0.64 in IGF1-differentiated myotubes (Suppl. Fig. S6D), well in line with the shift toward a more oxidative phenotype. Thus, the data did not suggest an increased uptake or effectiveness of metformin in IGF1-differentiated myotubes. It would have been interesting to investigate how the more pronounced oxidative phenotype of IGF1-differentiated myotubes affects the metformin-induced inhibition of complex I, since glycolytic ATP production dominates in myotubes differentiated without IGF1.

6.7 Blunted hypertrophic response under metformin: Is resistance exercise still effective?

Accounting for around 40% of the total body mass [97], the skeletal muscle is the largest organ of the human body and plays a crucial role in metabolic processes, energy expenditure and motion. Hence, maintaining muscle mass homeostasis is crucial for quality of life, and decreases in muscle mass and strength can serve as significant predictors of mortality [138, 173]. Diabetes is associated with a loss in muscle mass and strength, particularly in older adults with T2D compared to those without [136, 183], in addition to the decrease in muscle mass as part of the natural aging process. Metformin treatment of human myotubes induced a down-regulation of skeletal muscle transcripts, which are associated with hypertrophy.

Regular physical activity and in particular resistance exercise training has been shown to play a significant role in maintaining muscle mass homeostasis involving a complex interplay of mechanisms, including mechanical stimuli, metabolic stress, and secretion of hormones and growth factors, all of which can influence translational and transcriptional control of muscle mass homeostasis [20, 51, 214]. As a pro-hypertrophic pathway, the PI3K-Akt-mTOR signaling pathway plays a central role in the control of muscle protein synthesis and gets activated in the contracting muscle [73]. For this reason, we focused on metformin effects on mTORC1 at the protein level. We observed reduced phosphorylation of mTOR-Ser2448, a site linked to mTORC1 and suggested to be controlled by S6K [40]. In line, the downstream target RPS6 showed diminished phosphorylation, which

suggests that metformin can have a negative effect on the hypertrophic response in myotubes by blunting mTORC1/S6K1 signaling. The second down-stream target eukaryotic translation initiation factor 4E binding protein 1 (4E-BP1), which upon phosphorylation by mTORC1 promotes protein synthesis, was not investigated in the thesis.

At this point it should be mentioned that IGF1 is a known mediator of muscle hypertrophy by activating the PI3K-Akt-mTOR signaling pathway through binding to its receptor IGF1R [256]. This raises the question of whether metformin reverses the hypertrophic effects of IGF1 resulting in the diminished phosphorylation of mTORC1 and RPS6. However, we observed the same metformin effects in myotubes cultured according to *protocol A* in preliminary experiments, suggesting an IGF1-independent mechanism. Based on previously described mechanisms of metformin in skeletal muscle, it can be speculated that the metformin-mediated activation of AMPK could be underlying the reduced activation of mTORC1 [169, 241], since activation of AMPK can switch off mTOR signaling [72]. Consistent with this, we also show an increased dose-dependent activation of AMPK.

The inhibitory effect of metformin on mTORC1 is already described in non-muscle cell culture or in mice. Hepatic mTORC1 activity in mice was reported to be impaired in a dose-dependent manner, which involves AMPK and TSC complex at low doses (500 µM in hepatocytes) while alternative upstream targets seem to be of relevance at higher doses ($\geq$ 1 mM) [89]. Consistent with this, TSC/AMPK-independent suppression of mTORC1 activity was reported in fibroblasts subjected to high-dose metformin treatment (10 mM) [102]. In addition, there is an entire field of research that examines metformin in cancer therapy and should only be mentioned briefly here. The inhibition of mTOR by metformin has been associated with impaired cancer cell growth and migration, and has been shown to sensitize cancer cells to chemotherapy by targeting the mTOR pathway, suggesting its potential as an adjuvant therapy in cancer treatment [188].

In vivo evidence for a reduced hypertrophic response in muscle of metformin-treated subjects derives from the MASTERS trial [142, 241]. In this placebo-controlled study subjects at an average age of 70 years underwent 14 weeks of resistance training and thereby improved lean body mass, as well as thigh muscle mass, density and area. These parameters, indicating a hypertrophic response to the exercise stimulus, are attenuated in the metformin-treated cohort (1 700 mg/day). Further, in muscle biopsies the activation of AMPK is increased by metformin along with a trend for blunted phosphorylation of mTORC1. Hence, mTORC1 can be a target of metformin in human skeletal muscle, even if we observed the effect in myotubes only at supra-pharmacological concentrations. Additional transcriptomic analysis of the muscle biopsies from the MASTERS trial reveal that the exercise-induced up-regulation in a large number of ECM transcripts is dampened by metformin, which potentially also contributes to impaired muscle growth [120]. Further investigations are particularly important in view of the fact that half of patients with T2D are at an age of 53 to 75 years when they are first diagnosed [95], meaning that the age-related reduction of muscle mass as a physiological process has already begun [106] and regular physical activity as a counter-regulatory intervention becomes more important than ever. If necessary, consideration should be given to whether regular exercise and simultaneous metformin administration should be recommended for a certain population. Special attention should also be drawn at this point to the consideration of using metformin as a potential anti-aging drug.

Beside muscle hypertrophy, a gain in muscle strength is another important health-promoting effect of mainly resistance exercise. While Boulé et al. [21] report that metformin only blunts a gain in muscle mass without affecting muscle strength in response to a 22-week resistance exercise intervention, the MASTERS trial [241] report a trend toward reduced improvement in muscle strength along with impaired hypertrophy. This aspect cannot be investigated with the 2D monolayer culture of primary human myotubes used to date. A promising tissue engineering approach is the recent development of so-called myobundles as a 3D culture in which the myofiber is to be simulated by linearly aligned myotubes [107, 147]. Here it is possible to use force sensors at both ends of the

myobundle to measure the force during contraction induced by an electrical pulse. This model could therefore be used in the future to carry out metformin treatment and determine the influence on force development.

In summary, by demonstrating an impaired mTORC1/S6K1 signaling in metformin-treated myotubes we provide a mechanistic suggestion for how metformin may lead to an attenuated hypertrophic response in skeletal muscle and thus may have an influence on exercise adaptation processes, particularly to resistance exercise. Whether the interaction between metformin and exercise concerns only the increase in muscle mass or affects other aspects remains to be elucidated.

6.8 Electro-pulse stimulation as *in vitro* exercise model

EPS was established as a model during the last decades to mimic muscle-specific exercise-mediated effects in cell culture. By inserting electrodes that emit short electrical pulses into the cell culture medium, the *in vivo* function of motor nerves is simulated and the calcium release required for contraction is induced [63, 153, 213]. Exercise-induced effects on skeletal muscle like increased oxidative capacity and glucose metabolism, enhanced translation associated with skeletal muscle hypertrophy and secretion of cytokines can be induced by EPS [174]. Impaired contractility in response to EPS was already observed in metformin-treated myotubes at the lowest concentration of 16 µM. In order to systematically examine this initially visual observation, videos were analyzed using OpenHeartWare [91]. The software was initially developed for the investigation of cardiomyocyte contractility to calculate the beating motion in µm/s. Based on the underlying block-matching optical flow algorithm, the accuracy and thus the informative value of the generated beating kinetic curve is highly dependent on the quality of the input video and require high frames per second (fps). We used the highest possible 60 fps technically available to us to record the videos. This allows us to achieve a suitable visualization of the beating kinetics with a beating rate that matches the rate of electrical pulses applied. The results of the video analysis, which show an almost complete absence of the contraction peaks in the motion curve of metformin-treated myotubes ($\geq$ 39 µM), are consistent with the visual observation of a lost contraction during EPS. Whether even lower metformin concentrations cause already changes in beating kinetics that are not associated with inhibition of contraction, such as a shift in contraction or relaxation time, are not accessible by the obtained data. However, this could be an important question, especially with regard to transferability of the results to the *in vivo* situation and should be addressed in a follow-up experiment. For this purpose, an even higher number of fps of the recorded videos should be chosen to accurately determine the timing of maximum deflection and reaching the resting state as precisely as possible. Likewise, the magnification must be chosen carefully, as it is necessary to compromise over maximizing coverage of the growth area and thus imaging complete fused myotubes at low magnification, and achieving detailed resolution in the deflection range at high magnifications. Moreover, the pulse duration and frequency should be systematically varied in such an experiment to ensure that these parameters do not mask any metformin effects.

Previously, interactions between metformin and EPS-induced effects were reported on transcriptional and protein level in human myotubes [227, 241]. EPS forced the transcriptional up-regulation of *RSPO3*, *IL8*, *CXCL1*, *IL6* and *ABRA*, all of which were counter-regulated when metformin (1.25–5 mM) was administrated [227]. In addition, the enhanced phosphorylation of p70S6K1 after 8 h EPS was blunted in the presence of 10 mM metformin [241]. Not only the long duration of stimulation but also the high metformin concentrations used differ from our approach. The authors made no statement as to whether EPS results in visible contraction of the myotubes, a point that can generally be criticized in many studies applying EPS.

6.9 Explanatory approaches to the influence of metformin on myotube contraction

The impairment of EPS-induced myotube contraction by the administration of metformin raises the question of which mechanisms are responsible for this effect. Various aspects that are essential for muscle contraction *in vivo* can be considered:

- structural arrangement of proteins of the contractile apparatus
- sufficient energy supply in the form of ATP
- cellular calcium signaling

An elegant study in C2C12 myotubes demonstrate a delayed onset of contraction during EPS by approximately 30 min, which is caused by assembly processes of the sarcomere structure [63]. Immunostaining of the sarcomeric proteins α-actinin and titin reveals that the cells develop the typical striated pattern in response to the electrical simulation, suggesting that the ongoing protein arrangement process is necessary for myotube contraction. In contrast to differentiated C2C12 myotubes, which show poor sarcomeric arrangement [53, 63], the IGF1-differentiated human myotubes present a markedly striated pattern [47]. We therefore successfully verified that human myotubes were able to contract during a short 10-minute stimulus before the administration of metformin. The hypothesis that metformin has a reverse effect on the sarcomeric arrangement was not confirmed by immunostainings showing no impact of metformin on the striated pattern of the myotubes. Further, the initial identified reduced expression of myosin heavy chain genes *MYH1*, *MYH2* and *MYH7* was not conserved on protein level. A similar discrepancy between the metformin effect on RNA expression and protein abundance was found for ABRA, also known as striated muscle activator of Rho signaling (Stars), which is predominately localized in the I-band of the sarcomere [8]. Involving RhoA-signaling, it stabilizes the actin cytoskeleton by promoting the binding of G-actin to F-actin and forcing actin polymerization [8]. Thereby the inhibitory effect of G-actin on MRTF-A gets reversed and together with SRF, the transcription of target genes is activated including among others tropomyosin, MyoD, PGC1α, and some myosin light chains [8, 130]. In the context of metformin-exercise-interactions, ABRA is an interesting potential metformin target, as it was demonstrated that resistance exercise increases ABRA expression in humans, while a period of de-training reverted the effect [129]. A study in C2C12 myotubes demonstrated that the knockdown of ABRA increases marker of necrosis and inflammation leading to increased cell death [240] indicating that ABRA is a highly relevant protein in skeletal muscle. Since we did not find reduced ABRA protein levels despite the clearly reduced transcript levels in metformin-treated myotubes, we speculate that there are counter-regulatory mechanisms for stabilizing ABRA protein levels and thus buffering the metformin-induced transcriptional effects on *ABRA*. Based on these results, we currently assume that the metformin effect on contractility cannot be attributed to structural changes in the sarcomeres or myotubes. In support of this, high doses of metformin were required to reduce the transcripts of *ABRA* and myosin heavy chain genes well above the concentrations effective to impair contractility. The discrepancy between the regulation of RNA and protein abundance in metformin-treated myotubes would be another interesting question to investigate, but is beyond the scope of this thesis.

Further, we cannot exclude that metformin induces structural changes associated with reduced myotube contractility, which cannot be investigated with the immunofluorescence staininngs applied in this work. A recently pharmacologically utilized mechanism in heart muscle illustrates that the muscular contractility depends not only on the arrangement of the sarcomer proteins but also on the activity state of myosin [171]. Myosin in its super-relaxed (SRX) state is in a spatial arrangement that does not allow interaction with the actin filament. The transition to the disordered-relaxed (DRX) state, as a prerequisite for calcium-dependent interaction with the actin filament, is

regulated by phosphorylation processes in which regulatory light chains (RLCs) and myosin binding proteins (MyBPs) play a role [158, 171]. It would therefore be a further approach to investigate whether metformin influences the phosphorylation of the regulatory proteins in skeletal muscle and thus the activity state of myosin.

It is a consistent finding *in vitro* and *in vivo* that metformin exert some of its effects by a change in the cellular energy status. Several studies report increased AMPK activity in response to metformin indicating an increase in the AMP:ATP ratio [34, 169, 177, 243]. Acute stimulation for 2 h of hepatocytes and isolated rat muscle with 10 mM metformin result in a decrease in intracellular ATP levels [177, 178]. Prolonged metformin administration of up to 8 h lead to reduced ATP levels already at lower concentrations of 0.25 to 1 mM metformin in hepatocytes [60, 243]. The latter studies demonstrated in addition that the total nucleotide pool (AMP+ADP+ATP) is also reduced. Under conditions of heightened energy consumption, as it is the case during EPS, the reduced amount of available ATP under metformin might not be sufficient to support full contractility of the myotubes. We therefore investigated the hypothesis of whether metformin-induced cellular energy deficit affects EPS-induced contractility in myotubes. First, we provide evidence that low concentrations of metformin impair overall cellular ATP production along with a shift toward glycolytic ATP production in myotubes. In order to activate pathways to compensate for the energy deficiency under metformin, phosphorylation of AMPK was increased, corresponding to enhanced activity. In line, the downstream target ACC showed a higher level of phosphorylation in order to cover the cellular ATP demand by enhanced FAO. At the same time, the results of the quantification of the three single nucleotides AMP, ADP and ATP from metformin-treated myotubes do not support a change in the cellular energy status. Neither under basal condition nor under the energy-demanding conditions of EPS metformin impaired the absolute nucleotide levels and an AEC of average 0.74 indicate a healthy energy status of the myotubes [11]. Of note, myotubes had to be supplied with fresh cell culture medium before the application of EPS. Otherwise AEC was already dampened before the application of EPS, so that any potential effect of EPS in the combination with metformin would have been covered. The inhibitory effect of metformin on visual contraction of the myotubes remained even after the supply with fresh nutrients and seems to be independent of intracellular ATP levels. In support, there are findings indicating that comparable concentrations of metformin have no impact on cellular ATP levels in hepatocytes [6, 34]. However, Hunter and colleagues [93] mention in connection with the discussion of contradictory results around metformin-induced AMPK activation and cellular ATP levels, that the correct determination of nucleotides is technically challenging. They argue, that the cellular AMP concentration reacts very sensitively to stress factors with an increase and thus easily falsifies the results upward. They therefore suggest for investigations of cellular energy status using the more robust measurement of AMPK and its phosphorylation at Thr-172, which is sensitive to changes in cellular AMP levels. Despite the fact that the steps for preparing the samples for the quantification of the nucleotides by CE were reduced to a minimum, we assume that cell stress could not be completely avoided and thus may have influenced the measurement. In conclusion, we consider the results of increased AMPK activity by metformin to be more robust and assume that metformin has the ability to impair the cellular energy status in myotubes. Again, higher concentrations of metformin are required to induce AMPK phosphorylation compared to the inhibition of myotube contraction. Thus, whether an impaired cellular energy status in consequence affects myotube contractility during EPS cannot be conclusively clarified on the basis of the investigations in this thesis and leaves room for other mechanistic explanations.

In skeletal muscle impaired calcium signaling can significantly affect the ability to contract effectively and efficiently, leading to functional deficits in muscle performance [123]. The following considerations of a metformin-induced altered calcium signaling resulting in impaired myotube con-

traction are based on theoretical foundations but were not investigated experimentally as a part of the thesis. A decrease in the levels of cytosolic Ca^{2+}, which is essential for the activation of the actomyosin fibers responsible for muscle contraction, can lead to a reduction in the force of muscle contraction [16], as there may be insufficient Ca^{2+} to initiate the excitation contraction coupling (ECC) process. Relevant potential targets of metformin include the muscular calcium channels ryanodine receptors (RyRs) and sarcoplasmic/endoplasmic reticulum calcium ATPase (SERCA), which are responsible for the sarcoplasmatic release and uptake of Ca^{2+}, respectively. Functional analysis of Ca^{2+} fluxes in metformin-treated myotubes should also be conducted when addressing this research question. A suitable tool to do so is the application of calcium indicator dyes (e.g. FURA-2 AM) [17]. The dye binds to calcium and changes its fluorescence properties allow live imaging of intracellular Ca^{2+} levels through dual-wavelength excitation. Using such a setting, it would be possible to combine the measurements with the application of EPS in order to explore whether metformin has an impact on the sarcoplasmatic Ca^{2+} release in response to the electric pulses [63].

Calcium signaling is also essential for many processes including cell growth and differentiation, cellular metabolism, and regulation of gene expression. Alterations in cytosolic Ca^{2+} in skeletal muscle can also impact the activation of signal transduction cascades that are dependent on Ca^{2+}/calmodulin, including calmodulin kinases (CamK) or the Ca^{2+}/calmodulin-activated serine-threonine phosphatase calcineurin [38, 249]. Through Ca^{2+}-induced changes in the phosphorylation state of downstream proteins, skeletal muscle development and differentiation can be altered. Even if the latter effects do not have a direct impact on contraction, they are important in the context of the overarching question of interaction mechanisms between metformin and exercise adaptation processes and should be investigated in the future.

CHAPTER 7

Future Investigations and Concluding Remarks

The novel identified mechanism of increased lactate production by metformin in myotubes may only play a role *in vivo* in skeletal muscle under toxic conditions. However, in tissues and organs of higher metformin concentrations, this mechanism could be of relevance. One such organ is the intestine, which is already discussed as a source of increased plasma lactate levels under metformin therapy [203, 228]. Specific investigations are pending.

Regardless of the source of lactate, we provide further evidence of increased human plasma lactate levels that still remain within the physiological range. Future studies should investigate the question of which pleiotropic effects of metformin can be mediated by a slight chronic elevation of lactate levels and which mechanisms are involved. This gain of knowledge can help to identify new targets to harness specifically some of the effects of metformin.

Finally, the question remains as to the importance of the described interactions between metformin and adaptation processes to exercise *in vivo*. The currently available clinical data suggests that the individually positive effects of metformin and exercise do not translate into additive effects when combined or even have a negative influence on each other (Table 2). The understanding of underlying mechanisms is limited and future investigations are needed. As pointed out earlier, the reduced hypertrophic response due to metformin should be investigated in more detail, also with regard to the question of whether muscle mass and muscle strength are equally affected. Using 3D-myobundles as an *in vitro* model appears to be beneficial not only in this context. This model could also be helpful to understand the *in vivo* significance of the reduced contractility by metformin found in the traditional 2D culture of myotubes. In addition, the extended culture time of myobundles allows to simulate training via repetitive EPS sessions and thus come a step closer to the real-life situation.

Giving the increasing prevalence of T2D and the yet recommended treatment of metformin and regular physical activity, future *in vivo* studies are necessary to validate the potential negative interaction of both. Ideally, large cohort studies should be conducted to clarify whether there are specific groups of patient, that are particularly affected by the interactions. Similarly, risk factors such as concomitant medications could be identified that may have an exacerbating effect. Additionally, the question arises as to whether certain exercise modalities, such as HIIT, are preferable for patients with T2D under metformin therapy. In the course of this, the influence of the timing of metformin administration and the execution of a single exercise bout on the outcome should also be investigated. With this knowledge, the patient's therapy could be individually adapted to make the best possible use of the individual positive aspects of metformin and exercise together.

The potential interaction between metformin and exercise may not be relevant for every patient. At this point, however, attention should be drawn to elderly, who suffer from distinct age-related loss of muscle mass and strength or sarcopenia, which represents a more advanced stage of this process, with significant clinical consequences [41, 133]. Engaging in regular resistance exercise is the cornerstone of sarcopenia prevention and management, improving muscle mass and strength [31, 206] and thus a concomitant therapy of T2D with metformin could have a particularly negative impact on individual's health and quality of life. On the other hand, there is current research exploring the potential use of metformin in healthy individuals to extend lifespan and enhance healthspan [162]. Current clinical trials, some of which are still ongoing, on metformin as an anti-aging drug

include the Antecedent Metabolic Health and Metformin (ANTHEM) Aging study, the Targeting Aging with Metformin (TAME) study and the Metformin In Longevity Study (MILES) [18, 119, 122]. The latter suggest that metformin may induce transcriptional changes associated with anti-aging effects, but there is still a lack of evidence for an prolonged healthspan and lifespan under metformin treatment. Moreover, there are currently a few studies in rodents that explore metformin-exercise interactions in aging [85, 145, 144]. Initial evidence suggests that the metabolic health status of the animals attenuates the outcome [29]. Against this background, it is important to clarify whether in metabolically healthy individuals, metformin also interacts with adaptive responses to exercise. If it is the case, it is necessary to consider this when potentially using metformin as an anti-aging drug.

Supplementary Material

Supplementary tables

Table S1: Baseline characteristics of subjects donating muscle biopsies.

Sex		all		male		female	
Number of subjects		27		11		16	
Parameter baseline	**unit**	**mean**	**sd**	**mean**	**sd**	**mean**	**sd**
Age	**[years]**	29.67	7.95	33.00	5.35	27.88	8.79
Height	**[cm]**	171.21	9.92	181.01	6.04	164.09	4.13
Weight	**[kg]**	92.99	16.25	101.08	13.12	86.36	14.61
BMI	**[kg/m^2]**	31.59	4.04	30.82	3.52	31.94	4.37
Systolic blood pressure	**[mmHg]**	133.67	13.13	137.90	14.36	130.44	11.62
Diastolic blood pressure	**[mmHg]**	87.96	11.38	89.00	14.71	87.63	9.00
ISImats		8.79	4.83	9.30	6.50	8.22	3.38
HbA1c	**[mmol/mol]**	34.15	2.58	34.50	2.54	33.88	2.64
HbA1c	**[%]**	5.27	0.24	5.31	0.23	5.25	0.24

BMI, body mass index; ISI_{mats}, insulin sensitivity index estimated by Matsuda method; HbA1c, glycated haemoglobin A1c; sd, standard deviation.

Table S2: Clinical data on subjects participating in the crossover study used for *in vivo* studies of metformin effects in skeletal muscle.

Parameter	**unit**	**mean**	**sd**
Age	**[years]**	23.7	0.6
BMI	**[kg/m^2]**	22.3	2.0
VO_2peak	**[L/ min]**	3.5	0.6

Table S3: Baseline characteristics of subjects donating muscle biopsies used for RNA sequencing analysis.

Sex		all		male		female	
Number of subjects		10		6		4	
Parameter baseline	**unit**	**mean**	**sd**	**mean**	**sd**	**mean**	**sd**
Age	**[years]**	30.10	6.74	34.83	5.84	25.50	3.20
Height	**[cm]**	175.23	9.63	181.55	7.21	165.75	2.02
Weight	**[kg]**	94.61	9.69	96.93	9.19	91.13	9.36
BMI	**[kg/m^2]**	30.88	3.04	29.38	1.86	33.13	3.09
Systolic blood pressure	**[mm Hg]**	134.40	13.78	138.83	13.11	127.75	11.97
Diastolic blood pressure	**[mm Hg]**	89.90	13.16	91.67	15.18	87.25	8.70
ISI$_{mats}$		6.08	1.35	6.45	1.35	5.51	1.14
HbA1c	**[mmol/mol]**	34.10	2.55	34.67	3.09	33.25	0,83
HbA1c	**[%]**	5.27	0.23	5.32	0.28	5.19	0.08

BMI, body mass index; ISI$_{mats}$, insulin sensitivity index estimated by Matsuda method; HbA1c, glycated haemoglobin A1c; sd, standard deviation.

Table S4: Number of transcripts differentially regulated by the indicated treatment dose of metformin assessed by RNA sequencing analysis.

	Metformin				
statistical criteria	**16 µM**	**39 µM**	**78 µM**	**388 µM**	**776 µM**
adj.p < 0.1	1	6	3	3049	7208
adj.p < 0.1, FC±1.2	1	6	2	908	3791

adj. p value: Benjamini-Hochberg; FC: fold-change.

Supplementary figures

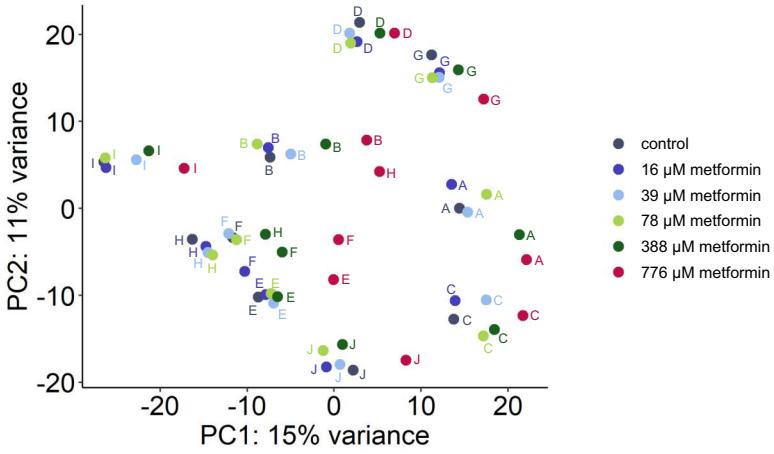

Figure S1: Principle component analysis of RNA sequencing data.
Principle component analysis using the 20 000 most variable genes detected by RNA sequencing was used to prove for outliers. Letters indicate single donors of analyzed myotubes.

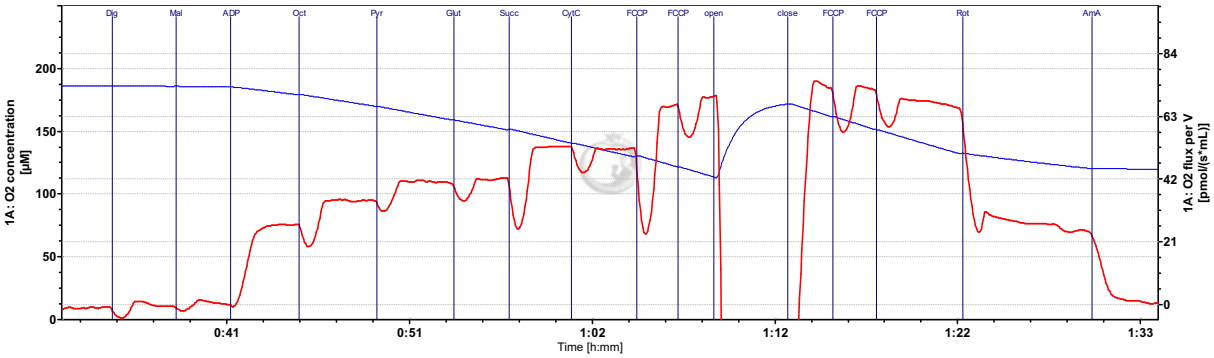

Figure S2: High resolution respirometry of primary human myotubes using the Oroboros system.
Representative measurement of one individual donor using the Oroboros system. Timepoints of substrate injections are labeled: digitonin (Dig), malate (Mal), ADP, octanylcarnitine (Oct), pyruvate (Pyr), glutamate (Glut), succinate (Succ), cytochrome c (CyC), carbonyl-cyanide-4-(trifluoromethoxy)phenylhydrazone (FCCP), rotenone (Rot), and antimycin A (AmA). Reoxygenation was carried out during the FCCP titration, which is indicated by the corresponding marking when opening and closing the measuring chamber. blue: O_2 concentration inside the chamber; red: O_2 flux per volume.

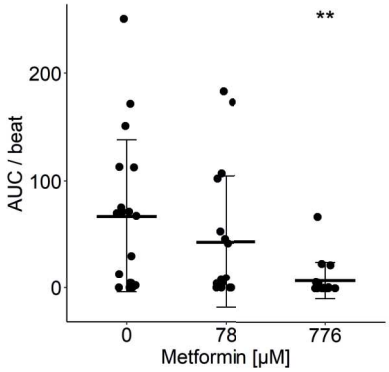

Figure S3: Impaired EPS-induced myotube contractility is not explained by acute changes in adenylate energy charge.
Motion analysis conducted using OpenHeartWare of EPS-stimulated myotubes, which were used for the subsequent nucleotide determination. Videos were recorded at the end of the 2 h stimulation period. All individual data points are displayed; bars represent means ± SD; t-test against 0 µM metformin: ns $p > 0.05$, ** $p < 0.01$.

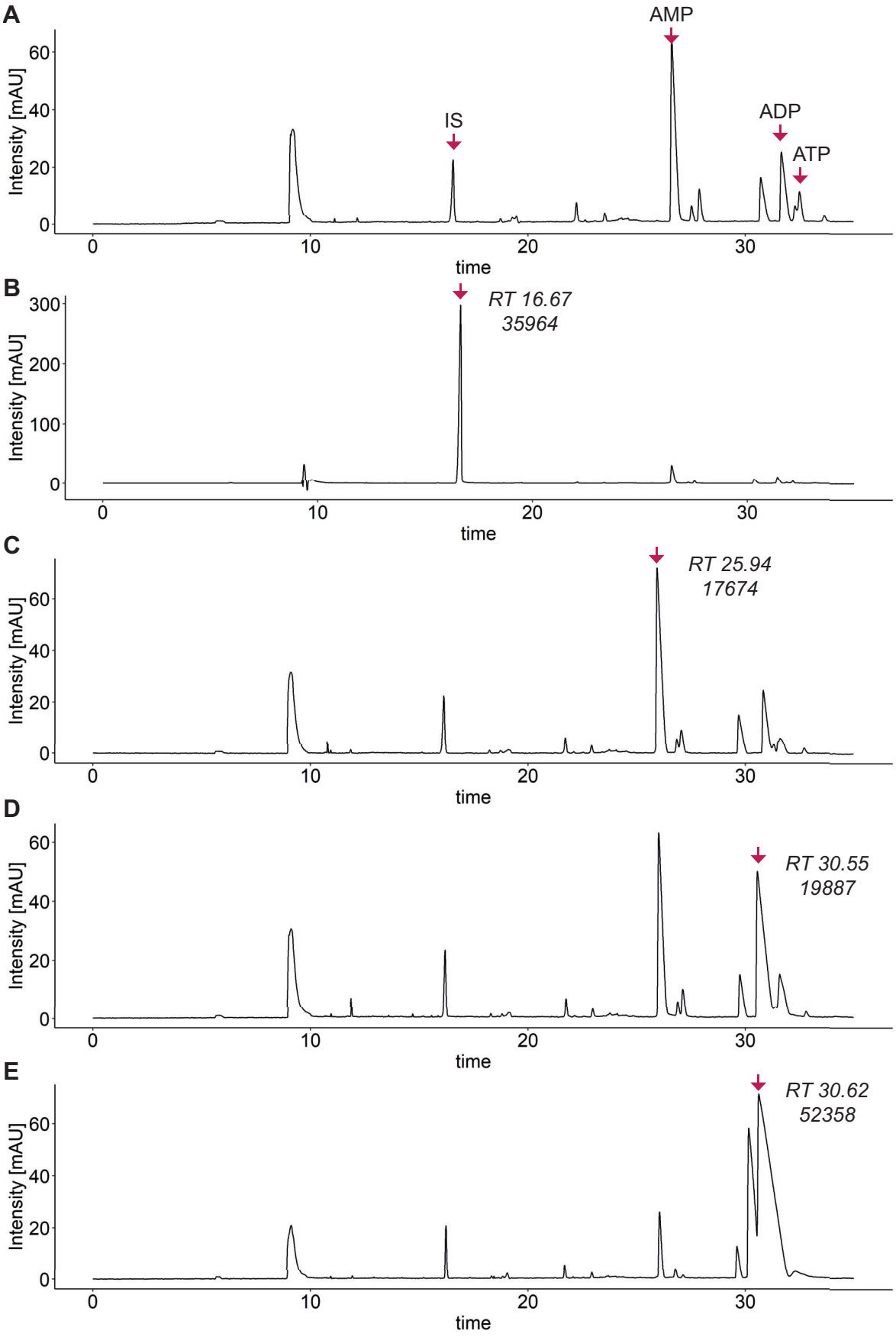

Figure S4: *– continued on next page*

– continued from previous page

Figure S4: Nucleotide quantification by capillary electrophoresis.
(A) Electropherogram of a representative sample including 40 µM of 8-bromoguanosine as internal standard. Peaks were identified by adding 2 mM (B) 8-bromoguanosine, (C) AMP, (D) ADP and (E) ATP separately. IS, internal standard; RT, retention time; lower numbers indicate peak area.

A

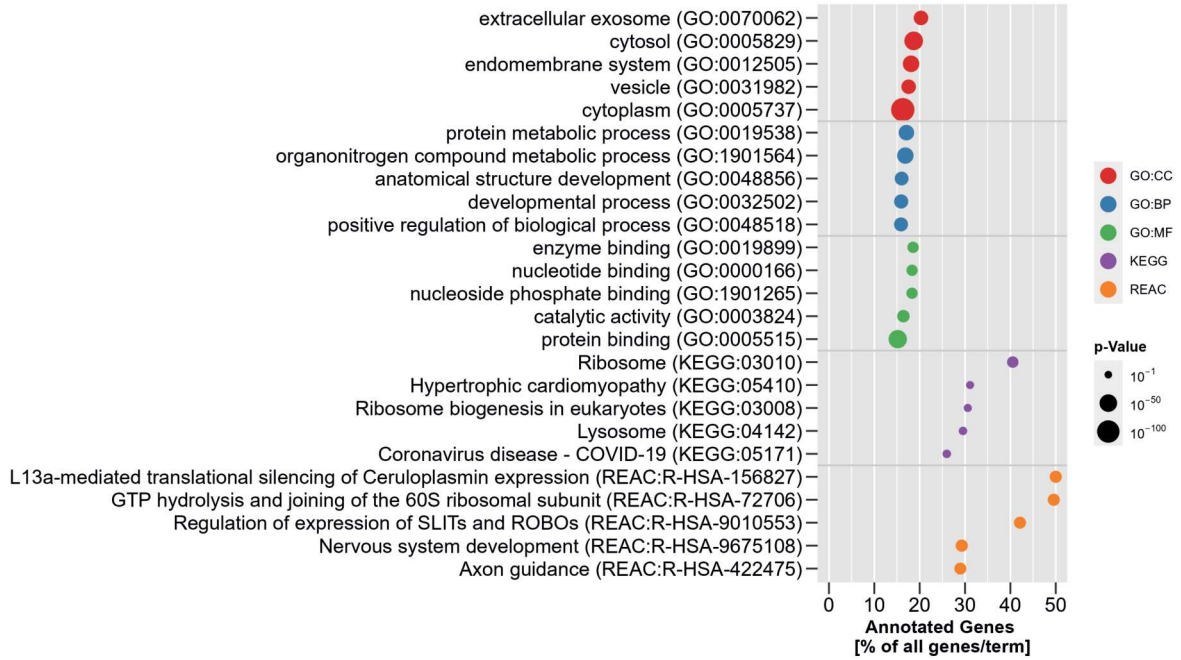

B

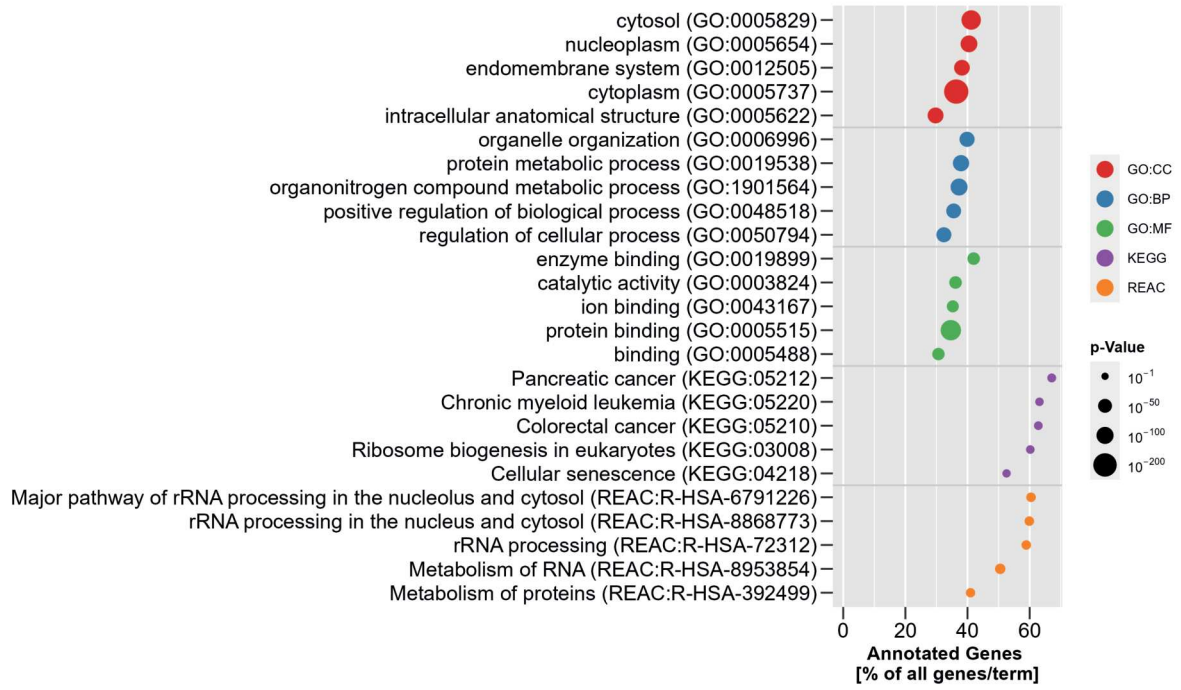

Figure S5: Enrichment analysis of differentially regulated genes by metformin in myotubes.
G:Profiler analysis based on RNA sequencing of primary human myotubes after 48 h treatment with (A) 388 µM and (B) 776 µM metformin (n = 10 donors). The top 5 terms based on the percentage of differentially regulated genes (adj.p < 0.1) annotated for the corresponding term are visualized for GO cellular component (red), GO biological process (blue), GO molecular function (green), KEGG (purple), and Reactome (orange).

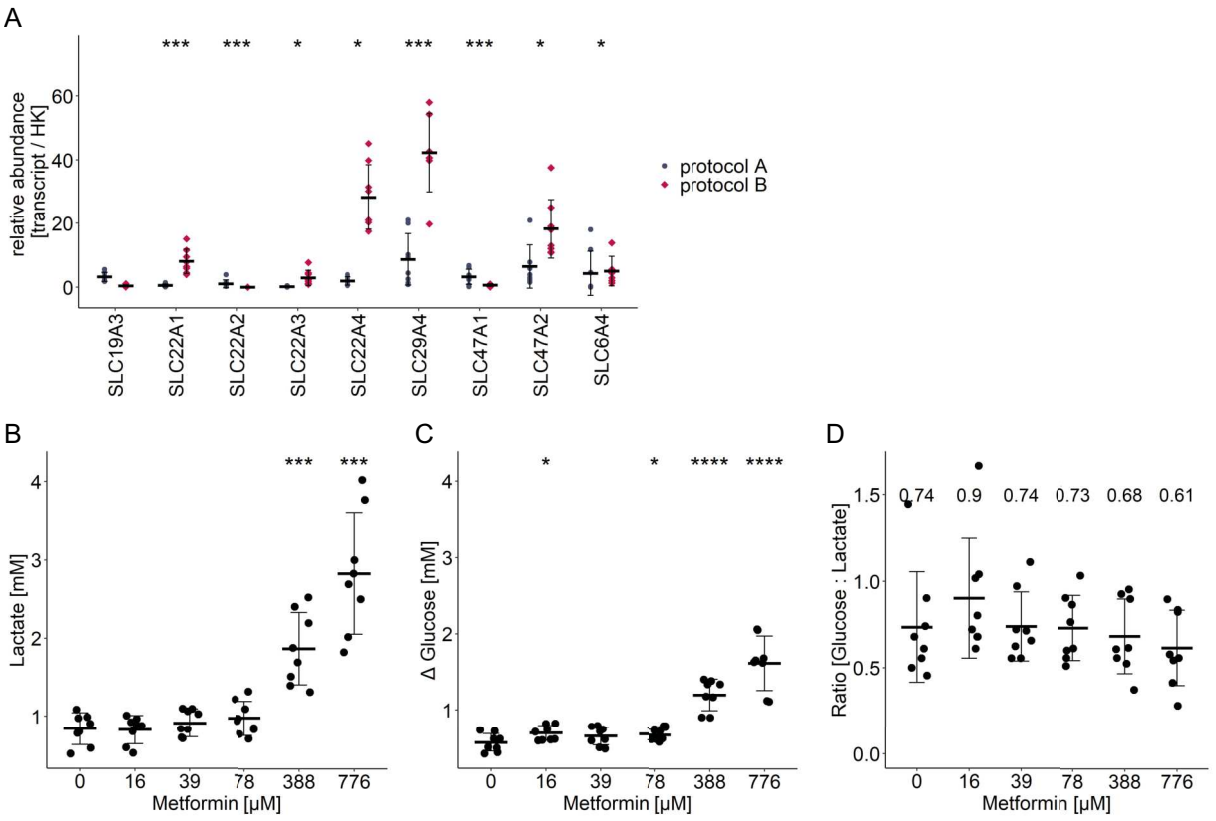

Figure S6: Metformin-induced lactate production is unaffected of IGF1 supplementation during myotube fusion.

(A) Basal expression of potential metformin transporters in myotubes fused according to *protocol A* (blue) and *protocol B* (red) determined by qRT-PCR. All individual data points are displayed (n = 8 donors); bars represent ± SD; t-test between both groups: ns $p > 0.05$, * $p < 0.01$, ** $p < 0.01$, *** $p < 0.01$. (B) Lactate production, (C) glucose consumption and (D) glucose:lactate ratio determined in the supernatant of metformin-treated myotubes according to *protocol B*. All individual data points are displayed (n = 4 donors as technical duplicates); bars represent ± SD; t-test against 0 µM metformin: ns $p > 0.05$, * $p < 0.01$, ** $p < 0.01$, *** $p < 0.01$, **** $p < 0.01$.

.

List of Figures

List of Tables

Bibliography

[1] Aas, V., Bakke, S. S., Feng, Y. Z., Kase, E. T., Jensen, J., Bajpeyi, S., Thoresen, G. H., and Rustan, A. C. (2013). Are cultured human myotubes far from home? *Cell Tissue Res*, 354(3):671–82.

[2] Aduen, J., Bernstein, W. K., Khastgir, T., Miller, J., Kerzner, R., Bhatiani, A., Lustgarten, J., Bassin, A. S., Davison, L., and Chernow, B. (1994). The use and clinical importance of a substrate-specific electrode for rapid determination of blood lactate concentrations. *JAMA*, 272(21):1678–1685.

[3] Al-Khalili, L., Forsgren, M., Kannisto, K., Zierath, J. R., Lönnqvist, F., and Krook, A. (2005). Enhanced insulin-stimulated glycogen synthesis in response to insulin, metformin or rosiglitazone is associated with increased mRNA expression of GLUT4 and peroxisomal proliferator activator receptor gamma co-activator 1. *Diabetologia*, 48(6):1173–9.

[4] Al-Oanzi, Z. H., Fountana, S., Moonira, T., Tudhope, S. J., Petrie, J. L., Alshawi, A., Patman, G., Arden, C., Reeves, H. L., and Agius, L. (2017). Opposite effects of a glucokinase activator and metformin on glucose-regulated gene expression in hepatocytes. *Diabetes Obes Metab*, 19(8):1078–1087.

[5] Al-Zahrani, A., Sandhu, M. S., Luben, R. N., Thompson, D., Baynes, C., Pooley, K. A., Luccarini, C., Munday, H., Perkins, B., Smith, P., Pharoah, P. D., Wareham, N. J., Easton, D. F., Ponder, B. A., and Dunning, A. M. (2006). IGF1 and IGFBP3 tagging polymorphisms are associated with circulating levels of IGF1, IGFBP3 and risk of breast cancer. *Hum Mol Genet*, 15(1):1–10.

[6] Alshawi, A. and Agius, L. (2019). Low metformin causes a more oxidized mitochondrial NADH/NAD redox state in hepatocytes and inhibits gluconeogenesis by a redox-independent mechanism. *J Biol Chem*, 294(8):2839–2853.

[7] American Diabetes Association (2023). Standards of care in diabetes - 2023. *DiabetesCare*, 46.

[8] Arai, A., Spencer, J. A., and Olson, E. N. (2002). STARS, a striated muscle activator of Rho signaling and serum response factor-dependent transcription. *J Biol Chem*, 277(27):24453–9.

[9] Argaud, D., Roth, H., Wiernsperger, N., and Leverve, X. M. (1993). Metformin decreases gluconeogenesis by enhancing the pyruvate kinase flux in isolated rat hepatocytes. *Eur J Biochem*, 213(3):1341–8.

[10] Ashcroft, S. P., Stocks, B., Egan, B., and Zierath, J. R. (2024). Exercise induces tissue-specific adaptations to enhance cardiometabolic health. *Cell Metab*, 36(2):278–300.

[11] Atkinson, D. E. (1968). Energy charge of the adenylate pool as a regulatory parameter. Interaction with feedback modifiers. *Biochemistry*, 7(11):4030–4034.

[12] Bahne, E., Sun, E. W. L., Young, R. L., Hansen, M., Sonne, D. P., Hansen, J. S., Rohde, U., Liou, A. P., Jackson, M. L., de Fontgalland, D., Rabbitt, P., Hollington, P., Sposato, L., Due, S., Wattchow, D. A., Rehfeld, J. F., Holst, J. J., Keating, D. J., Vilsbøll, T., and Knop, F. K. (2018). Metformin-induced glucagon-like peptide-1 secretion contributes to the actions of metformin in type 2 diabetes. *JCI Insight*, 3(23).

[13] Bailey, C. J. (2012). Insulin plus metformin for T2DM - are there benefits? *Nature Reviews Endocrinology*, 8(8):449–450.

[14] Bailey, C. J. (2017). Metformin: historical overview. *Diabetologia*, 60(9):1566–1576.

[15] Bailey, C. J., Wilcock, C., and Scarpello, J. H. (2008). Metformin and the intestine. *Diabetologia*, 51(8):1552–3.

[16] Baker, A. J., Longuemare, M. C., Brandes, R., and Weiner, M. W. (1993). Intracellular tetanic calcium signals are reduced in fatigue of whole skeletal muscle. *American Journal of Physiology-Cell Physiology*, 264(3):C577–C582.

[17] Barreto-Chang, O. L. and Dolmetsch, R. E. (2009). Calcium imaging of cortical neurons using Fura-2 AM. *J Vis Exp*, (23).

[18] Barzilai, N., Crandall, J. P., Kritchevsky, S. B., and Espeland, M. A. (2016). Metformin as a tool to target aging. *Cell Metab*, 23(6):1060–1065.

[19] Becker, M. L., Visser, L. E., van Schaik, R. H., Hofman, A., Uitterlinden, A. G., and Stricker, B. H. (2009). Genetic variation in the multidrug and toxin extrusion 1 transporter protein influences the glucose-lowering effect of metformin in patients with diabetes: a preliminary study. *Diabetes*, 58(3):745–9.

[20] Bersiner, K., Park, S. Y., Schaaf, K., Yang, W. H., Theis, C., Jacko, D., and Gehlert, S. (2023). Resistance exercise: a mighty tool that adapts, destroys, rebuilds and modulates the molecular and structural environment of skeletal muscle. *Phys Act Nutr*, 27(2):78–95.

[21] Boulé, N. G., Kenny, G. P., Larose, J., Khandwala, F., Kuzik, N., and Sigal, R. J. (2013). Does metformin modify the effect on glycaemic control of aerobic exercise, resistance exercise or both? *Diabetologia*, 56(11):2378–82.

[22] Boulé, N. G., Robert, C., Bell, G. J., Johnson, S. T., Bell, R. C., Lewanczuk, R. Z., Gabr, R. Q., and Brocks, D. R. (2011). Metformin and exercise in type 2 diabetes: Examining treatment modality interactions. *Diabetes Care*, 34(7):1469–1474.

[23] Bowker-Kinley, M. M., Davis, W. I., Wu, P., Harris, R. A., and Popov, K. M. (1998). Evidence for existence of tissue-specific regulation of the mammalian pyruvate dehydrogenase complex. *Biochem J*, 329 (Pt 1)(Pt 1):191–6.

[24] Braun, B., Eze, P., Stephens, B. R., Hagobian, T. A., Sharoff, C. G., Chipkin, S. R., and Goldstein, B. (2008). Impact of metformin on peak aerobic capacity. *Appl Physiol Nutr Metab*, 33(1):61–7.

[25] Bridges, H. R., Jones, A. J., Pollak, M. N., and Hirst, J. (2014). Effects of metformin and other biguanides on oxidative phosphorylation in mitochondria. *Biochem J*, 462(3):475–87.

[26] Brooks, G. A. (1985). Lactate: Glycolytic end product and oxidative substrate during sustained exercise in mammals - "the lactate shuttle". In Gilles, R., editor, *Circulation, Respiration, and Metabolism*, pages 208–218. Springer Berlin Heidelberg.

[27] Brooks, G. A. (2020). Lactate as a fulcrum of metabolism. *Redox Biol*, 35:101454.

[28] Brunmair, B., Staniek, K., Gras, F., Scharf, N., Althaym, A., Clara, R., Roden, M., Gnaiger, E., Nohl, H., Waldhäusl, W., and Fürnsinn, C. (2004). Thiazolidinediones, like metformin, inhibit respiratory complex I: a common mechanism contributing to their antidiabetic actions? *Diabetes*, 53(4):1052–9.

[29] Bubak, M. P., Davidyan, A., O'Reilly, C. L., Mondal, S. A., Keast, J., Doidge, S. M., Borowik, A. K., Taylor, M. E., Volovičeva, E., Kinter, M. T., Britton, S. L., Koch, L. G., Stout, M. B., Lewis, T. L., and Miller, B. F. (2024). Metformin treatment results in distinctive skeletal muscle mitochondrial remodeling in rats with different intrinsic aerobic capacities. *bioRxiv*.

[30] Buono, M. J. and Yeager, J. E. (1986). Intraerythrocyte and plasma lactate concentrations during exercise in humans. *Eur J Appl Physiol Occup Physiol*, 55(3):326–9.

[31] Burton, L. A. and Sumukadas, D. (2010). Optimal management of sarcopenia. *Clin Interv Aging*, 5:217–28.

[32] Buse, J. B., DeFronzo, R. A., Rosenstock, J., Kim, T., Burns, C., Skare, S., Baron, A., and Fineman, M. (2016). The primary glucose-lowering effect of metformin resides in the gut, not the circulation: Results from short-term pharmacokinetic and 12-week dose-ranging studies. *Diabetes Care*, 39(2):198–205.

[33] Cadeddu, C., Nocco, S., Cugusi, L., Deidda, M., Bina, A., Fabio, O., Bandinu, S., Cossu, E., Baroni, M. G., and Mercuro, G. (2014). Effects of metformin and exercise training, alone or in association, on cardio-pulmonary performance and quality of life in insulin resistance patients. *Cardiovasc Diabetol*, 13:93.

[34] Cao, J., Meng, S., Chang, E., Beckwith-Fickas, K., Xiong, L., Cole, R. N., Radovick, S., Wondisford, F. E., and He, L. (2014). Low concentrations of metformin suppress glucose production in hepatocytes through AMP-activated protein kinase (AMPK). *J Biol Chem*, 289(30):20435–46.

[35] Chen, C. T., Chen, W., Chung, H. H., Cheng, K. C., Yeh, C. H., and Cheng, J. T. (2011). Activation of imidazoline I-2B receptor by metformin to increase glucose uptake in skeletal muscle. *Horm Metab Res*, 43(10):708–13.

[36] Chen, E. C., Liang, X., Yee, S. W., Geier, E. G., Stocker, S. L., Chen, L., and Giacomini, K. M. (2015). Targeted disruption of organic cation transporter 3 attenuates the pharmacologic response to metformin. *Mol Pharmacol*, 88(1):75–83.

[37] Chen, L., Pawlikowski, B., Schlessinger, A., More, S. S., Stryke, D., Johns, S. J., Portman, M. A., Chen, E., Ferrin, T. E., Sali, A., and Giacomini, K. M. (2010). Role of organic cation transporter 3 (SLC22A3) and its missense variants in the pharmacologic action of metformin. *Pharmacogenet Genomics*, 20(11):687–99.

[38] Chin, E. R., Olson, E. N., Richardson, J. A., Yang, Q., Humphries, C., Shelton, J. M., Wu, H., Zhu, W., Bassel-Duby, R., and Williams, R. S. (1998). A calcineurin-dependent transcriptional pathway controls skeletal muscle fiber type. *Genes Dev*, 12(16):2499–509.

[39] Clarke, J. D., Dzierlenga, A. L., Nelson, N. R., Li, H., Werts, S., Goedken, M. J., and Cherrington, N. J. (2015). Mechanism of altered metformin distribution in nonalcoholic steatohepatitis. *Diabetes*, 64(9):3305–13.

[40] Copp, J., Manning, G., and Hunter, T. (2009). TORC-specific phosphorylation of mammalian target of rapamycin (mTOR): Phospho-Ser2481 is a marker for intact mTOR signaling complex 2. *Cancer Research*, 69(5):1821–1827.

[41] Csete, M. E. (2021). Basic science of frailty-biological mechanisms of age-related sarcopenia. *Anesth Analg*, 132(2):293–304.

[42] Cusi, K., Consoli, A., and DeFronzo, R. A. (1996). Metabolic effects of metformin on glucose and lactate metabolism in noninsulin-dependent diabetes mellitus. *J Clin Endocrinol Metab*, 81(11):4059–67.

[43] Da Silva, D., Zancan, P., Coelho, W. S., Gomez, L. S., and Sola-Penna, M. (2010). Metformin reverses hexokinase and 6-phosphofructo-1-kinase inhibition in skeletal muscle, liver and adipose tissues from streptozotocin-induced diabetic mouse. *Arch Biochem Biophys*, 496(1):53–60.

[44] Davis, T. M., Jackson, D., Davis, W. A., Bruce, D. G., and Chubb, P. (2001). The relationship between metformin therapy and the fasting plasma lactate in type 2 diabetes: The Fremantle Diabetes Study. *Br J Clin Pharmacol*, 52(2):137–44.

[45] Day, E. A., Ford, R. J., Smith, B. K., Mohammadi-Shemirani, P., Morrow, M. R., Gutgesell, R. M., Lu, R., Raphenya, A. R., Kabiri, M., McArthur, A. G., McInnes, N., Hess, S., Paré, G., Gerstein, H. C., and Steinberg, G. R. (2019). Metformin-induced increases in GDF15 are important for suppressing appetite and promoting weight loss. *Nature Metabolism*, 1(12):1202–1208.

[46] DeFronzo, R. A. and Goodman, A. M. (1995). Efficacy of metformin in patients with non-insulin-dependent diabetes mellitus. The Multicenter Metformin Study Group. *N Engl J Med*, 333(9):541–9.

[47] Dreher, S. I., Grubba, P., Toerne, C. v., Moruzzi, A., Maurer, J., Goj, T., Birkenfeld, A. L., Peter, A., Loskill, P., Hauck, S. M., and Weigert, C. (2024). IGF1 promotes human myotube differentiation toward a mature metabolic and contractile phenotype. *American Journal of Physiology-Cell Physiology*.

[48] Dreher, S. I., Irmler, M., Pivovarova-Ramich, O., Kessler, K., Jürchott, K., Sticht, C., Fritsche, L., Schneeweiss, P., Machann, J., Pfeiffer, A. F. H., Hrabě de Angelis, M., Beckers, J., Birkenfeld, A. L., Peter, A., Niess, A. M., Weigert, C., and Moller, A. (2023). Acute and long-term exercise adaptation of adipose tissue and skeletal muscle in humans: a matched transcriptomics approach after 8-week training-intervention. *Int J Obes (Lond)*, 47(4):313–324.

[49] Duca, F. A., Bauer, P. V., Hamr, S. C., and Lam, T. K. (2015). Glucoregulatory relevance of small intestinal nutrient sensing in physiology, bariatric surgery, and pharmacology. *Cell Metab*, 22(3):367–80.

[50] Dykens, J. A., Jamieson, J., Marroquin, L., Nadanaciva, S., Billis, P. A., and Will, Y. (2008). Biguanide-induced mitochondrial dysfunction yields increased lactate production and cytotoxicity of aerobically-poised HepG2 cells and human hepatocytes in vitro. *Toxicol Appl Pharmacol*, 223(2):203–10.

[51] Egan, B. and Zierath, J. R. (2013). Exercise metabolism and the molecular regulation of skeletal muscle adaptation. *Cell Metab*, 17(2):162–84.

[52] El-Mir, M. Y., Nogueira, V., Fontaine, E., Avéret, N., Rigoulet, M., and Leverve, X. (2000). Dimethylbiguanide inhibits cell respiration via an indirect effect targeted on the respiratory chain complex I. *J Biol Chem*, 275(1):223–8.

[53] Engler, A. J., Griffin, M. A., Sen, S., Bönnemann, C. G., Sweeney, H. L., and Discher, D. E. (2004). Myotubes differentiate optimally on substrates with tissue-like stiffness: pathological implications for soft or stiff microenvironments. *J Cell Biol*, 166(6):877–87.

[54] Eppenga, W. L., Lalmohamed, A., Geerts, A. F., Derijks, H. J., Wensing, M., Egberts, A., De Smet, P. A., and de Vries, F. (2014). Risk of lactic acidosis or elevated lactate concentrations in metformin users with renal impairment: a population-based cohort study. *Diabetes Care*, 37(8):2218–24.

[55] Esefeld, K., Kress, S., Behrens, M., Zimmer, P., Stumvoll, M., Thurm, U., Gehr, B., Halle, M., and Brinkmann, C. (2023). Diabetes, Sport und Bewegung. *Diabetol Stoffwechs*, 18(S 02):S314–S323.

[56] Federation, I. D. (2021). IDF diabetes atlas, 10th edn. *Brussels, Belgium*.

[57] Fontaine, E. (2014). Metformin and respiratory chain complex I: the last piece of the puzzle? *Biochem J*, 463(3):e3–5.

[58] Fontaine, E. (2018). Metformin-induced mitochondrial complex I inhibition: facts, uncertainties, and consequences. *Front Endocrinol (Lausanne)*, 9:753.

[59] Foretz, M., Guigas, B., and Viollet, B. (2019). Understanding the glucoregulatory mechanisms of metformin in type 2 diabetes mellitus. *Nat Rev Endocrinol*, 15(10):569–589.

[60] Foretz, M., Hébrard, S., Leclerc, J., Zarrinpashneh, E., Soty, M., Mithieux, G., Sakamoto, K., Andreelli, F., and Viollet, B. (2010). Metformin inhibits hepatic gluconeogenesis in mice independently of the LKB1/AMPK pathway via a decrease in hepatic energy state. *J Clin Invest*, 120(7):2355–69.

[61] Fowler, M. J. (2008). Microvascular and macrovascular complications of diabetes. *Clinical Diabetes*, 26(2):77–82.

[62] Friess, U., Lehmann, R., Weigert, C., Haering, H. U., Voelter, W., and Schleicher, E. (2002). Single-run determination of adenylate nucleotides, and of cellular energy status, by a simple and improved capillary electrophoretic method. *Chromatographia*, 56(5):375–378.

[63] Fujita, H., Nedachi, T., and Kanzaki, M. (2007). Accelerated de novo sarcomere assembly by electric pulse stimulation in C2C12 myotubes. *Exp Cell Res*, 313(9):1853–65.

[64] Fullerton, M. D., Galic, S., Marcinko, K., Sikkema, S., Pulinilkunnil, T., Chen, Z. P., O'Neill, H. M., Ford, R. J., Palanivel, R., O'Brien, M., Hardie, D. G., Macaulay, S. L., Schertzer, J. D., Dyck, J. R., van Denderen, B. J., Kemp, B. E., and Steinberg, G. R. (2013). Single phosphorylation sites in Acc1 and Acc2 regulate lipid homeostasis and the insulin-sensitizing effects of metformin. *Nat Med*, 19(12):1649–54.

[65] Galuska, D., Nolte, L. A., Zierath, J. R., and Wallberg-Henriksson, H. (1994). Effect of metformin on insulin-stimulated glucose transport in isolated skeletal muscle obtained from patients with NIDDM. *Diabetologia*, 37(8):826–32.

[66] Galuska, D., Zierath, J. R., Thörne, A., Sonnenfeld, T., and Wallberg-Henriksson, H. (1991). Metformin increases insulin-stimulated glucose transport in insulin-resistant human skeletal muscle. *Diabete Metab*, 137(1 Pt 2):159–63.

[67] Giaccari, A., Solini, A., Frontoni, S., and Del Prato, S. (2021). Metformin benefits: Another example for alternative energy substrate mechanism? *Diabetes Care*, 44(3):647–654.

[68] Gillespie, Z. E., Wang, C., Vadan, F., Yu, T. Y., Ausió, J., Kuskalik, A., and Eskiw, C. H. (2019). Metformin induces the AP-1 transcription factor network in normal dermal fibroblasts. *Sci Rep*, 9(1):5369.

[69] Glancy, B., Kane, D. A., Kavazis, A. N., Goodwin, M. L., Willis, W. T., and Gladden, L. B. (2021). Mitochondrial lactate metabolism: history and implications for exercise and disease. *The Journal of Physiology*, 599(3):863–888.

[70] Gong, Q., Zhang, P., Wang, J., Ma, J., An, Y., Chen, Y., Zhang, B., Feng, X., Li, H., Chen, X., Cheng, Y. J., Gregg, E. W., Hu, Y., Bennett, P. H., and Li, G. (2019). Morbidity and mortality after lifestyle intervention for people with impaired glucose tolerance: 30-year results of the Da Qing Diabetes Prevention Outcome Study. *Lancet Diabetes Endocrinol*, 7(6):452–461.

[71] Gontier, E., Fourme, E., Wartski, M., Blondet, C., Bonardel, G., Le Stanc, E., Mantzarides, M., Foehrenbach, H., Pecking, A. P., and Alberini, J. L. (2008). High and typical 18F-FDG bowel uptake in patients treated with metformin. *Eur J Nucl Med Mol Imaging*, 35(1):95–9.

[72] González, A., Hall, M. N., Lin, S. C., and Hardie, D. G. (2020). AMPK and TOR: The yin and yang of cellular nutrient sensing and growth control. *Cell Metab*, 31(3):472–492.

[73] Goodman, C. A. (2019). Role of mTORC1 in mechanically induced increases in translation and skeletal muscle mass. *Journal of Applied Physiology*, 127(2):581–590.

[74] Goodwin, M. L., Harris, J. E., Hernández, A., and Gladden, L. B. (2007). Blood lactate measurements and analysis during exercise: a guide for clinicians. *J Diabetes Sci Technol*, 1(4):558–69.

[75] Gormsen, L. C., Sundelin, E. I., Jensen, J. B., Vendelbo, M. H., Jakobsen, S., Munk, O. L., Hougaard Christensen, M. M., Brøsen, K., Frøkiær, J., and Jessen, N. (2016). In vivo imaging of human 11C-metformin in peripheral organs: dosimetry, biodistribution, and kinetic analyses. *J Nucl Med*, 57(12):1920–1926.

[76] Graham, G. G., Punt, J., Arora, M., Day, R. O., Doogue, M. P., Duong, J., Furlong, T. J., Greenfield, J. R., Greenup, L. C., Kirkpatrick, C. M., Ray, J. E., Timmins, P., and Williams, K. M. (2011). Clinical pharmacokinetics of metformin. *Clinical Pharmacokinetics*, 50(2):81–98.

[77] Green, B. D., Irwin, N., Duffy, N. A., Gault, V. A., O'Harte, F. P. M., and Flatt, P. R. (2006). Inhibition of dipeptidyl peptidase-IV activity by metformin enhances the antidiabetic effects of glucagon-like peptide-1. *European Journal of Pharmacology*, 547(1):192–199.

[78] Group, U. P. D. S. U. (1998). Effect of intensive blood-glucose control with metformin on complications in overweight patients with type 2 diabetes (UKPDS 34). UK Prospective Diabetes Study (UKPDS) group. *Lancet*, 352(9131):854–65.

[79] Gudi, R., Bowker-Kinley, M. M., Kedishvili, N. Y., Zhao, Y., and Popov, K. M. (1995). Diversity of the pyruvate dehydrogenase kinase gene family in humans. *J Biol Chem*, 270(48):28989–94.

[80] Gudiksen, A., Qoqaj, A., Ringholm, S., Wojtaszewski, J., Plomgaard, P., and Pilegaard, H. (2022). Ameliorating effects of lifelong physical activity on healthy aging and mitochondrial function in human white adipose tissue. *J Gerontol A Biol Sci Med Sci*, 77(6):1101–1111.

[81] Haines, M. S., Dichtel, L. E., Santoso, K., Torriani, M., Miller, K. K., and Bredella, M. A. (2020). Association between muscle mass and insulin sensitivity independent of detrimental adipose depots in young adults with overweight/obesity. *International Journal of Obesity*, 44(9):1851–1858.

[82] Han, T. K., Proctor, W. R., Costales, C. L., Cai, H., Everett, R. S., and Thakker, D. R. (2015). Four cation-selective transporters contribute to apical uptake and accumulation of metformin in Caco-2 cell monolayers. *J Pharmacol Exp Ther*, 352(3):519–28.

[83] He, L., Sabet, A., Djedjos, S., Miller, R., Sun, X., Hussain, M. A., Radovick, S., and Wondisford, F. E. (2009). Metformin and insulin suppress hepatic gluconeogenesis through phosphorylation of CREB binding protein. *Cell*, 137(4):635–46.

[84] He, L. and Wondisford, F. E. (2015). Metformin action: concentrations matter. *Cell Metab*, 21(2):159–162.

[85] Hernández-Álvarez, D., Mena-Montes, B., Toledo-Pérez, R., Pedraza-Vázquez, G., López-Cervantes, S. P., Morales-Salazar, A., Hernández-Cruz, E., Lazzarini-Lechuga, R., Vázquez-Cárdenas, R. R., Vilchis-DeLaRosa, S., Posadas-Rodríguez, P., Santín-Márquez, R., Rosas-Carrasco, O., Ibañez-Contreras, A., Alarcón-Aguilar, A., López-Díazguerrero, N. E., Luna-López, A., and Königsberg, M. (2019). Long-term moderate exercise combined with metformin treatment induces an hormetic response that prevents strength and muscle mass loss in old female wistar rats. *Oxid Med Cell Longev*, 2019:3428543.

[86] Hoffmann, C., Hockele, S., Kappler, L., Hrabe de Angelis, M., Haring, H. U., and Weigert, C. (2018). The effect of differentiation and TGFbeta on mitochondrial respiration and mitochondrial enzyme abundance in cultured primary human skeletal muscle cells. *Sci Rep*, 8(1):737.

[87] Hoffmann, C., Schneeweiss, P., Randrianarisoa, E., Schnauder, G., Kappler, L., Machann, J., Schick, F., Fritsche, A., Heni, M., Birkenfeld, A., Niess, A. M., Häring, H. U., Weigert, C., and Moller, A. (2020). Response of mitochondrial respiration in adipose tissue and muscle to 8 weeks of endurance exercise in obese subjects. *J Clin Endocrinol Metab*, 105(11).

[88] Hou, W. L., Yin, J., Alimujiang, M., Yu, X. Y., Ai, L. G., Bao, Y. Q., Liu, F., and Jia, W. P. (2018). Inhibition of mitochondrial complex I improves glucose metabolism independently of AMPK activation. *J Cell Mol Med*, 22(2):1316–1328.

[89] Howell, J. J., Hellberg, K., Turner, M., Talbott, G., Kolar, M. J., Ross, D. S., Hoxhaj, G., Saghatelian, A., Shaw, R. J., and Manning, B. D. (2017). Metformin inhibits hepatic mTORC1 signaling via dose-dependent mechanisms involving AMPK and the TSC complex. *Cell Metab*, 25(2):463–471.

[90] Huang, W., Castelino, R. L., and Peterson, G. M. (2017). Lactate levels with chronic metformin use: A narrative review. *Clin Drug Investig*, 37(11):991–1007.

[91] Huebsch, N., Loskill, P., Mandegar, M. A., Marks, N. C., Sheehan, A. S., Ma, Z., Mathur, A., Nguyen, T. N., Yoo, J. C., Judge, L. M., Spencer, C. I., Chukka, A. C., Russell, C. R., So, P. L., Conklin, B. R., and Healy, K. E. (2015). Automated video-based analysis of contractility and calcium flux in human-induced pluripotent stem cell-derived cardiomyocytes cultured over different spatial scales. *Tissue Eng Part C Methods*, 21(5):467–79.

[92] Hundal, H. S., Ramlal, T., Reyes, R., Leiter, L. A., and Klip, A. (1992). Cellular mechanism of metformin action involves glucose transporter translocation from an intracellular pool to the plasma membrane in L6 muscle cells. *Endocrinology*, 131(3):1165–73.

[93] Hunter, R. W., Hughey, C. C., Lantier, L., Sundelin, E. I., Peggie, M., Zeqiraj, E., Sicheri, F., Jessen, N., Wasserman, D. H., and Sakamoto, K. (2018). Metformin reduces liver glucose production by inhibition of fructose-1-6-bisphosphatase. *Nat Med*, 24(9):1395–1406.

[94] Inzucchi, S. E., Maggs, D. G., Spollett, G. R., Page, S. L., Rife, F. S., Walton, V., and Shulman, G. I. (1998). Efficacy and metabolic effects of metformin and troglitazone in type II diabetes mellitus. *New England Journal of Medicine*, 338(13):867–873.

[95] Jacobs, E., Rathmann, W., Tönnies, T., Arendt, D., Marchowez, M., Veith, L., Kuss, O., Brinks, R., and Hoyer, A. (2020). Age at diagnosis of type 2 diabetes in germany: a nationwide analysis based on claims data from 69 million people. *Diabetic Medicine*, 37(10):1723–1727.

[96] Jalling, O. and Olsen, C. (1984). The effect of metformin compared to the effects of phenformin on the lactate production and the metabolism of isolated parenchymal rat liver cell. *Acta Pharmacol Toxicol (Copenh)*, 54(5):327–32.

[97] Janssen, I., Heymsfield, S. B., Wang, Z., and Ross, R. (2000). Skeletal muscle mass and distribution in 468 men and women aged 18–88 yr. *Journal of Applied Physiology*, 89(1):81–88.

[98] Jensen, J. B., Sundelin, E. I., Jakobsen, S., Gormsen, L. C., Munk, O. L., Frøkiær, J., and Jessen, N. (2016). [11C]-labeled metformin distribution in the liver and small intestine using dynamic positron emission tomography in mice demonstrates tissue-specific transporter dependency. *Diabetes*, 65(6):1724–30.

[99] Juel, C., Klarskov, C., Nielsen, J. J., Krustrup, P., Mohr, M., and Bangsbo, J. (2004). Effect of high-intensity intermittent training on lactate and H^+ release from human skeletal muscle. *American Journal of Physiology-Endocrinology and Metabolism*, 286(2):E245–E251.

[100] Junien, J. L., Brohon, J., Guillaume, M., and Sterne, J. (1979). DBM mice as a pharmacological model of maturity onset diabetes. studies with metformin. *Arch Int Pharmacodyn Ther*, 241(1):165–76.

[101] Kajbaf, F., De Broe, M. E., and Lalau, J.-D. (2016). Therapeutic concentrations of metformin: A systematic review. *Clinical Pharmacokinetics*, 55(4):439–459.

[102] Kalender, A., Selvaraj, A., Kim, S. Y., Gulati, P., Brûlé, S., Viollet, B., Kemp, B. E., Bardeesy, N., Dennis, P., Schlager, J. J., Marette, A., Kozma, S. C., and Thomas, G. (2010). Metformin, independent of AMPK, inhibits mTORC1 in a Rag GTPase-dependent manner. *Cell Metab*, 11(5):390–401.

[103] Kamel, K. S., Oh, M. S., and Halperin, M. L. (2020). L-lactic acidosis: pathophysiology, classification, and causes; emphasis on biochemical and metabolic basis. *Kidney Int*, 97(1):75–88.

[104] Kane, D. A., Anderson, E. J., Price, J. W., r., Woodlief, T. L., Lin, C. T., Bikman, B. T., Cortright, R. N., and Neufer, P. D. (2010). Metformin selectively attenuates mitochondrial H_2O_2 emission without affecting respiratory capacity in skeletal muscle of obese rats. *Free Radic Biol Med*, 49(6):1082–7.

[105] Karlsson, H. K., Hällsten, K., Björnholm, M., Tsuchida, H., Chibalin, A. V., Virtanen, K. A., Heinonen, O. J., Lönnqvist, F., Nuutila, P., and Zierath, J. R. (2005). Effects of metformin and rosiglitazone treatment on insulin signaling and glucose uptake in patients with newly diagnosed type 2 diabetes: a randomized controlled study. *Diabetes*, 54(5):1459–67.

[106] Keller, K. and Engelhardt, M. (2013). Strength and muscle mass loss with aging process. Age and strength loss. *Muscles Ligaments Tendons J*, 3(4):346–50.

[107] Khodabukus, A., Madden, L., Prabhu, N. K., Koves, T. R., Jackman, C. P., Muoio, D. M., and Bursac, N. (2019). Electrical stimulation increases hypertrophy and metabolic flux in tissue-engineered human skeletal muscle. *Biomaterials*, 198:259–269.

[108] Kido, K., Ato, S., Yokokawa, T., Makanae, Y., Sato, K., and Fujita, S. (2016). Acute resistance exercise-induced IGF1 expression and subsequent GLUT4 translocation. *Physiol Rep*, 4(16).

[109] Kim, M. H., Jee, J. H., Park, S., Lee, M. S., Kim, K. W., and Lee, M. K. (2014). Metformin enhances glucagon-like peptide 1 via cooperation between insulin and Wnt signaling. *J Endocrinol*, 220(2):117–28.

[110] Kimura, N., Masuda, S., Tanihara, Y., Ueo, H., Okuda, M., Katsura, T., and Inui, K. (2005). Metformin is a superior substrate for renal organic cation transporter OCT2 rather than hepatic OCT1. *Drug Metab Pharmacokinet*, 20(5):379–86.

[111] Kirwan, J. P., Solomon, T. P., Wojta, D. M., Staten, M. A., and Holloszy, J. O. (2009). Effects of 7 days of exercise training on insulin sensitivity and responsiveness in type 2 diabetes mellitus. *Am J Physiol Endochrinol Metab*, 297(1):E151–6.

[112] Knowler, W. C., Barrett-Connor, E., Fowler, S. E., Hamman, R. F., Lachin, R. F., Walker, E. A., and Nathan, D. N. (2002). Reduction in the incidence of type 2 diabetes with lifestyle intervention or metformin. *New England Journal of Medicine*, 346(6).

[113] Koffert, J. P., Mikkola, K., Virtanen, K. A., Andersson, A.-M. D., Faxius, L., Hällsten, K., Heglind, M., Guiducci, L., Pham, T., Silvola, J. M. U., Virta, J., Eriksson, O., Kauhanen, S. P., Saraste, A., Enerbäck, S., Iozzo, P., Parkkola, R., Gomez, M. F., and Nuutila, P. (2017). Metformin treatment significantly enhances intestinal glucose uptake in patients with type 2 diabetes: Results from a randomized clinical trial. *Diabetes Research and Clinical Practice*, 131:208–216.

[114] Konopka, A. R., Laurin, J. L., Schoenberg, H. M., Reid, J. J., Castor, W. M., Wolff, C. A., Musci, R. V., Safairad, O. D., Linden, M. A., Biela, L. M., Bailey, S. M., Hamilton, K. L., and Miller, B. F. (2019). Metformin inhibits mitochondrial adaptations to aerobic exercise training in older adults. *Aging Cell*, 18(1):e12880.

[115] Korotchkina, L. G., Khailova, L. S., and Severin, S. E. (1995). The effect of phosphorylation on pyruvate dehydrogenase. *FEBS Lett*, 364(2):185–8.

[116] Koziris, L. P., Hickson, R. C., Chatterton, R. T., J., Groseth, R. T., Christie, J. M., Goldflies, D. G., and Unterman, T. G. (1999). Serum levels of total and free IGF-I and IGFBP-3 are increased and maintained in long-term training. *J Appl Physiol (1985)*, 86(4):1436–42.

[117] Kristensen, J. M., Larsen, S., Helge, J. W., Dela, F., and Wojtaszewski, J. F. (2013). Two weeks of metformin treatment enhances mitochondrial respiration in skeletal muscle of AMPK kinase dead but not wild type mice. *PLoS One*, 8(1):e53533.

[118] Kristensen, J. M., Lillelund, C., Kjøbsted, R., Birk, J. B., Andersen, N. R., Nybo, L., Mellberg, K., Balendran, A., Richter, E. A., and Wojtaszewski, J. F. P. (2019). Metformin does not compromise energy status in human skeletal muscle at rest or during acute exercise: A randomised, crossover trial. *Physiol Rep*, 7(23):e14307.

[119] Kulkarni, A. S., Brutsaert, E. F., Anghel, V., Zhang, K., Bloomgarden, N., Pollak, M., Mar, J. C., Hawkins, M., Crandall, J. P., and Barzilai, N. (2018). Metformin regulates metabolic and nonmetabolic pathways in skeletal muscle and subcutaneous adipose tissues of older adults. *Aging Cell*, 17(2).

[120] Kulkarni, A. S., Peck, B. D., Walton, R. G., Kern, P. A., Mar, J. C., Windham, S. T., Bamman, M. M., Barzilai, N., and Peterson, C. A. (2020). Metformin alters skeletal muscle transcriptome adaptations to resistance training in older adults. *Aging (Albany NY)*, 12(20):19852–19866.

[121] Kumar, N. and Dey, C. S. (2002). Metformin enhances insulin signalling in insulin-dependent and -independent pathways in insulin resistant muscle cells. *Br J Pharmacol*, 137(3).

[122] Kumari, S., Bubak, M. T., Schoenberg, H. M., Davidyan, A., Elliehausen, C. J., Kuhn, K. G., VanWagoner, T. M., Karaman, R., Scofield, R. H., Miller, B. F., and Konopka, A. R. (2022). Antecedent Metabolic Health and Metformin (ANTHEM) aging study: rationale and study design for a randomized controlles trial. *J Gerontol A Biol Sci Med Sci*, 77(12).

[123] Kuo, I. Y. and Ehrlich, B. E. (2015). Signaling in muscle contraction. *Cold Spring Harb Perspect Biol*, 7(2):a006023.

[124] Kwong, S. C. and Brubacher, J. (1998). Phenformin and lactic acidosis: a case report and review. *J Emerg Med*, 16(6).

[125] Kyu, H. H., Bachman, V. F., Alexander, L. T., Mumford, J. E., Afshin, A., Estep, K., Veerman, J. L., Delwiche, K., Iannarone, M. L., Moyer, M. L., Cercy, K., Vos, T., Murray, C. J., and Forouzanfar, M. H. (2016). Physical activity and risk of breast cancer, colon cancer, diabetes, ischemic heart disease, and ischemic stroke events: systematic review and dose-response meta-analysis for the Global Burden of Disease Study 2013. *Bmj*, 354:i3857.

[126] Lalau, J. D., Lacroix, C., Compagnon, P., Cagny, B. d., Rigaud, J. P., Bleichner, G., Chauveau, P., Dulbecco, P., Guérin, C., Haegy, J. M., Loirat, P., Marchand, B., Ravaud, Y., Weyne, P., and Fournier, A. (1995). Role of metformin accumulation in metformin-associated lactic acidosis. *Diabetes Care*, 18(6):779–784.

[127] Lalau, J. D. and Race, J. M. (2001). Lactic acidosis in metformin therapy: searching for a link with metformin in reports of 'metformin-associated lactic acidosis'. *Diabetes Obes Metab*, 3(3):195–201.

[128] LaMoia, T. E. and Shulman, G. I. (2021). Cellular and molecular mechanisms of metformin action. *Endocr Rev*, 42(1):77–96.

[129] Lamon, S., Wallace, M. A., Léger, B., and Russell, A. P. (2009). Regulation of STARS and its downstream targets suggest a novel pathway involved in human skeletal muscle hypertrophy and atrophy. *J Physiol*, 587(Pt 8):1795–803.

[130] Lamon, S., Wallace, M. A., and Russell, A. P. (2014). The STARS signaling pathway: a key regulator of skeletal muscle function. *Pflugers Arch*, 466(9):1659–71.

[131] Landgraf, R., Aberle, J., Birkenfeld, A. L., Gallwitz, B., Kellerer, M., Klein, H. H., Müller-Wieland, D., Nauck, M. A., Wiesner, T., and Siegel, E. (2023). Therapie des Typ-2-Diabetes. *Diabetologie und Stoffwechsel*, 18(S 02):S162–S217.

[132] Larsen, S., Rabøl, R., Hansen, C. N., Madsbad, S., Helge, J. W., and Dela, F. (2012). Metformin-treated patients with type 2 diabetes have normal mitochondrial complex I respiration. *Diabetologia*, 55(2):443–9.

[133] Larsson, L., Degens, H., Li, M., Salviati, L., Lee, Y. I., Thompson, W., Kirkland, J. L., and Sandri, M. (2019). Sarcopenia: Aging-related loss of muscle mass and function. *Physiol Rev*, 99(1):427–511.

[134] Learsi, S. K., Bastos-Silva, V. J., Lima-Silva, A. E., Bertuzzi, R., and De Araujo, G. G. (2015). Metformin improves performance in high-intensity exercise, but not anaerobic capacity in healthy male subjects. *Clin Exp Pharmacol Physiol*, 42(10):1025–9.

[135] Lee, J. O., Lee, S. K., Jung, J. H., Kim, J. H., You, G. Y., Kim, S. J., Park, S. H., Uhm, K. O., and Kim, H. S. (2011). Metformin induces Rab4 through AMPK and modulates GLUT4 translocation in skeletal muscle cells. *J Cell Physiol*, 226(4):974–81.

[136] Leenders, M., Verdijk, L. B., van der Hoeven, L., Adam, J. J., van Kranenburg, J., Nilwik, R., and van Loon, L. J. (2013). Patients with type 2 diabetes show a greater decline in muscle mass, muscle strength, and functional capacity with aging. *J Am Med Dir Assoc*, 14(8):585–92.

[137] Li, D. J., Huang, F., Lu, W. J., Jiang, G. J., Deng, Y. P., and Shen, F. M. (2015). Metformin promotes irisin release from murine skeletal muscle independently of AMP-activated protein kinase activation. *Acta Physiol (Oxf)*, 213(3):711–21.

[138] Li, R., Xia, J., Zhang, X. I., Gathirua-Mwangi, W. G., Guo, J., Li, Y., McKenzie, S., and Song, Y. (2018). Associations of muscle mass and strength with all-cause mortality among US older adults. *Med Sci Sports Exerc*, 50(3):458–467.

[139] Liang, X. and Giacomini, K. M. (2017). Transporters involved in metformin pharmacokinetics and treatment response. *J Pharm Sci*, 106(9):2245–2250.

[140] Lindström, J., Louheranta, A., Mannelin, M., Rastas, M., Salminen, V., Eriksson, J., Uusitupa, M., and Tuomilehto, J. (2003). The Finnish Diabetes Prevention Study (DPS): lifestyle intervention and 3-year results on diet and physial activity. *Diabetes Care*, 26(12):3230–6.

[141] London: National Institute for Health and Care Excellence (NICE) (2022). Type 2 diabetes in adults: management. *NICE guideline*.

[142] Long, D. E., Peck, B. D., Martz, J. L., Tuggle, S. C., Bush, H. M., McGwin, G., Kern, P. A., Bamman, M. M., and Peterson, C. A. (2017). Metformin to Augment Strength Training Effective Response in Seniors (MASTERS): study protocol for a randomized controlled trial. *Trials*, 18(2):192.

[143] Luizon, M., Eckalbar, W. L., Wang, Y., Jones, S. L., Smith, R. P., Laurance, M., Lin, L., Gallins, P. J., Etheridge, A. S., Wright, F., Zhou, Y., Molony, C., Innocenti, F., Yee, S. W., Giacomini, K. M., and Ahituv, N. (2016). Genomic characterization of metformin hepatic response. *PLoS Genet*, 12(11):e1006449.

[144] Lyu, Q., Wen, Y., He, B., Zhang, X., Chen, J., Sun, Y., Zhao, Y., Xu, L., Xiao, Q., and Deng, H. (2022). The ameliorating effects of metformin on disarrangement ongoing in gastrocnemius muscle of sarcopenic and obese sarcopenic mice. *Biochim Biophys Acta Mol Basis Dis*, 1868(11):166508.

[145] López-Cervantes, S. P., Sánchez, N. S., Calahorra, M., Mena-Montes, B., Pedraza-Vázquez, G., Hernández-Álvarez, D., Esparza-Perusquía, M., Peña, A., López-Díazguerrero, N. E., Alarcón-Aguilar, A., Luna-López, A., Flores-Herrera, O., and Königsberg, M. (2022). Moderate exercise combined with metformin-treatment improves mitochondrial bioenergetics of the quadriceps muscle of old female wistar rats. *Arch Gerontol Geriatr*, 102:104717.

[146] Ma, T., Tian, X., Zhang, B., Li, M., Wang, Y., Yang, C., Wu, J., Wei, X., Qu, Q., Yu, Y., Long, S., Feng, J. W., Li, C., Zhang, C., Xie, C., Wu, Y., Xu, Z., Chen, J., Yu, Y., Huang, X., He, Y., Yao, L., Zhang, L., Zhu, M., Wang, W., Wang, Z. C., Zhang, M., Bao, Y., Jia, W., Lin, S. Y., Ye, Z., Piao, H. L., Deng, X., Zhang, C. S., and Lin, S. C. (2022). Low-dose metformin targets the lysosomal AMPK pathway through PEN2. *Nature*, 603(7899):159–165.

[147] Madden, L., Juhas, M., Kraus, W. E., Truskey, G. A., and Bursac, N. (2015). Bioengineered human myobundles mimic clinical responses of skeletal muscle to drugs. *Elife*, 4:e04885.

[148] Madiraju, A. K., Erion, D. M., Rahimi, Y., Zhang, X. M., Braddock, D. T., Albright, R. A., Prigaro, B. J., Wood, J. L., Bhanot, S., MacDonald, M. J., Jurczak, M. J., Camporez, J. P., Lee, H. Y., Cline, G. W., Samuel, V. T., Kibbey, R. G., and Shulman, G. I. (2014). Metformin suppresses gluconeogenesis by inhibiting mitochondrial glycerophosphate dehydrogenase. *Nature*, 510(7506):542–6.

[149] Madiraju, A. K., Qiu, Y., Perry, R. J., Rahimi, Y., Zhang, X. M., Zhang, D., Camporez, J. G., Cline, G. W., Butrico, G. M., Kemp, B. E., Casals, G., Steinberg, G. R., Vatner, D. F., Petersen, K. F., and Shulman, G. I. (2018). Metformin inhibits gluconeogenesis via a redox-dependent mechanism in vivo. *Nat Med*, 24(9):1384–1394.

[150] Magkos, F., Hjorth, M. F., and Astrup, A. (2020). Diet and exercise in the prevention and treatment of type 2 diabetes mellitus. *Nat Rev Endocrinol*, 16(10):545–555.

[151] Malin, S. K. and Braun, B. (2013). Effect of metformin on substrate utilization after exercise training in adults with impaired glucose tolerance. *Appl Physiol Nutr Metab*, 38(4):427–30.

[152] Malin, S. K., Gerber, R., Chipkin, S. R., and Braun, B. (2012). Independent and combined effects of exercise training and metformin on insulin sensitivity in individuals with prediabetes. *Diabetes Care*, 35(1):131–6.

[153] Manabe, Y., Miyatake, S., Takagi, M., Nakamura, M., Okeda, A., Nakano, T., Hirshman, M. F., Goodyear, L. J., and Fujii, N. L. (2012). Characterization of an acute muscle contraction model using cultured C2C12 myotubes. *PloS One*, 7(12):e52592.

[154] Mann, G., Riddell, M. C., and Adegoke, O. A. J. (2022). Effects of acute muscle contraction on the key molecules in insulin and Akt signaling in skeletal muscle in health and in insulin resistant states. *Diabetology*, 3(3):423–446.

[155] Mannucci, E., Tesi, F., Bardini, G., Ognibene, A., Petracca, M. G., Ciani, S., Pezzatini, A., Brogi, M., Dicembrini, I., Cremasco, F., Messeri, G., and Rotella, C. M. (2004). Effects of metformin on glucagon-like peptide-1 levels in obese patients with and without type 2 diabetes. *Diabetes Nutr Metab*, 17(6):336–42.

[156] Maurer, J., Zhao, X., Irmler, M., Gudiksen, A., Pilmark, N. S., Li, Q., Goj, T., Beckers, J., Hrabě de Angelis, M., Birkenfeld, A., Peter, A., Lehmann, R., Pilegaard, H., Karstoft, K., Xu, G., and Weigert, C. (2023). Redox state and altered pyruvate metabolism contribute to a dose-dependent metformin-induced lactate production of human myotubes. *Am J Physiol Cell Physiol*.

[157] McKenzie, A. I., Mahmassani, Z. S., Petrocelli, J. J., de Hart, N., Fix, D. K., Ferrara, P. J., LaStayo, P. C., Marcus, R. L., Rondina, M. T., Summers, S. A., Johnson, J. M., Trinity, J. D., Funai, K., and Drummond, M. J. (2022). Short-term exposure to a clinical dose of metformin increases skeletal muscle mitochondrial H_2O_2 emission and production in healthy, older adults: A randomized controlled trial. *Exp Gerontol*, 163:111804.

[158] McNamara, J. W., Singh, R. R., and Sadayappan, S. (2019). Cardiac myosin binding protein-c phosphorylation regulates the super-relaxed state of myosin. *Proc Natl Acad Sci U S A*, 116(24):11731–11736.

[159] Meex, R. C., Schrauwen-Hinderling, V. B., Moonen-Kornips, E., Schaart, G., Mensink, M., Phielix, E., van de Weijer, T., Sels, J. P., Schrauwen, P., and Hesselink, M. K. (2010). Restoration of muscle mitochondrial function and metabolic flexibility in type 2 diabetes by exercise training is paralleled by increased myocellular fat storage and improved insulin sensitivity. *Diabetes*, 59(3):572–9.

[160] Mikines, K. J., Sonne, B., Farrell, P. A., Tronier, B., and Galbo, H. (1988). Effect of physical exercise on sensitivity and responsiveness to insulin in humans. *American Journal of Physiology-Endocrinology and Metabolism*, 254(3):E248–E259.

[161] Miller, R. A., Chu, Q., Xie, J., Foretz, M., Viollet, B., and Birnbaum, M. J. (2013). Biguanides suppress hepatic glucagon signalling by decreasing production of cyclic AMP. *Nature*, 494(7436):256–60.

[162] Mohammed, I., Hollenberg, M. D., Ding, H., and Triggle, C. R. (2021). A critical review of the evidence that metformin is a putative anti-aging drug that enhances healthspan and extends lifespan. *Front Endocrinol (Lausanne)*, 12:718942.

[163] Mohankumar, K., Lee, J., Wu, C. S., Sun, Y., and Safe, S. (2018). Bis-indole-derived NR4A1 ligands and metformin exhibit NR4A1-dependent glucose metabolism and uptake in C2C12 cells. *Endocrinology*, 159(5):1950–1963.

[164] Moonira, T., Chachra, S. S., Ford, B. E., Marin, S., Alshawi, A., Adam-Primus, N. S., Arden, C., Al-Oanzi, Z. H., Foretz, M., Viollet, B., Cascante, M., and Agius, L. (2020). Metformin lowers glucose 6-phosphate in hepatocytes by activation of glycolysis downstream of glucose phosphorylation. *J Biol Chem*, 295(10):3330–3346.

[165] Moreno-Cabañas, A., Morales-Palomo, F., Alvarez-Jimenez, L., Ortega, J. F., and Mora-Rodriguez, R. (2022). Effects of chronic metformin treatment on training adaptations in men and women with hyperglycemia: a prospective study. *Obesity (Silver Spring)*, 30(6):1219–1230.

[166] Morita, M., Gravel, S. P., Chénard, V., Sikström, K., Zheng, L., Alain, T., Gandin, V., Avizonis, D., Arguello, M., Zakaria, C., McLaughlan, S., Nouet, Y., Pause, A., Pollak, M., Gottlieb, E., Larsson, O., St-Pierre, J., Topisirovic, I., and Sonenberg, N. (2013). mTORC1 controls mitochondrial activity and biogenesis through 4E-BP-dependent translational regulation. *Cell Metab*, 18(5):698–711.

[167] Mueller, W. M., Stanhope, K. L., Gregoire, F., Evans, J. L., and Havel, P. J. (2000). Effects of metformin and vanadium on leptin secretion from cultured rat adipocytes. *Obesity Research*, 8(7):530–539.

[168] Musi, N., Fujii, N., Hirshman, M. F., Ekberg, I., Fröberg, S., Ljungqvist, O., Thorell, A., and Goodyear, L. J. (2001). AMP-activated protein kinase (AMPK) is activated in muscle of subjects with type 2 diabetes during exercise. *Diabetes*, 50(5):921–7.

[169] Musi, N., Hirshman, M. F., Nygren, J., Svanfeldt, M., Bavenholm, P., Rooyackers, O., Zhou, G., Williamson, J. M., Ljunqvist, O., Efendic, S., Moller, D. E., Thorell, A., and Goodyear, L. J. (2002). Metformin increases AMP-activated protein kinase activity in skeletal muscle of subjects with type 2 diabetes. *Diabetes*, 51(7):2074–81.

[170] Nadkarni, P., Chepurny, O. G., and Holz, G. G. (2014). *Chapter Two - Regulation of Glucose Homeostasis by GLP-1*, volume 121, pages 23–65. Academic Press.

[171] Nag, S., Gollapudi, S. K., del Rio, C. L., Spudich, J. A., and McDowell, R. (2023). Mavacamten, a precision medicine for hypertrophic cardiomyopathy: From a motor protein to patients. *Science Advances*, 9(30):eabo7622.

[172] National Center for Biotechnology Information (2023). *PubChem Compound Summary for CID 14219, Metformin Hydrochloride.* Accessed: 2023-11-09.

[173] Newman, A. B., Kupelian, V., Visser, M., Simonsick, E. M., Goodpaster, B. H., Kritchevsky, S. B., Tylavsky, F. A., Rubin, S. M., and Harris, T. B. (2006). Strength, but not muscle mass, is associated with mortality in the health, aging and body composition study cohort. *J Gerontol A Biol Sci Med Sci*, 61(1):72–7.

[174] Nikolić, N., Görgens, S. W., Thoresen, G. H., Aas, V., Eckel, J., and Eckardt, K. (2017). Electrical pulse stimulation of cultured skeletal muscle cells as a model for in vitro exercise - possibilities and limitations. *Acta Physiol (Oxf)*, 220(3):310–331.

[175] Ong, K. L., Stafford, L. K., McLaughlin, S. A., Boyko, E. J., Vollset, S. E., Smith, A. E., Dalton, B. E., Duprey, J., Cruz, J. A., Hagins, H., et al. (2023). Global, regional, and national burden of diabetes from 1990 to 2021, with projections of prevalence to 2050: a systematic analysis for the Global Burden of Disease Study 2021. *The Lancet*, 402(10397):203–234.

[176] Ortega, J. F., Hamouti, N., Fernández-Elías, V. E., de Prada, M. V., Martínez-Vizcaíno, V., and Mora-Rodríguez, R. (2014). Metformin does not attenuate the acute insulin-sensitizing effect of a single bout of exercise in individuals with insulin resistance. *Acta Diabetol*, 51(5):749–55.

[177] Oshima, R., Yamada, M., Kurogi, E., Ogino, Y., Serizawa, Y., Tsuda, S., Ma, X., Egawa, T., and Hayashi, T. (2015). Evidence for organic cation transporter-mediated metformin transport and 5'-adenosine monophosphate-activated protein kinase activation in rat skeletal muscles. *Metabolism*, 64(2):296–304.

[178] Ota, S., Horigome, K., Ishii, T., Nakai, M., Hayashi, K., Kawamura, T., Kishino, A., Taiji, M., and Kimura, T. (2009). Metformin suppresses glucose-6-phosphatase expression by a complex I inhibition and AMPK activation-independent mechanism. *Biochem Biophys Res Commun*, 388(2):311–6.

[179] Ouyang, J., Parakhia, R. A., and Ochs, R. S. (2011). Metformin activates AMP kinase through inhibition of AMP deaminase. *J Biol Chem*, 286(1):1–11.

[180] Owen, M. R., Doran, E., and Halestrap, A. P. (2000). Evidence that metformin exerts its anti-diabetic effects through inhibition of complex 1 of the mitochondrial respiratory chain. *Biochem J*, 348 Pt 3(Pt 3):607–14.

[181] Panfoli, I., Puddu, A., Bertola, N., Ravera, S., and Maggi, D. (2021). The hormetic effect of metformin: "less is more"? *Int J Mol Sci*, 22(12).

[182] Park, S., Jeon, J. H., Min, B. K., Ha, C. M., Thoudam, T., Park, B. Y., and Lee, I. K. (2018). Role of the pyruvate dehydrogenase complex in metabolic remodeling: Differential pyruvate dehydrogenase complex functions in metabolism. *Diabetes Metab J*, 42(4):270–281.

[183] Park, S. W., Goodpaster, B. H., Strotmeyer, E. S., de Rekeneire, N., Harris, T. B., Schwartz, A. V., Tylavsky, F. A., and Newman, A. B. (2006). Decreased muscle strength and quality in older adults with type 2 diabetes: the health, aging, and body composition study. *Diabetes*, 55(6):1813–8.

[184] Parker, E. D., Lin, J., Mahoney, T., Ume, N., Yang, G., Gabbay, R. A., ElSayed, N. A., and Bannuru, R. R. (2023). Economic costs of diabetes in the U.S. in 2022. *Diabetes Care*.

[185] Pavlovic, K., Krako Jakovljevic, N., Isakovic, A. M., Ivanovic, T., Markovic, I., and Lalic, N. M. (2022). Therapeutic vs. suprapharmacological metformin concentrations: Different effects on energy metabolism and mitochondrial function in skeletal muscle cells in vitro. *Frontiers in Pharmacology*, 13.

[186] Pedersen, B. K. and Saltin, B. (2015). Exercise as medicine - evidence for prescribing exercise as therapy in 26 different chronic diseases. *Scand J Med Sci Sports*, 25 Suppl 3:1–72.

[187] Perakakis, N., Triantafyllou, G. A., Fernández-Real, J. M., Huh, J. Y., Park, K. H., Seufert, J., and Mantzoros, C. S. (2017). Physiology and role of irisin in glucose homeostasis. *Nat Rev Endocrinol*, 13(6):324–337.

[188] Pernicova, I. and Korbonits, M. (2014). Metformin - mode of action and clinical implications for diabetes and cancer. *Nat Rev Endocrinol*, 10(3):143–56.

[189] Piel, S., Ehinger, J. K., Elmér, E., and Hansson, M. J. (2015). Metformin induces lactate production in peripheral blood mononuclear cells and platelets through specific mitochondrial complex I inhibition. *Acta Physiol (Oxf)*, 213(1):171–80.

[190] Pilmark, N. S., Lyngbæk, M., Oberholzer, L., Elkjær, I., Petersen-Bønding, C., Kofoed, K., Siebenmann, C., Kellenberger, K., van Hall, G., Abildgaard, J., Ellingsgaard, H., Lauridsen, C., Ried-Larsen, M., Pedersen, B. K., Hansen, K. B., and Karstoft, K. (2021a). The interaction between metformin and physical activity on postprandial glucose and glucose kinetics: a randomised, clinical trial. *Diabetologia*, 64(2):397–409.

[191] Pilmark, N. S., Oberholzer, L., Halling, J. F., Kristensen, J. M., Bønding, C. P., Elkjær, I., Lyngbæk, M., Elster, G., Siebenmann, C., Holm, N. F. R., Birk, J. B., Larsen, E. L., Lundby, A. M., Wojtaszewski, J., Pilegaard, H., Poulsen, H. E., Pedersen, B. K., Hansen, K. B., and Karstoft, K. (2022). Skeletal muscle adaptations to exercise are not influenced by metformin treatment in humans: secondary analyses of 2 randomized, clinical trials. *Appl Physiol Nutr Metab*, 47(3):309–320.

[192] Pilmark, N. S., Petersen-Bønding, C., Holm, N. F. R., Johansen, M. Y., Pedersen, B. K., Hansen, K. B., and Karstoft, K. (2021b). The effect of metformin on self-selected exercise intensity in healthy, lean males: a randomized, crossover, counterbalanced trial. *Front Endocrinol (Lausanne)*, 12:599164.

[193] Pleus, S., Tytko, A., Landgraf, R., Heinemann, L., Werner, C., Müller-Wieland, D., Ziegler, A.-G., Müller, U. A., Freckmann, G., Kleinwechter, H., Schleicher, E., Nauck, M., and Petersmann, A. (2023). Definition, Klassifikation, Diagnostik und Differenzialdiagnostik des Diabetes mellitus: Update 2023. *Diabetologie und Stoffwechsel*, 18(S 02):S100–S113.

[194] Proctor, W. R., Bourdet, D. L., and Thakker, D. R. (2008). Mechanisms underlying saturable intestinal absorption of metformin. *Drug Metab Dispos*, 36(8):1650–8.

[195] Protti, A., Lecchi, A., Fortunato, F., Artoni, A., Greppi, N., Vecchio, S., Fagiolari, G., Moggio, M., Comi, G. P., Mistraletti, G., Lanticina, B., Faraldi, L., and Gattinoni, L. (2012). Metformin overdose causes platelet mitochondrial dysfunction in humans. *Crit Care*, 16(5):R180.

[196] Protti, A., Properzi, P., Magnoni, S., Santini, A., Langer, T., Guenzani, S., Ferrero, S., Bassani, G., Stocchetti, N., and Gattinoni, L. (2016). Skeletal muscle lactate overproduction during metformin intoxication: An animal study with reverse microdialysis. *Toxicol Lett*, 255:43–6.

[197] R Core Team (2022). *R: A Language and Environment for Statistical Computing*. R Foundation for Statistical Computing, Vienna, Austria.

[198] Rardin, M. J., Wiley, S. E., Naviaux, R. K., Murphy, A. N., and Dixon, J. E. (2009). Monitoring phosphorylation of the pyruvate dehydrogenase complex. *Anal Biochem*, 389(2):157–64.

[199] Raudvere, U., Kolberg, L., Kuzmin, I., Arak, T., Adler, P., Peterson, H., and Vilo, J. (2019). g:profiler: a web server for functional enrichment analysis and conversions of gene lists (2019 update). *Nucleic Acids Research*, 47(W1):W191–W198.

[200] Ravindran, S., Kuruvilla, V., Wilbur, K., and Munusamy, S. (2017). Nephroprotective effects of metformin in diabetic nephropathy. *J Cell Physiol*, 232(4):731–742.

[201] Richter, E. A., Sylow, L., and Hargreaves, M. (2021). Interactions between insulin and exercise. *Biochem J*, 478(21):3827–3846.

[202] Ricoult, S. J. and Manning, B. D. (2013). The multifaceted role of mTORC1 in the control of lipid metabolism. *EMBO Rep*, 14(3):242–51.

[203] Rittig, N., Aagaard, N. K., Sundelin, E., Villadsen, G. E., Sandahl, T. D., Holst, J. J., Hartmann, B., Brøsen, K., Grønbaek, H., and Jessen, N. (2021). Metformin stimulates intestinal glycolysis and lactate release: A single-dose study of metformin in patients with intrahepatic portosystemic stent. *Clin Pharmacol Ther*, 110(35):1329–1336.

[204] Robergs, R. A., Ghiasvand, F., and Parker, D. (2004). Biochemistry of exercise-induced metabolic acidosis. *Am J Physiol Regul Integr Comp Physiol*, 287(3):R502–16.

[205] Robergs, R. A., McNulty, C. R., Minett, G. M., Holland, J., and Trajano, G. (2018). Lactate, not lactic acid, is produced by cellular cytosolic energy catabolism. *Physiology (Bethesda)*, 33(1):10–12.

[206] Roth, S. M., Ferrell, R. F., and Hurley, B. F. (2000). Strength training for the prevention and treatment of sarcopenia. *J Nutr Health Aging*, 4(3):143–55.

[207] Rowles, J., Scherer, S. W., Xi, T., Majer, M., Nickle, D. C., Rommens, J. M., Popov, K. M., Harris, R. A., Riebow, N. L., Xia, J., Tsui, L. C., Bogardus, C., and Prochazka, M. (1996). Cloning and characterization of PDK4 on 7q21.3 encoding a fourth pyruvate dehydrogenase kinase isoenzyme in human. *J Biol Chem*, 271(37):22376–82.

[208] RStudio Team (2020). *RStudio: Integrated Development Environment for R*. RStudio, PBC., Boston, MA.

[209] Sahlin, K., Harris, R., Nylind, B., and Hultman, E. (1976). Lactate content and pH in muscle obtained after dynamic exercise. *Pflugers Arch*, 367(2):143–9.

[210] Sajan, M. P., Bandyopadhyay, G., Miura, A., Standaert, M. L., Nimal, S., Longnus, S. L., Van Obberghen, E., Hainault, I., Foufelle, F., Kahn, R., Braun, U., Leitges, M., and Farese, R. V. (2010). AICAR and metformin, but not exercise, increase muscle glucose transport through AMPK-, ERK-, and PDK1-dependent activation of atypical PKC. *Am J Physiol Endocrinol Metab*, 298(2):E179–92.

[211] Sarabia, V., Lam, L., Burdett, E., Leiter, L. A., and Klip, A. (1992). Glucose transport in human skeletal muscle cells in culture. stimulation by insulin and metformin. *J Clin Invest*, 90(4):1386–95.

[212] Scheen, A. J. (1996). Clinical pharmacokinetics of metformin. *Clinical Pharmacokinetics*, 30(5):359–371.

[213] Scheler, M., de Angelis, M. H., Al-Hasani, H., Häring, H. U., Weigert, C., and Lehr, S. (2015). Methods for proteomics-based analysis of the human muscle secretome using an in vitro exercise model. *Methods Mol Biol*, 1295:55–64.

[214] Schiaffino, S., Reggiani, C., Akimoto, T., and Blaauw, B. (2021). Molecular mechanisms of skeletal muscle hypertrophy. *Journal of Neuromuscular Diseases*, 8:169–183.

[215] Schneider, O., Zeifang, L., Fuchs, S., Sailer, C., and Loskill, P. (2019). User-friendly and parallelized generation of human induced pluripotent stem cell-derived microtissues in a centrifugal heart-on-a-chip. *Tissue Eng Part A*, 25(9-10):786–798.

[216] Scott, B., Day, E. A., O'Brien, K. L., Scanlan, J., Cromwell, G., Scannail, A. N., McDonnell, M. E., Finlay, D. K., and Lynch, L. (2024). Metformin and feeding increase levels of the appetite-suppressing metabolite Lac-Phe in humans. *Nature Metabolism*.

[217] Shah, M. and Vella, A. (2014). Effects of GLP-1 on appetite and weight. *Rev Endocr Metab Disord*, 15(3):181–7.

[218] Sharoff, C. G., Hagobian, T. A., Malin, S. K., Chipkin, S. R., Yu, H., Hirshman, M. F., Goodyear, L. J., and Braun, B. (2010). Combining short-term metformin treatment and one bout of exercise does not increase insulin action in insulin-resistant individuals. *Am J Physiol Endocrinol Metab*, 298(4):E815–23.

[219] Shaw, R. J., Lamia, K. A., Vasquez, D., Koo, S. H., Bardeesy, N., Depinho, R. A., Montminy, M., and Cantley, L. C. (2005). The kinase LKB1 mediates glucose homeostasis in liver and therapeutic effects of metformin. *Science*, 310(5754):1642–6.

[220] Shu, Y., Sheardown, S. A., Brown, C., Owen, R. P., Zhang, S., Castro, R. A., Ianculescu, A. G., Yue, L., Lo, J. C., Burchard, E. G., Brett, C. M., and Giacomini, K. M. (2007). Effect of genetic variation in the organic cation transporter 1 (OCT1) on metformin action. *J Clin Invest*, 117(5):1422–31.

[221] Spriet, L. L. and Heigenhauser, G. J. (2002). Regulation of pyruvate dehydrogenase (PDH) activity in human skeletal muscle during exercise. *Exerc Sport Sci Rev*, 30(2):91–5.

[222] Srikanthan, P. and Karlamangla, A. S. (2011). Relative muscle mass is inversely associated with insulin resistance and prediabetes. Findings from the third national health and nutrition examination survey. *The Journal of Clinical Endocrinology & Metabolism*, 96(9):2898–2903.

[223] Stanford, K. I. and Goodyear, L. J. (2014). Exercise and type 2 diabetes: molecular mechanisms regulating glucose uptake in skeletal muscle. *Adv Physiol Educ*, 38(4):308–14.

[224] Stumvoll, M., Nurjhan, N., Perriello, G., Dailey, G., and Gerich, J. E. (1995). Metabolic effects of metformin in non-insulin-dependent diabetes mellitus. *N Engl J Med*, 333(9):550–4.

[225] Sugano, T., Shiota, M., Tanaka, T., Miyamae, Y., Shimada, M., and Oshino, N. (1980). Intracellular redox state and stimulation of gluconeogenesis by glucagon and norepinephrine in the perfused rat liver. *J Biochem*, 87(1):153–66.

[226] Sun, S., Li, H., Chen, J., and Qian, Q. (2017). Lactic acid: no longer an inert and end-prodct of glycolysis. *Physiology (Bethesda)*, 32(6):453–463.

[227] Takahashi, T., Li, Y., Chen, W., Nyasha, M. R., Ogawa, K., Suzuki, K., Koide, M., Hagiwara, Y., Itoi, E., Aizawa, T., Tsuchiya, M., Suzuki, N., Aoki, M., and Kanzaki, M. (2022). RSPO3 is a novel contraction-inducible factor identified in an "in vitro exercise model" using primary human myotubes. *Sci Rep*, 12(1):14291.

[228] Tobar, N., Rocha, G. Z., Santos, A., Guadagnini, D., Assalin, H. B., Camargo, J. A. Gonçalves, A., Pallis, F. R., Oliveira, A. G., Rocco, S. A., Neto, R. M., de Sousa, I. L., Alborghetti, M. R., Sforça, M. L., Rodrigues, P. B., Ludwig, R. G., Vanzela, E. C., Brunetto, S. Q., Boer, P. A., Gontijo, J. A. R., Geloneze, B., Carvalho, C. R. O., Prada, P. O., Folli, F., Curi, R., Mori, M. A., Vinolo, M. A. R., Ramos, C. D., Franchini, K. G., Tormena, C. F., and Saad, M. J. A. (2023). Metformin acts in the gut and induces gut-liver crosstalk. *Proc Natl Acad Sci U S A*, 120(4):e2211933120.

[229] Toyama, K., Yonezawa, A., Masuda, S., Osawa, R., Hosokawa, M., Fujimoto, S., Inagaki, N., Inui, K., and Katsura, T. (2012). Loss of multidrug and toxin extrusion 1 (MATE1) is associated with metformin-induced lactic acidosis. *Br J Pharmacol*, 166(3):1183–91.

[230] Tsuda, M., Terada, T., Minzuno, T., Katsura, T., Shimakura, J., and Inui, K. (2009). Targeted disruption of the multidrug and toxin extrusion 1 (MATE1) gene in mice reduces renal secretion of metformin. *Molecular Pharmacology*, 75(6):1280.

[231] Tucker, G., Casey, C., Phillips, P., Connor, H., Ward, J., and Woods, H. (1981). Metformin kinetics in healthy subjects and in patients with diabetes mellitus. *British Journal of Clinical Pharmacology*, 12(2):235–246.

[232] Turban, S., Stretton, C., Drouin, O., Green, C. J., Watson, M. L., Gray, A., Ross, F., Lantier, L., Viollet, B., Hardie, D. G., Marette, A., and Hundal, H. S. (2012). Defining the contribution of AMP-activated protein kinase (AMPK) and protein kinase c (PKC) in regulation of glucose uptake by metformin in skeletal muscle cells. *J Biol Chem*, 287(24):20088–99.

[233] Tzvetkov, M. V., Vormfelde, S. V., Balen, D., Meineke, I., Schmidt, T., Sehrt, D., Sabolić, I., Koepsell, H., and Brockmöller, J. (2009). The effects of genetic polymorphisms in the organic cation transporters OCT1, OCT2, and OCT3 on the renal clearance of metformin. *Clinical Pharmacology & Therapeutics*, 86(3):299–306.

[234] van Berlo-van de Laar, I. R., Vermeij, C. G., and Doorenbos, C. J. (2011). Metformin associated lactic acidosis: incidence and clinical correlation with metformin serum concentration measurements. *J Clin Pharm Ther*, 36(3):376–82.

[235] van Hall, G. (2010). Lactate kinetics in human tissues at rest and during exercise. *Acta Physiol (Oxf)*, 199(4):499–508.

[236] Vestergaard, P. F., Hansen, M., Frystyk, J., Espelund, U., Christiansen, J. S., Jørgensen, J. O., and Fisker, S. (2014). Serum levels of bioactive IGF1 and physiological markers of ageing in healthy adults. *Eur J Endocrinol*, 170(2):229–36.

[237] Vial, G., Detaille, D., and Guigas, B. (2019). Role of mitochondria in the mechanism(s) of action of metformin. *Front Endocrinol (Lausanne)*, 10:294.

[238] Viskochil, R., Malin, S. K., Blankenship, J. M., and Braun, B. (2017). Exercise training and metformin, but not exercise training alone, decreases insulin production and increases insulin clearance in adults with prediabetes. *J Appl Physiol (1985)*, 123(1):243–248.

[239] Vukovich, M. D., Arciero, P. J., Kohrt, W. M., Racette, S. B., Hansen, P. A., and Holloszy, J. O. (1996). Changes in insulin action and GLUT-4 with 6 days of inactivity in endurance runners. *J Appl Physiol (1985)*, 80(1):240–4.

[240] Wallace, M. A. and Russell, A. P. (2013). Striated muscle activator of Rho signaling is required for myotube survival but does not influence basal protein synthesis or degradation. *Am J Physiol Cell Physiol*, 305(4):C414–26.

[241] Walton, R. G., Dungan, C. M., Long, D. E., Tuggle, S. C., Kosmac, K., Peck, B. D., Bush, H. M., Villasante Tezanos, A. G., McGwin, G., Windham, S. T., Ovalle, F., Bamman, M. M., Kern, P. A., and Peterson, C. A. (2019). Metformin blunts muscle hypertrophy in response to progressive resistance exercise training in older adults: a randomized, double-blind, placebo-controlled, multicenter trial: the MASTERS trial. *Aging Cell*, 18(6):e13039.

[242] Wang, D. S., Jonker, J. W., Kato, Y., Kusuhara, H., Schinkel, A. H., and Sugiyama, Y. (2002). Involvement of organic cation transporter 1 in hepatic and intestinal distribution of metformin. *J Pharmacol Exp Ther*, 302(2):510–5.

[243] Wang, Y., An, H., Liu, T., Qin, C., Sesaki, H., Guo, S., Radovick, S., Hussain, M., Maheshwari, A., Wondisford, F. E., O'Rourke, B., and He, L. (2019). Metformin improves mitochondrial respiratory activity through activation of AMPK. *Cell Rep*, 29(6):1511–1523.e5.

[244] Wessels, B., Ciapaite, J., van den Broek, N. M., Nicolay, K., and Prompers, J. J. (2014). Metformin impairs mitochondrial function in skeletal muscle of both lean and diabetic rats in a dose-dependent manner. *PLoS One*, 9(6):e100525.

[245] White, A. T. and Schenk, S. (2012). NAD^+/NADH and skeletal muscle mitochondrial adaptations to exercise. *Am J Physiol Endocrinol Metab*, 303(3):E308–21.

[246] Wilcock, C. and Bailey, C. J. (1994). Accumulation of metformin by tissues of the normal and diabetic mouse. *Xenobiotica*, 24(1):49–57.

[247] Wu, C.-Y. and Benet, L. Z. (2005). Predicting drug disposition via application of BCS: transport/absorption/elimination interplay and development of a Biopharmaceutics DrugDisposition Classification System. *Pharmaceutical Research*, 22(1):11–23.

[248] Wu, G., Dai, Y., Yan, Y., Zheng, X., Zhang, H., Li, H., and Chen, W. (2022). The lactate receptor GPR81 mediates hepatic lipid metabolism and the therapeutic effect of metformin on experimental NAFLDs. *Eur J Pharmacol*, 924:174959.

[249] Wu, H., Kanatous, S. B., Thurmond, F. A., Gallardo, T., Isotani, E., Bassel-Duby, R., and Williams, R. S. (2002). Regulation of mitochondrial biogenesis in skeletal muscle by CaMK. *Science*, 296(5566):349–52.

[250] Xiao, S., Li, V. L., Lyu, X., Chen, X., Wei, W., Abbasi, F., Knowles, J. W., Tung, A. S., Deng, S., Tiwari, G., Shi, X., Zheng, S., Farrell, L., Chen, Z. Z., Taylor, K. D., Guo, X., Goodarzi, M. O., Wood, A. C., Ida Chen, Y. D., Lange, L. A., Rich, S. S., Rotter, J. I., Clish, C. B., Tahir, U. A., Gerszten, R. E., Benson, M. D., and Long, J. Z. (2024). Lac-Phe mediates the effects of metformin on food intake and body weight. *Nature metabolism*.

[251] Xiao, Y., Xu, M., Alimujiang, M., Bao, Y., Wei, L., and Yin, J. (2018). Bidirectional regulation of adenosine 5'-monophosphate-activated protein kinase activity by berberine and metformin in response to changes in ambient glucose concentration. *J Cell Biochem*, 119(12):9910–9920.

[252] Yang, M., Darwish, T., Larraufie, P., Rimmington, D., Cimino, I., Goldspink, D. A., Jenkins, B., Koulman, A., Brighton, C. A., Ma, M., Lam, B. Y. H., Coll, A. P., O'Rahilly, S., Reimann, F., and Gribble, F. M. (2021). Inhibition of mitochondrial function by metformin increases glucose uptake, glycolysis and GDF-15 release from intestinal cells. *Sci Rep*, 11(1):2529.

[253] Yang, Z., Chen, X., Chen, Y., and Zhao, Q. (2015). PGC-1 mediates the regulation of metformin in muscle irisin expression and function. *Am J Transl Res*, 7(10):1850–9.

[254] Yendapally, R., Sikazwe, D., Kim, S. S., Ramsinghani, S., Fraser-Spears, R., Witte, A. P., and La-Viola, B. (2020). A review of phenformin, metformin, and imeglimin. *Drug Dev Res*, 81(4):390–401.

[255] Yki-Järvinen, H., Bogardus, C., and Foley, J. E. (1990). Regulation of plasma lactate concentration in resting human subjects. *Metabolism*, 39(8):859–64.

[256] Yoshida, T. and Delafontaine, P. (2020). Mechanisms of IGF-1-mediated regulation of skeletal muscle hypertrophy and atrophy. *Cells*, 9(9).

[257] Zaharenko, L., Kalnina, I., Geldnere, K., Konrade, I., Grinberga, S., Židzik, J., Javorský, M., Lejnieks, A., Nikitina-Zake, L., Fridmanis, D., Peculis, R., Radovica-Spalvina, I., Hartmane, D., Pugovics, O., Tkáč, I., Klimčáková, L., Pīrāgs, V., and Klovins, J. (2016). Single nucleotide polymorphisms in the intergenic region between metformin transporter OCT2 and OCT3 coding genes are associated with short-term response to metformin monotherapy in type 2 diabetes mellitus patients. *European Journal of Endocrinology*, 175(6):531–540.

[258] Zake, D. M., Kurlovics, J., Zaharenko, L., Komasilovs, V., Klovins, J., and Stalidzans, E. (2021). Physiologically based metformin pharmacokinetics model of mice and scale-up to humans for the estimation of concentrations in various tissues. *PLoS One*, 16(4):e0249594.

[259] Zhao, M., Veeranki, S. P., Magnussen, C. G., and Xi, B. (2020). Recommended physical activity and all cause and cause specific mortality in US adults: prospective cohort study. *Bmj*, 370:m2031.

[260] Zhou, G., Myers, R., Li, Y., Chen, Y., Shen, X., Fenyk-Melody, J., Wu, M., Ventre, J., Doebber, T., Fujii, N., Musi, N., Hirshman, M. F., Goodyear, L. J., and Moller, D. E. (2001). Role of AMP-activated protein kinase in mechanism of metformin action. *J Clin Invest*, 108(8):1167–74.

[261] Żebrowska, A., Waśkiewicz, Z., Zając, A., Gąsior, Z., Galbo, H., and Langfort, J. (2013). IGF-1 response to arm exercise with eccentric and concentric muscle contractions in resistance-trained athletes with left ventricular hypertrophy. *Int J Sports Med*, 34(2):116–22.

Acknowledgement

It's your road, and yours alone.
Others may walk it with you,
but no one can walk it for you.
- Rumi

In diesem Sinne gibt es eine Reihe an Personen, bei denen ich mich gerne namentlich bedanken möchte, dafür dass sie mich auf meinem Weg bis zur Fertigstellung dieser Doktorarbeit begleitet haben. Ohne euch alle wäre das so nicht möglich gewesen!

Als erstes möchte ich ein großes Dankeschön an Prof. Cora Weigert für die Betreuung dieser Arbeit richten. Danke dafür, dass du deine Rolle als Mentor mit viel Verantwortung übernommen hast und an mich und mein Potential geglaubt hast. Ich weiß sehr zu schätzen, dass mir deine Bürotüre jederzeit offen stand und du immer mit Expertise, Ideen und kritischem Feedback zur Seite warst.

Ebenso möchte ich mir für die Unterstützung bei Prof. Peter Ruth bedanken. Mit ihrem kritischen Feedback und anregenden Diskussionen und Vorschlägen haben Sie entscheidend zum Erfolg dieser Arbeit beigetragen.

Ich schätze mich glücklich eine tolle Arbeitsgruppe zu haben und möchte daher Danke sagen an meine Kollegen Miriam Hoene, Simon Dreher, Thomas Goj, Bruno Taschke, Ann-Kathrin Horlacher, Nadine Sanabria Valdés, Paul Grubba, Kolja Leffek, und Katharina Zorn. Danke, dass ihr euch immer Zeit genommen habt, um mich und meine Arbeit zu unterstützen. Ein ganz besonderes Danke an Thomas, dafür, dass du immer mit Rat und Tat zur Seite warst, ganz egal ob es einen Fehler in meinem R Code gab oder ich Latex Unterstützung gebraucht habe und dafür, dass du dir jeden Morgen Zeit für einen Kaffee mit mir genommen hast. Ein weiteres Danke geht an Nadine und Paul für eure Unterstützung bei allem, was im Labor angefallen ist und natürlich ganz besonders für euren technischen und moralischen Support bei meinen geliebten Western Blots.

Ich möchte mich auch beim erweiterten Kreis der Kollegen – Andreas Peter, Rainer Lehmann, Sebastian Hörber, Marija Kocijancic, Alena Merz, Amalia Salca, Alke Guirguis, Karin Schweitzer, Melanie Weisser, Roman Werner – bedanken. Danke, dass ihr mit mir bei den Freitags-Vorträgen immer angeregt diskutiert habt, inspirirende Ideen für mich parat hattet und auch immer mit einer helfenden Hand im Labor zur Stelle wart.

Ich möchte mich auch ganz herzlich bei allen Kooperationspartner bedanken, die zu dieser Arbeit beigetragen haben. Danke an alle Kollegen aus dem Zentrallabor für die Messung unzähliger Zellkulturüberstände. Danke an Carolin Huhn und insbesondere an Nadja Kalinke für die tatkräftige Unterstützung bei den Messungen an der CE und die Geduld bei der Etablierung der Probenaufarbeitung. Danke auch an die Arbeitsgruppe von Prof. Guowang Xu in Dalian und an Kristian Karstoft und Kollegen vom Rigshospital in Kopenhagen. Ein besonderes Dankeschön geht an Henriette Pilegaard und Anders Gudiksen für ein herzliches Willkommen und einen inspirierenden Aufenthalt in eurem Labor in Kopenhagen.

Ein ganz besonders großes Danke möchte ich auch an meine Eltern Doris und Ralf und meinen Bruder Flo richten. Ihr habt mir immer die Freiheit gelassen meinen eigenen Weg zu gehen und mich dabei immer bedingungslos unterstützt. Ich weiß, dass ich immer auf euch zählen kann.

Ebenso dankbar bin ich für meine Freundin Christin. Danke, dass du dich gemeinsam mit mir durchs Studium gekämpft hast und sich so überhaupt erst die Möglichkeit zur Promotion ergeben hat. Ich hatte dir immer versprochen später einmal nicht mit Diabetes zu arbeiten. Das hat wohl nicht so ganz geklappt. Danke, dass du dir trotzdem die Zeit genommen hast, diese Arbeit zu lesen.

Danke auch an Stefan für die kurzen gemeinsamen Auszeiten am Berg und deine investierte Zeit, um dieser Arbeit den letzten Schliff zu verleihen.

Zu guter Letzt möchte ich mich noch aus tiefstem Herzen bei Niklas bedanken. Danke, dass du mich über all die Jahre hinweg auf meinem Weg begleitest und immer an mich glaubst. Manchmal sogar mehr als ich selbst. Du hast es immer wieder geschafft, dass ich das Beste aus mir herausholen konnte und wieder ein Stückchen über mich selbst hinauswachsen konnte. Und natürlich danke für all deinen geleisteten IT und Coding Support zu jeder Tages- und Nachtzeit.

DANKE!

Declaration

I hereby declare that I have independently written the thesis submitted for doctoral studies entitled “Metformin-induced Effects on Human Skeletal Muscle Metabolism and Function”, that I have used only the sources and aids indicated and that I have marked passages taken over verbatim or in citations as such. I declare that the guidelines for ensuring good scientific practice at the University of Tübingen (resolution of the Senate of 25.5.2000) have been observed. I affirm in lieu of oath that this information is true and that I have not concealed anything. I am aware that making a false affirmation in lieu of an oath is punishable by imprisonment of up to three years or a fine.

At the moment I am not accepted or registered at another university as doctoral student. There were no former interrupted or terminated PhD procedures or corresponding examinations, which I have taken. This work has not been submitted for any other degree or professional qualification except as specified. I did not take part in any commercially arranged opportunities to take up the current PhD procedure. I especially did not contact any organizations which engage in the active search for supervisors for the PhD thesis and receive money for this service. I also do clearly exclude that I used such organizations, which adopt the applicants obligations and take care of the academic records partially or entirely. Furthermore, I confirm to be aware of the legal consequences of using a commercial thesis writing agency (exclusion from acceptance as a doctoral student and exclusion from admission to the doctoral qualification process, an end to the doctoral qualification process and annulment of the degree). I have no penal convictions, disciplinary measures and pending criminal- and disciplinary proceedings to declare.

Part of this work has been published: Maurer J, Zhao X, Irmler M, Gudiksen A, Pilmark NS, Li Q, Goj T, Beckers J, Hrabě de Angelis M, Birkenfeld A, Peter A, Lehmann R, Pilegaard H, Karstoft K, Xu G, Weigert C. Redox state and altered pyruvate metabolism contribute to a dose-dependent metformin-induced lactate production of human myotubes. Am J Physiol Cell Physiol. 2023 Sep 11; 325:4, C1131-C1143; doi: 10.1152/ajpcell.00186.2023.

Jennifer Maurer
Tübingen, 08.04.2024

Publications and Conference Contributions

Publications

- **Maurer J.**, Hoene M., Weigert C., Signals from the Circle: Tricarboxylic Acid Cycle Intermediates as Myometabokines. Metabolites. 2021 Jul 23;11(8):474. doi: 10.3390/metabo11080474
- **Maurer J.**, Zhao X., Irmler M., Gudiksen A., Pilmark N.S., Li Q., Goj T., Beckers J., Hrabě de Angelis M., Birkenfeld A.L., Peter A., Lehmann R., Pilegaard H., Karstoft K., Xu G., Weigert C., Redox state and altered pyruvate metabolism contribute to a dose-dependent metformin-induced lactate production of human myotubes. Am J Physiol Cell Physiol. 2023 Sep 11; 325:4, C1131-C1143; doi: 10.1152/ajpcell.00186.2023
- Dreher S.I., Grubba P., von Toerne C., Moruzzi A., **Maurer J.**, Goj T., Birkenfeld A.L., Peter A., Loskill P., Hauck S.M., Weigert C., IGF1 promotes human myotube differentiation toward a mature metabolic and contractile phenotype. American Journal of Physiology-Cell Physiology 2024 Feb 26. doi: 10.1152/ajpcell.00654.2023

Conference Contributions

- **Maurer J**, Irmler M, Beckers J, Birkenfeld A, Peter A, Weigert C. Redox state and altered pyruvate metabolism explain the dose-dependent metformin-induced lactate production of human myotubes. Diabetologie und Stoffwechsel 2022; 17(S 01): S13. doi: 10.1055/s-0042-1746246
- **Maurer J**, Irmler M, Beckers J, Birkenfeld A, Peter A, Weigert C. Structural changes in human myotubes lead to impaired human myotube contractility under metformin treatment. Diabetologie und Stoffwechsel 2023; 18(S 01): S67-S68.doi: 10.1055/s-0043-1768003

EBERHARD KARLS
UNIVERSITÄT
TÜBINGEN

Mathematisch-Naturwissenschaftliche Fakultät

Erklärung nach § 5 Abs. 2 Nr. 8 der Promotionsordnung der Math.-Nat. Fakultät
-Anteil an gemeinschaftlichen Veröffentlichungen-

Declaration according to § 5 Abs. 2 No. 8 of the PhD regulations of the Faculty of Science
-Collaborative Publications-

Last Name, First Name: Maurer, Jennifer

List of Publications
1. Maurer J, Zhao X, Irmler M, Gudiksen A, Pilmark NS, Li Q, Goj T, Beckers J, HrabÄ› de Angelis M, Birkenfeld A, Peter A, Lehmann R, Pilegaard H, Karstoft K, Xu G, Weigert C. Redox state and altered pyruvate metabolism contribute to a dose-dependent metformininduced lactate production of human myotubes. Am J Physiol Cell Physiol. 2023 Sep 11. doi: 10.1152/ajpcell.00186.2023. PMID: 37694284.

Nr.	**Accepted publication yes/no**	**List of authors**	Position of candidate in list of authors	Scientific ideas by the candidate (%)	Data generation by the candidate (%)	Analysis and Interpretation by the candidate (%)	Paper writing done by the candidate (%)
1	yes	see above	1	70	70	90	100

I confirm that the above-stated is correct.

_____

Date, Signature of the candidate

I/We certify that the above-stated is correct.

_____

Date, Signature of the doctoral committee or at least of one of the supervisors